

**RAPID ASSESSMENT OF INFILL DRILLING POTENTIAL USING A
SIMULATION-BASED INVERSION APPROACH**

A Dissertation

by

HUI GAO

Submitted to the Office of Graduate Studies of
Texas A&M University
in partial fulfillment of the requirements for the degree of

DOCTOR OF PHILOSOPHY

May 2005

Major Subject: Petroleum Engineering

**RAPID ASSESSMENT OF INFILL DRILLING POTENTIAL USING A
SIMULATION-BASED INVERSION APPROACH**

A Dissertation

by

HUI GAO

Submitted to Texas A&M University
in partial fulfillment of the requirements
for the degree of

DOCTOR OF PHILOSOPHY

Approved as to style and content by:

Duane McVay
(Chair of Committee)

Jerry Jensen
(Member)

Akhil Datta-Gupta
(Member)

Richard Gibson
(Member)

Stephen Holditch
(Head of Department)

May 2005

Major Subject: Petroleum Engineering

ABSTRACT

Rapid Assessment of Infill Drilling Potential Using a Simulation-Based
Inversion Approach. (May 2005)

Hui Gao, B.S., University of Petroleum (East China)

M.S., University of Petroleum (BeiJing)

Chair of Advisory Committee: Dr. Duane McVay

It is often difficult to quantify the drilling and recompletion potential in producing gas fields, due to large variability in rock quality, well spacing, well completion practices, and the large number of wells involved. Given the marginal nature of many of these fields, it is often prohibitively expensive to conduct conventional reservoir characterization and simulation studies to determine infill potential. There is a need for rapid, cost-efficient technology to evaluate infill potential in gas reservoirs, particularly tight gas reservoirs. Some authors have used moving window statistical methods, which are useful screening tools for identifying potential areas or groups of wells for further study. But the accuracy of the moving window method in very heterogeneous reservoirs is limited, based on the analysis of some authors.

This study presents a new simulation-based inversion approach for rapid assessment of infill well potential. It differs from typical simulation inversion applications in that, instead of focusing on small-scale, high-resolution problems, it focuses on large-scale, coarse-resolution studies consisting of hundreds or, potentially thousands, of wells. In an initial application, the method employs well locations, production data, an approximate reservoir description and, accordingly, is able to identify potential areas or groups of wells for infill development quickly and inexpensively. Prediction accuracy can be increased commensurate with reservoir characterization effort, time and costs. Thus, the method provides a consistent basis for transition from screening studies to conventional reservoir studies.

The proposed approach is demonstrated to be more accurate than moving window statistical methods in synthetic cases, with comparable analysis times and costs. In a blind validation study of a field case with 40 years of production history, the method was able to accurately predict performance for a group of 19 infill wells.

DEDICATION

To my parents, Shengxing Gao and Yuhuan Ma for their love and support throughout this study.

To my husband Bo and my daughter Megan for their love and understanding.

ACKNOWLEDGMENTS

I would like to express my deep gratitude to my advisor, Dr. Duane McVay, for his valuable advice, financial support, and especially for his academic guidance.

I would like to thank Dr. Akhil Datta-Gupta, Dr. Jerry Jensen and Dr. Richard Gibson for serving as members of my advisory committee and for their advice and guidance in this study.

I would like to thank Dr. Zhan Wu and Ill Nam for their valuable discussions in this study.

TABLE OF CONTENTS

	Page
ABSTRACT.....	iii
DEDICATION.....	v
ACKNOWLEDGMENTS.....	vi
TABLE OF CONTENTS.....	vii
LIST OF TABLES.....	ix
LIST OF FIGURES.....	xi
CHAPTER I INTRODUCTION.....	1
1.1 Background and literature review.....	1
1.2 Objectives of research.....	5
CHAPTER II FUNDAMENTALS OF INVERSE METHOD.....	6
2.1 Overview.....	6
2.2 Forward model.....	7
2.3 Minimization methods.....	8
2.4 Sensitivity coefficient computation.....	13
2.5 Objective function.....	16
2.6 Calculating infill well performance.....	18
CHAPTER III VALIDATION OF INVERSE METHOD.....	19
3.1 Synthetic case introduction.....	19
3.2 Comparison with moving window method.....	23
3.3 Comparison of inverse method with SimOpt by Case 2.....	43
CHAPTER IV RESERVOIR PARAMETERS SENSITIVITY STUDY.....	52
4.1 Introduction of synthetic cases generated for sensitivity study.....	52
4.2 The effect of pore volume on predicted infill performance.....	56
4.3 The effect of skin factors on predicted infill performance.....	63
CHAPTER V FIELD CASE APPLICATION OF INVERSE METHOD.....	67
5.1 Field case description.....	67
5.2 Procedures for dealing with the new field database.....	69
5.3 Construct reservoir model.....	71

	Page
5.4 Field test results.....	72
5.5 Sensitivity to weighting factors.....	85
5.6 Comparison of inverse method and SimOpt by field case.....	93
CHAPTER VI SUMMARY AND CONCLUSIONS.....	99
NOMENCLATURE.....	103
REFERENCES.....	107
VITA.....	111

LIST OF TABLES

TABLE	Page
3.1 Description of four synthetic cases.....	20
3.2 The parameters used in the four synthetic cases.....	21
3.3 Regression results for the four synthetic cases.....	27
3.4 Comparison of the inverse and moving window method.....	38
3.5 Comparison of average BY_{inf} for three methods.....	51
3.6 Comparison of average percent error of individual wells for three methods.....	51
3.7 Comparison of computation efficiency of the inverse method and SimOpt in synthetic case.....	51
4.1 The parameters used in the base case.....	55
4.2 Description of four synthetic cases in sensitivity study of pore volume.....	57
4.3 Relative error with different pore volume.....	62
4.4 Average percent error with different pore volume.....	63
4.5 The properties of skin factors.....	64
4.6 Percent error distribution for $Sk1_{actual}$	66
4.7 Percent error distribution for $Sk2_{zero}$	66
5.1 Formation ID corresponding to formation name.....	70
5.2 Other parameters used in the field case.....	72
5.3 Summary of percent error for group wells	81
5.4 Different combination of weighting factors.....	88
5.5 Percent error distribution using weighting factors as 1(Type 1).....	89

TABLE	Page
5.6 Percent error distribution with Type 2 weighting factors.....	89
5.7 Percent error distribution with Type 3 weighting factors (normalized).....	90
5.8 Percent error distribution with Type 4 weighting factors.....	90
5.9 Percent error distribution with schemes of Type 2 and Type 3 weighting..	90
5.10 Percent error distribution with schemes of Type 2 and Type 4 weighting..	91
5.11 Percent error by inverse method.....	97
5.12 Percent error by SimOpt matching only on permeability.....	97
5.13 Percent error by SimOpt matching both on permeability and pore volume.....	97
5.14 Comparison of computation efficiency in field case.....	98

LIST OF FIGURES

FIGURE	Page
2.1 Four steps used in the inverse method.....	7
3.1 Date of first production for 100 wells	20
3.2 Actual permeability distribution for Case 2	21
3.3 Actual permeability distribution for Case 3.....	22
3.4 Actual permeability distribution for Case 4.....	22
3.5 Field cumulative production history match for Case 2.....	23
3.6 Field production rate history match for Case 2.....	24
3.7 History matching of Well 2 for Case 2.....	24
3.8 History matching of Well 81 for Case 2.....	25
3.9 History matching of Well 61 for Case 2.....	25
3.10 History matching of Well 94 for Case 2.....	26
3.11 Objective functions for the four synthetic cases.....	27
3.12 Estimated permeability distribution for Case 1.....	28
3.13 Actual and estimated permeability distribution for Case 2.....	29
3.14 Actual and estimated permeability distribution for Case 3.....	29
3.15 Actual and estimated permeability distribution for Case 4.....	30
3.16 The effect of smoothness factor on permeability misfit and objective function.....	30
3.17 Infill potential map of Case 2.....	31
3.18 Pressure map of Case 2.....	32

FIGURE	Page
3.19 Simulation well regions.....	34
3.20 Infill BY from simulation and inverse method for Case 2.....	35
3.21 Infill BY from simulation and moving window method for Case 2.....	36
3.22 Infill BY from simulation and inverse method for Case 1.....	39
3.23 Infill BY from simulation and moving window method for Case 1.....	40
3.24 Infill BY from simulation and inverse method for Case 3.....	41
3.25 Infill BY from simulation and moving window method for Case 3.....	41
3.26 Infill BY from simulation and inverse method for Case 4.....	42
3.27 Infill BY from simulation and moving window method for Case 4.....	42
3.28 Objective function by inverse method.....	47
3.29 Objective function by SimOpt.....	47
3.30 History match of field production rate by SimOpt	48
3.31 Good individual history match from SimOpt for Case 2 – Well 49.....	48
3.32 Bad individual history match from SimOpt for Case 2 – Well 42.....	49
3.33 Estimated permeability distribution for Case 2 by SimOpt	50
4.1 The distribution of date of first production for the base case	54
4.2 The distribution of actual thickness for the base case	54
4.3 The distribution of actual porosity for the base case.....	55
4.4 Well locations in the base case.....	56
4.5 Objective function for four synthetic cases.....	58
4.6 Estimated permeability for Pv1_actual.....	59
4.7 Estimated permeability for Pv2_average.....	60
4.8 Estimated permeability for Pv3_high	60

FIGURE	Page
4.9 Estimated permeability for Pv4_low.....	61
4.10 Objective function with different skin factors.....	65
4.11 Estimated permeability distribution for Sk2_zero.....	66
5.1 Histogram of date of first production for the field case.....	68
5.2 Objective function for the field case.....	73
5.3 Estimated permeability for the field case at the end of the 152-well history.....	74
5.4 History match of field cumulative production.....	75
5.5 History match of field production rate.....	75
5.6 History match of Well 12.....	76
5.7 History match of Well 48.....	76
5.8 History match of Well 53.....	77
5.9 History match of Well 2.....	77
5.10 Estimated permeability distribution for the field case.....	79
5.11 Predicted field cumulative production for 105 existing wells that produced during the prediction period.....	80
5.12 Predicted field cumulative production for 19 infill wells.....	80
5.13 Predicted field cumulative production for 26 step-out wells.....	81
5.14 Prediction for infill Well 163.....	82
5.15 Prediction for infill Well 173.....	83
5.16 Prediction for step-out Well 170.....	83
5.17 Prediction for step-out Well 177.....	84
5.18 Distribution of relative percent error for 3 group wells.....	88
5.19 Distribution of median of percent error for 3 group wells.....	89

FIGURE	Page
5.20 Predicted field cumulative production for 105 existing wells with weighting scheme 6.	91
5.21 Predicted field cumulative production for 19 infill wells with weighting scheme 6.....	92
5.22 Predicted field cumulative production for 26 step-out wells with weighting scheme 6...	92
5.23 Objective function by SimOpt matching only on permeability.....	94
5.24 Objective function by SimOpt matching on both permeability and pore volume.....	94
5.25 Estimated permeability distribution by SimOpt matching on permeability only.....	95
5.26 Estimated permeability distribution by SimOpt matching on permeability and porosity	95
5.27 Estimated pore volume distribution by SimOpt matching on permeability and porosity.....	96

CHAPTER I

INTRODUCTION

1.1 Background and Literature Review

Natural gas plays a vital role in meeting energy requirements and today provides almost a quarter of the United State's energy portfolio. The demand for natural gas increases yearly, while the decline rate of existing production continues to increase as well. To meet U.S. natural gas demand, unconventional gas, which refers to natural gas extracted from coalbeds, low-permeability sandstone and shale formations, has become an increasingly important component of total U.S. domestic production over the past decade. From 18% (3.2 trillion cubic feet) of total gas production in 1990, the unconventional gas share grew to 24% (4.5 trillion cubic feet) by 1998. Although unconventional gas sources are abundant, they are generally more costly to produce.¹ Infill drilling is an alternative to exploration of unconventional gas in existing basins. However, quantifying the drilling and recompletion potential in producing gas basins is often challenging, due to large variability in rock quality, well spacing, well completion practices, and the large number of wells involved. It is not uncommon for an operator to have hundreds of infill candidates from which to choose in a particular campaign.²

The most accurate way to determine infill-drilling potential in a gas basin is to conduct a complete reservoir evaluation, which includes developing a geological model of the study area, estimating distributions of static reservoir properties of such as porosity and permeability,

This dissertation follows the style of SPE Journal.

constructing and calibrating a reservoir simulation model of the area, and then using the reservoir model to predict future production and reserves at potential infill well locations. In the history matching process, a reservoir simulation model has to be adjusted until a close match is obtained between the simulated production response and the production response observed in the field. This task has been performed traditionally by trial and error, and it is often time consuming and expensive. Automatic history matching has been used to reduce the time for calibrating reservoir models significantly. There are some example applications for determining reservoir parameters in gas reservoirs. Coats³ presented a method that used the least squares and linear programming techniques to determine a reservoir description from given performance data. Example applications presented in his paper include cases of single-phase gas flow, single-phase oil flow and two-phase gas-water flow. In these particular applications the method Coats proposed gave accurate reservoir description with a small number of simulation runs. Chung. And Kravaris⁴ developed a regularization history-matching algorithm that is capable of incorporating prior information on the unknown reservoir parameters like porosity and permeability. The prior information is considered to consist of order-of-magnitude point estimates that are directly measured from core sample analysis, or are extracted from other field tests. Their approach remains a deterministic one, and contrasts with other methods of incorporating prior information that are largely based on a statistical formulation. In this paper,⁴ their proposed approach is compared with statistically-based methods of incorporating prior information with respect to the mechanism of constraining the parameter space. The proposed method is evaluated through numerical simulations on history-matching of a two-dimensional ideal gas reservoir. The results showed that incorporation of a prior point estimates enhances the accuracy the regularized estimate by recovering the spatial distribution on a local scale.

Some authors have combined conventional reservoir simulation with automated methods to determine infill potential. For example, Coats⁵ presented a two-dimensional numerical calculation method for calculating the semi-steady-state pressure distribution and individual well deliverabilities in a gas field producing under a specified total rate schedule. The method he described minimizes new well requirements at each successive stage of depletion by selecting optimal locations for additional wells. The method accounts for the effects on well deliverability of reservoir heterogeneity, irregular spacing, and well interference. The calculation method he proposed can be employed to estimate field performance for any given combination of producing well locations or may be used to determine an optimal drilling order for a given set of admissible well sites. Coats also pointed out that the optimal selection of additional well sites depends upon well interference phenomena as well as the reservoir kh and ϕh distributions. It is important to have good estimations of reservoir parameter distributions, particularly kh and ϕh , since these distributions have a significant effect on the optimization.

While conventional reservoir simulation studies may be the most accurate way to determine infill potential, they are also time-consuming and expensive. This is especially true of large infill drilling studies in low-permeability gas basins, which may involve the analysis of 1000's of wells. While use of automatic history matching methods can reduce time and cost requirements, the time and costs associated with reservoir characterization can still make conventional studies prohibitively expensive, particularly for marginal reservoirs.

As an alternative approach to detailed reservoir studies, some authors have proposed statistical methods. McCain *et al.*⁶ proposed a statistical method to evaluate the need for infill drilling in complex, low-permeability gas reservoirs. It is a practical means of applying advanced analysis techniques to an entire field. This proposed statistical production analysis allows the use of a small number of localized advanced evaluations, and provides areal locations where

conclusions from the localized studies can be applied. The study in this paper includes the geological description of Cotton Valley formation, critical evaluation of all available pressure measurements, statistical comparison of production data for all wells in the field, careful and tedious logging interpretation activities and analysis, objective selection of cutoffs for determination of net pay and evaluation by some simulation studies. The statistical analysis is inexpensive to perform, and the advanced analysis is limited to a few small areas, keeping costs to a reasonable level. However, the author also needed the tedious logging interpretations in their research to assure the accuracy of net pay thickness calculation.

As an improvement to McCain *et al.*'s⁶ statistical method, Voneiff and Cipolla⁷ presented a moving window statistical method to determine infill potential in complex, low-permeability gas reservoirs. This new technique is a set of empirically derived approximations, comparisons, and statistical tests that attempt to mimic what a reservoir engineer does when faced with a single infill location evaluation. It looks at surrounding well performance, compares new wells to old wells for signs of depletion, calculates effective well density, and, once linked to a scattering of conventional estimates of drainage area, provides estimates of undrained acreage and infill reserves. The analyses are applied within a moving window of 5 to 15 wells at a time to minimize the effects of areal changes in rock properties. The primary advantages of the moving window technique are that it is easy to apply and it relies on only publicly available well location and production data, making a 1,000-well study a manageable task. It has been successfully applied to the Ozona (Canyon) Gas Sands, East Texas Cotton Valley, and the Austin Chalk to determine optimum well spacing and quantify infill potential.⁷⁻⁹

Guan *et al.*¹⁰ assessed the accuracy of the moving window technique for selecting infill candidate wells in low-permeability gas reservoirs by analyzing synthetically generated production data. The technology they showed in this paper is an extension of the method

described by Voneiff and Cipolla.⁷ It also includes a local analysis, each in an areal window centered around an existing well. However, a more rigorous, model-based analysis is applied in each window, which is a 4D regression based on combinations of material balance equation and the pseudo-steady state flow equation. The result of their analysis is a prediction of BY for a new infill well offsetting each existing well. In this paper, they show that the moving window technique can predict average infill performance of a group of wells reasonably well and, importantly, it appears to provide a conservative estimate. Thus, it can serve as a useful screening tool. However, as reservoir heterogeneity increases, the error in predicted individual infill well performance increases, to as much as +/-50% or more. Also, with this technique it is difficult to incorporate other types of data, particularly non-well based-data such as seismic data.

Therefore, considering the limitations of both conventional methods and moving window techniques in identifying infill drilling areas, there is still a need for new methods to quantify the infill potential in large gas reservoirs to be rapid, cost-efficient, but reasonably accurate.

1.2 Objectives of research

The objective of my work was to develop improved technology for rapid assessment of infill drilling and recompletion potential in large gas reservoirs. Specifically, I sought to combine the greater accuracy of simulation-based methods with the short analysis times and low costs associated with statistical methods, to yield a method intermediate in both.

In the following section, I presented the methodology of the proposed method. Then I compared the accuracy of the inverse method with the moving window technique by four synthetic cases, and showed the comparisons with SimOpt as well. Finally, I applied the inverse method in a field case to validate its accuracy.

CHAPTER II

FUNDAMENTALS OF INVERSE METHODS

2.1 Overview

My proposed method uses reservoir simulation combined with advanced automatic history matching technology. A reservoir simulator serves as the forward model, which calculates well production responses from reservoir description data. Sensitivity coefficients are calculated internally and used in the inversion of historical production data to estimate the permeability field. Using the estimated permeability field and forward model, I then determine the expected performance of potential infill wells.

Since the method is simulation-based, all the data required to initialize a reservoir simulator (e.g., reservoir property distributions, PVT properties, reservoir pressure) are required to apply the method. However, since my goal is rapid, approximate estimation of infill potential, I do not conduct a detailed reservoir characterization study. Instead, in an initial application, I simply use whatever data are available. For example, I use reservoir property maps if they are available; otherwise, I initialize the model with uniform average values. Since estimates of individual well skin factors will generally not be available, I assume a uniform value for all wells or apply a correlation of skin factor with completion type. In addition, since I rely primarily upon readily available well location and production data, I invert production data with constant pressure production modeling rather than inverting pressure data with constant rate modeling.

My proposed use of reservoir simulation inversion technology also differs from typical uses in the scale of application. The ultimate is to determine infill or recompletion potential over large areas and for large numbers of wells, often at scales exceeding individual reservoirs. To do

this I determine large-scale, coarse-resolution permeability fields, rather than small-scale, fine-resolution property fields obtained in conventional studies of individual reservoirs.

As I described in the Overview, the proposed approach includes four steps (**Fig. 2.1**). I introduce each of these steps in the following sections.

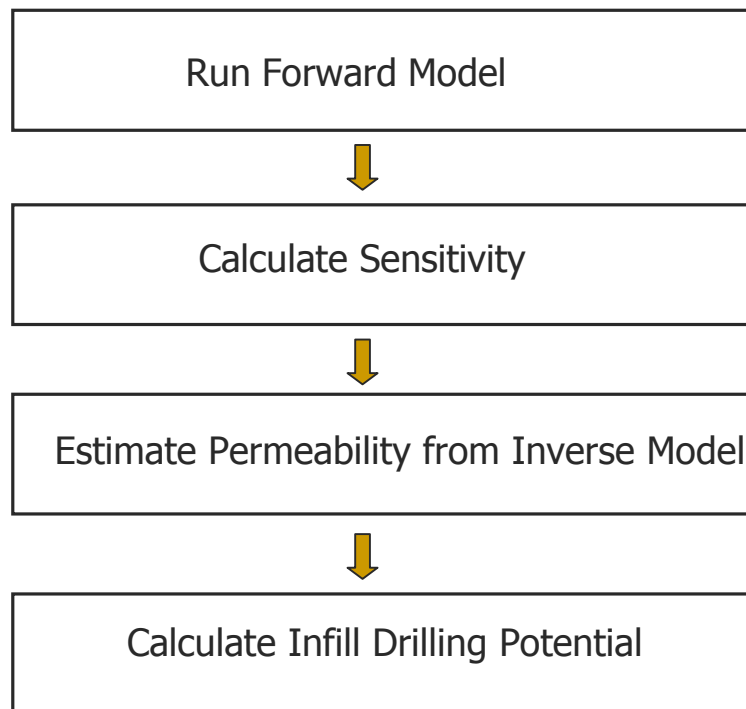


Fig. 2.1 - Four steps used in the inverse method

2.2 Forward model

The forward model used to calculate reservoir and well performance is a conventional 2D, single-phase, finite-difference gas reservoir simulator. This forward model is based on GasSim, a single-phase simulator for modeling real-gas flow in gas reservoirs.¹¹ The main equations used in this simulator are defined as following:

- Real-gas pseudopressure:

$$p_p(p) = 2 \int_0^p \frac{p}{z\mu} dp \quad \dots\dots\dots (2.1)$$

- 2D flow equation:

$$-a_N p_{pi,j-1}^{n+1} - a_W p_{pi-1,j}^{n+1} + a_C p_{pi,j}^{n+1} - a_E p_{pi+1,j}^{n+1} - a_S p_{pi,j+1}^{n+1} = d \quad \dots\dots\dots (2.2)$$

$$\text{Where } a_C = a_N + a_W + a_E + a_S + \alpha \quad \dots\dots\dots (2.3)$$

$$d = \alpha p_{pi,j}^n - q \quad \dots\dots\dots (2.4)$$

$$\alpha = \frac{1}{\Delta t} \left(\frac{T_{sc}}{p_{sc} T} \right) \frac{\left(\frac{V_p p}{z} \right)_i^{n+1} - \left(\frac{V_p p}{z} \right)_i^n}{p_{pi}^{n+1} - p_{pi}^n} \quad \dots\dots\dots (2.5)$$

- PI equation:

$$q = J' (p_{pi,j}^{n+1} - p_{pwf}) \quad \dots\dots\dots (2.6)$$

$$\text{Where } J' = \frac{0.01988khT_{sc}}{p_{sc} T \left(\ln \frac{r_o}{r_w} + s \right)} \quad \dots\dots\dots (2.7)$$

2.3 Minimization methods

Automatic history matching involves minimization of an objective function quantifying the mismatch between simulated and observed data. In the past, many methods¹²⁻¹⁶ have been used

for minimization. Generally, these approaches can be broadly classified into three categories: derivative-free methods, gradient-based methods and sensitivity-coefficient methods.

2.3.1 Derivative-free method

The derivative-free approaches such as simulated annealing can combine data from many different sources such as cores, logs, seismic traces and interwell tracer data.

2.3.1.1 Simulated annealing

Simulated annealing is an algorithm initially developed for the solution of combinatorial optimization problems. The central idea behind simulated annealing is an analogy with thermodynamics, specifically with the way liquids freeze and crystallize, or metals cool and anneal. The essential components of an annealing algorithm are the objective function, a procedure to update the objective function, a perturbation mechanism, and some empirical procedure for lowering the temperature or reducing the control parameter.

The general algorithm may be described with the following steps:

1. Generate an initial image
2. Establish an initial control parameter c and a schedule for lowering it as the looping progresses.
3. Perturb the image.
4. Compute a new objective function F_{new} .
5. Establish the acceptance probability distribution:

$$P\{accept\} = \begin{cases} 1, & \text{if } F_{new} < F_{old} \\ \exp\left[\frac{F_{old} - F_{new}}{c}\right], & \text{otherwise} \end{cases} \dots\dots\dots (2.8)$$

6. Draw from that probability distribution. If the perturbation is accepted then update the image and reset the objective function $F_{old} = F_{new}$
7. Return to step 3 until the objective function is low enough or there has not been any significant improvement in many successive iterations.

This derivative-free method is very flexible since it does not require derivative computations. It can also account for a wide variety of data as I mentioned above. But it is also computationally demanding because of the large number of rejection moves it makes as annealing progresses. Thus, this method is not practical for field-scale applications.

2.3.2 Gradient-based method

For the gradient-based algorithms, it is classified according to its search direction into steepest descent, Newton, quasi-Newton, and conjugate gradient. In the following, I introduced steepest descent and Newton method.

2.3.2.1 Steepest descent method

Taking the Taylor series of objective function $F(x)$,

$$F(x_k + p_k) = F(x_k) + q_k^T p_k \quad \dots\dots\dots (2.9)$$

where q_k is the gradient of F . The search direction that minimize Eq. 2.9 is

$$p_k = -q_k \quad \dots\dots\dots (2.10)$$

The steepest-descent method usually works satisfactorily when the search is far away from the minimum. However, it progresses very slowly in the vicinity of the minimum. A better rate of convergence can be obtained by choosing the search direction from the second-order approximation to the objective function like Newton method does.

2.3.2.2 Newton method

Taking the Taylor series of objective function $F(x)$ to second-order,

$$F(x_k + p) = F(x_k) + q_k^T p + \frac{1}{2} p^T H_k p \quad \dots\dots\dots (2.11)$$

The minimum of the Eq. 2.11 will be given by

$$p = -H_k^{-1} q_k \quad \dots\dots\dots (2.12)$$

This is the algorithm for Newton method. The rate of convergence for Newton's method is quadratic, which is higher than steepest descent method. However, computation of Hessian matrix is very expensive for reservoir history matching problems. It requires a number of reservoir simulations at least on the order of the dimensionality of the problems.

2.3.3 Sensitivity-based method

Gauss-Newton and Levenberg-Marquard methods are considered one of the Newton-type of search algorithm. But they need to calculate the sensitivity coefficients which are the gradients of production responses with respect to the model parameters, instead of the gradient of objective function as steep-descent method does. They are commonly used to get the maximum a posteriori estimate (MAP) from the posterior distribution by knowing the sensitivity coefficients.

2.3.3.1 Gauss-Newton method

Gauss-Newton method has avoided the computation of Hessian matrix in Newton method by ignoring the second term in H_k and computes a search direction by

$$J_k^T J_k p_k = -J_k^T e_k \quad \dots\dots\dots (2.13)$$

where, e is residual, $e = \begin{bmatrix} C_n^{-1/2} (d - g(x)) \\ C_x^{-1/2} (x - \mu) \end{bmatrix}$, \dots\dots\dots (2.14)

and J is Jacobin matrix, $J_{i,j} = \frac{\partial e_i}{\partial x_j} = \begin{bmatrix} -C_n^{-1/2} G(x) \\ C_x^{-1/2} \end{bmatrix}$ (2.15)

G(x) in Eq2.15 is sensitivity coefficient matrix.

2.3.3.2 Levenberg-Marquardt method

The Gauss-Newton method can run into problems if $J_k^T J_k$ is singular or nearly singular. This is corrected by Levenberg-Marquardt method by making the Hessian diagonally dominated,

$$(J_k^T J_k + \lambda_k I) p_k = -J_k^T e_k \quad \text{..... (2.16)}$$

Gauss-Newton and Levenberg-Marquardt method has fast quadratic convergence, and can be computationally efficient in large-scale problems.

2.3.3.3 LSQR (Lease squares QR factorization)

LSQR method is developed to find a solution for solving equation $Ax = b$ or minimize $\|Ax - b\|_2$. It's based on the Lanczos bidiagonalization procedure of Golub and Kahan. It generates a sequence of approximations $\{x_k\}$ such that the residual norm $\|r_k\|_2 = \|Ax - b\|_2$ decreases monotonically. In reservoir history matching problems, LSQR is used to minimize $\|G\delta m - \varepsilon\|_2$, where, G is sensitivity coefficient matrix, δm is the perturbation of reservoir parameter, and ε is vector of data misfit.

LSQR is commonly used for large tomographic problems and especially suited for large sparse system as encountered in reservoir simulation, and it can also works for ill-posed matrices. LSQR method is extremely efficient, requiring only a few iterations.

Sensitivity-based method has faster convergence rate compared to derivative-free and gradient-based method, and it is preferred for large-scale problems. For sensitivity-based method, a key step is the computation of sensitivity coefficient matrix.

2.4 Sensitivity coefficient computation

Sensitivity coefficients are partial derivatives of production response variables with respect to reservoir parameters (permeability in my work). Calculation of sensitivity coefficients is a critical part of inversion. Reducing the cost for calculating sensitivity coefficients can significantly improve the computation efficiency of the whole inversion process. I investigated several of methods for computation of sensitivity coefficients.¹²

2.4.1 Direct method

The time-honored method for calculating sensitivities is the direct or influence coefficient method.¹⁷ In this method, I first run the simulator using an initial estimate of the permeability distribution to obtain the first set of production responses. I then perturb one of the parameters, e.g., permeability of one grid block, k_i , and rerun the simulator to get the second set of production responses. From these two simulations, I obtain the sensitivities of all the production responses to the permeability k_i . Thus, to determine all the sensitivity coefficients using this method requires $M+1$ simulation runs, where M is the number of parameters, in this case the number of grid blocks. It is usually impractical to compute sensitivity coefficients using the direct method. In addition, if the magnitude of the perturbation is poorly chosen, it is possible for sensitivity coefficients from this direct method to be in error.¹⁸

2.4.2 Gradient Simulator Method

The Gradient Simulator Method was proposed first by Yeh¹⁹ in ground water hydrology literature as the Sensitivity Equation method. It was introduced to the petroleum engineering literature by Anterion *et al.*²⁰ In this method, the sensitivity coefficients are obtained by

differentiating the simulation equations. The advantage of the gradient simulator method is that the matrix problem solved to obtain sensitivity coefficients involves the same coefficient matrix as the one used to solve for production data at the same time step. With this method, in one simulation run, one actually obtains the sensitivity coefficients of production responses for all gridblocks with respect to each model parameter. However, since we only have observation data in the gridblocks with wells, most of the calculated sensitivity coefficients are unnecessary, which makes the Gradient Simulator Method low in computational efficiency.

2.4.3 MGPST method

To avoid calculation of the sensitivity coefficients for all gridblocks with respect to each model parameter, Chu *et al.*¹⁷ used the basic ideas of Tang *et al.*²¹ to develop a Modified Generalized Pulse-Spectrum Technique (MGPST). This method produces the sensitivity coefficients in one simulation run. The linear system to be solved depends on the number of wells (N_w) as opposed to the number of parameters (M) for the direct method and Gradient Simulator method. Thus the MGPST method is more efficient, particularly for determining sensitivity coefficients for a large number of parameters.

In my work, I calculated sensitivity coefficients with the MGPST method. As mentioned before, typical applications of automatic history matching involve small-scale, high-resolution problems. Wells are typically rate-constrained, using historical production rates. The derived sensitivity coefficients are usually bottomhole pressure, water cut and/or gas-oil ratio with respect to parameters such as permeability and porosity. In my approach, I constrain wells at constant flowing bottomhole pressure and match on production data. Thus, the derived sensitivity coefficients are production rate with respect to permeabilities. Derivation of the sensitivity coefficients that I used in my approach is discussed below.

The simplified governing flow equation is,

$$Ap = b, \quad \dots\dots\dots (2.17)$$

where A is the matrix of flow elements, p is the vector of well block pressures, and b is comprised of the known pressures, flow rate, and α (Eq. 2.5), which is related to time step, isothermal compressibility and pore volume.¹¹

Taking the partial derivative of Eq. 2.17 with respect to the i -th grid block permeability, and simplifying it, we obtain

$$\frac{\partial p}{\partial k_i} = A^{-1} \left(\frac{\partial b}{\partial k_i} - \frac{\partial A}{\partial k_i} p \right) \quad \dots\dots\dots (2.18)$$

Taking the partial derivative of Peaceman's equation,

$$q = J(p - p_{wf}) \quad \dots\dots\dots (2.19)$$

with respect to the i -th grid block permeability, we obtain

$$\frac{\partial q}{\partial k_i} = \frac{\partial J}{\partial k_i} (p - p_{wf}) + J \frac{\partial p}{\partial k_i} \quad \dots\dots\dots (2.20)$$

Substituting $\frac{\partial p}{\partial k_i}$ from Eq. 2.18 into Eq. 2.20, I obtain the following expression for sensitivity

coefficients of production rate in all the grid blocks to one permeability value, k_i .

$$\frac{\partial q}{\partial k_i} = \frac{\partial J}{\partial k_i} (p - p_{wf}) + JA^{-1} \left(\frac{\partial b}{\partial k_i} - \frac{\partial A}{\partial k_i} p \right) \quad \dots\dots\dots (2.21)$$

When I calculate $\frac{\partial q}{\partial k_i}$ in Eq. 2.21, I only need to calculate the sensitivity coefficients in the gridblocks with wells. This means I do not need to calculate the inverse matrix of A . I only need to calculate the rows of A^{-1} corresponding to the well blocks. This saves a lot of computation time. If I use $\frac{\partial p_l}{\partial k_i}$ for the sensitivity coefficient of block pressure of the l -th well with respect to

the i -th grid block permeability, Eq. 2.8 should be

$$\frac{\partial p_l}{\partial k_i} = \left(\frac{\partial A}{\partial k_i} p \right)^r x_l, \quad \dots\dots\dots (2.22)$$

where, x_l is the l -th column for A^{-1} .

2.5 Objective function

During inverse modeling, the objective is to minimize the differences between observed and simulated responses. Mathematically, this can be expressed as

$$\min \|d - g[m]\|_2^2 \quad \dots\dots\dots (2.23)$$

where d is the vector of N observation data points, g is the forward model, m is the vector of M parameters (permeabilities in my problem), and $\|\cdot\|_2$ denotes the Euclidean norm.

At the l -th iteration step, I take a first order Taylor series expansion of $g[m]$ around m_l ,

$$g[m] = g[m_l] + G\delta m, \quad \dots\dots\dots (2.24)$$

where m_l is the vector of M parameters at the l -th iteration step, G is the sensitivity coefficients matrix, and δm is the vector of parameter changes at the l -th iteration step.

The residual (data misfit) vector ε at the l -th iteration will be given

$$\varepsilon = d - g[m_l] \quad \dots\dots\dots (2.25)$$

Now I solve Eq. 2.23 by minimizing

$$\|\varepsilon - G \delta m\|_2^2 = \left[\sum_{i=1}^N \left(\varepsilon_i - \sum_{j=1}^M G_{ij} \delta m_j \right)^2 \right] \dots\dots\dots (2.26)$$

and update the parameter vector

$$m = m_i + \delta m \dots\dots\dots (2.27)$$

Since typically there are a large number of parameters compared to the amount of data, the inverse problem is often ill-posed and can result in non-unique and unstable solutions. In order to remedy the ill-posedness of the inverse problem, the objective function was augmented by adding another two terms.²² Thus, the penalized objective function is given by

$$\|\varepsilon - G \delta m\|_2^2 + \gamma_1 \|\delta m\|_2^2 + \gamma_2 \|L_h \delta m\|_2^2 \dots\dots\dots (2.28)$$

In Eq. 2.20, the first term is the data misfit term, which minimizes the difference between the observed and calculated production responses. The second term, the norm constraint, ensures that the final model is not significantly different from the initial model. This helps preserve geologic realism because the initial model already contains available geologic and static information related to the reservoir. The smoothness constraint, the third term in Eq. 2.20, provides some spatial continuity of reservoir properties by resolving large-structures rather than small-scale property variations. In this penalized objective function, γ_1 and γ_2 are user-specified weighting factors that determine the relative strengths of the prior model and the smoothness term. In general, the inversion results will be sensitive to the choice of these weights. L_h is the second-order spatial-difference operator.^{22, 23}

Mathematically, minimizing the objective function, Eq. 2.20, is equal to solving the following augmented matrix,

$$\min \left\| \begin{bmatrix} G \\ \gamma_1 I \\ \gamma_2 L_h \end{bmatrix} \delta m - \begin{bmatrix} \varepsilon \\ 0 \\ 0 \end{bmatrix} \right\|_2^2 \quad \dots\dots\dots (2.29)$$

I use LSQR²⁴ to solve this augmented linear system efficiently. Solution yields the permeability perturbations, δm . I use δm to update the permeability field, iterating until convergence is obtained. In this study, the convergence criteria I used is that the objective function does not have significant improvement in some (like 3 or 4 iterations) successive iterations. Or, from the plot of the misfit versus the number of iteration, the curve becomes almost parallel to the x-coordinate. Under either of these two conditions, I terminated the iteration of regression.

2.6 Calculating infill well performance

My method for calculating infill well performance is similar to the method proposed by Coats.⁵ In Coats' paper, he proposed a two-dimensional numerical calculation for calculating semi-steady-state pressure distribution and individual well deliverabilities in a producing gas field. Being simulation-based, my method applies for both transient and pseudo-steady flow. We estimate infill and recompletion potential using the reservoir model and the permeability field resulting from inversion. We first make a base case forecast with existing wells. We then place a new well in the first grid block of the reservoir model and make a forecast to determine the incremental fieldwide production attributable to a new well in this grid block. We repeat this for each grid block in the system, thus generating a distribution of the incremental fieldwide production attributable to one new well at all the possible grid locations in the reservoir. With this information we can generate colorfill maps of infill well production indicators that can be used to assess infill drilling potential in different areas of the field.

CHAPTER III

VALIDATION OF INVERSE METHOD

In this chapter, I used four synthetic cases presented in Guan *et al.*¹⁰ to evaluate the proposed inverse method and compare it to the moving window methods proposed by Voneiff and Cipolla.⁷

3.1 Synthetic case introduction

The four synthetic cases with varying heterogeneity were defined on a 54*54*1 simulation grid of a 9-township area. Case 1 is the homogeneous case. For Cases 2-4, a log-normal distribution was used to generate a base random permeability field. Heterogeneity increases with case number, as indicated in **Table 3.1** by the standard deviation and coefficient of variation. Average permeability is the same for all four cases, 0.2 md. There are 100 wells in the reservoir, which were drilled at different dates over approximately 40 years. **Figure 3.1** shows the date of first production for 100 wells which represents several rounds of infill drilling implemented. The distributions of current well spacing and first production date are realistic as they were derived from actual well data from a shallow gas basin in North America. Other parameters used in the simulation, listed in **Table 3.2**, are the same for all 4 cases.¹⁰

For each case, I generated the synthetic production history using the actual permeability distribution, then inverted the synthetic production data using the methodology described in Chapter II to determine the permeability field. I matched on average production rate of every other year, yielding a total of 752 observation points. In all 4 cases, all the other parameters are known and fixed except permeability which is the only parameter to be matched. For the three heterogeneous cases (**Figs. 3.2-3.4**), I started the regression with a uniform permeability field of

$k = 0.2$ md. In the homogeneous case, 0.25 md was used as the initial uniform permeability since the actual permeability value was 0.2 md.

Table 3.1 – Description of four synthetic cases

Case	Average permeability, md	Standard deviation of permeability, md	Coefficient of variation of permeability
1	0.2	0	0
2	0.2	0.06	0.33
3	0.2	0.14	0.70
4	0.2	0.24	1.25

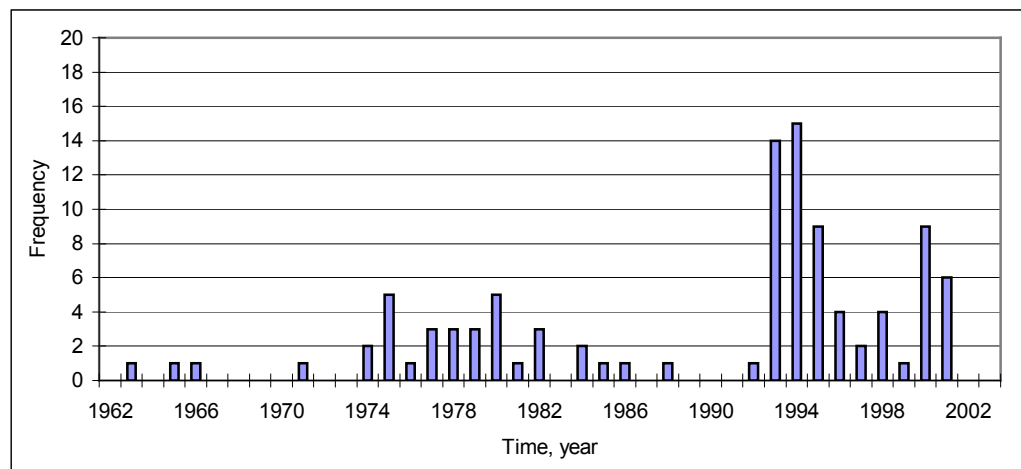


Fig. 3.1 - Date of first production for 100 wells

Table 3.2 – The parameters used in the four synthetic cases

Number of wells	100
Porosity (%)	12
Initial reservoir pressure (psia)	1100
Flowing bottom hole pressure (psia)	250
Well skin factor	-3
Well bore radius (ft)	0.3
Water saturation (%)	40

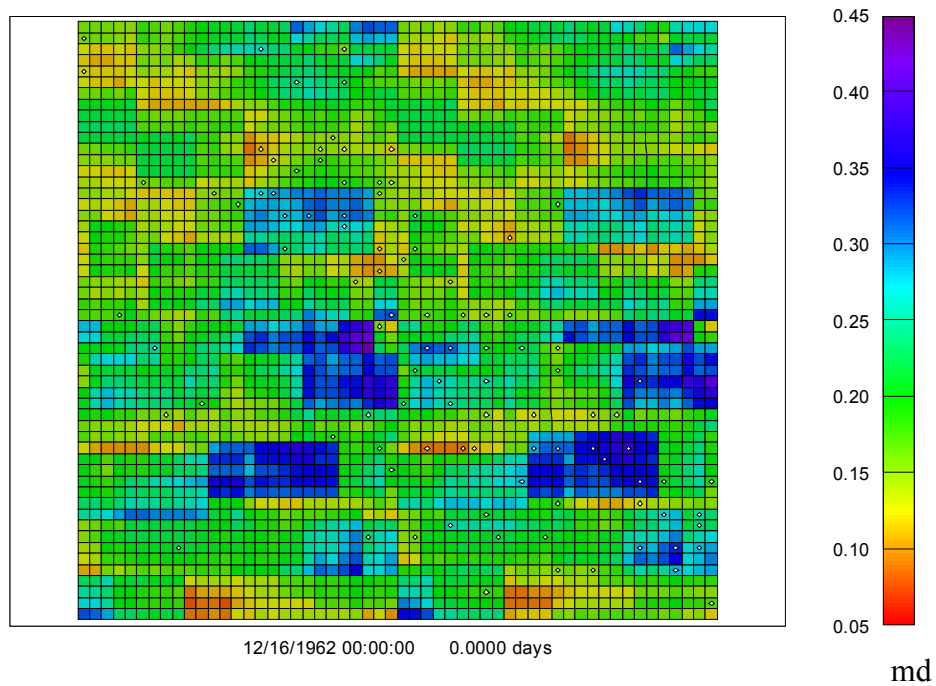


Fig. 3.2 - Actual permeability distribution for Case 2

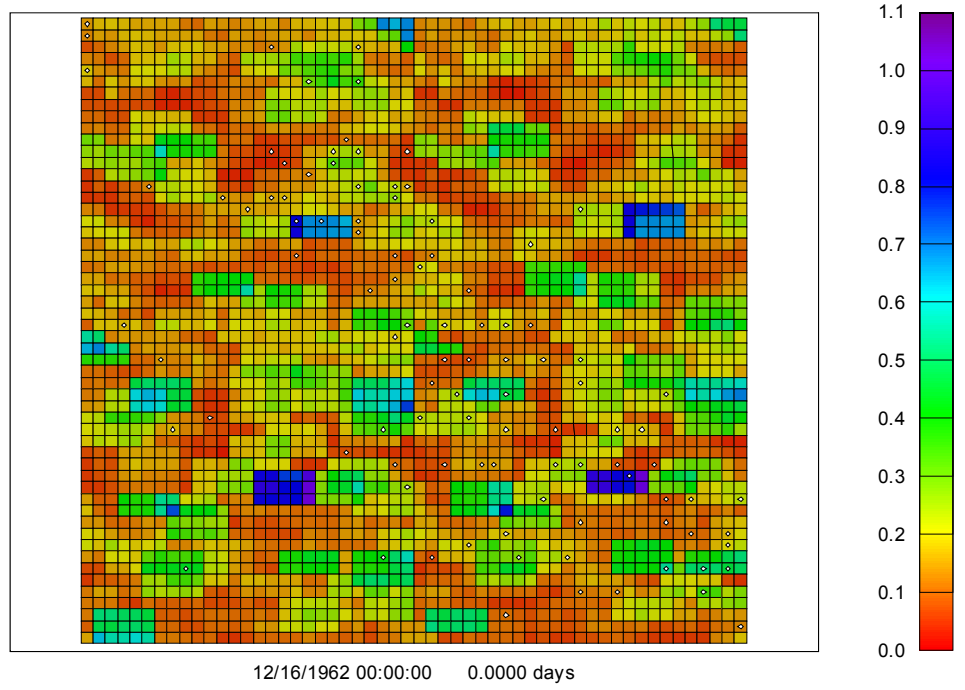


Fig. 3.3 - Actual permeability distribution for Case 3

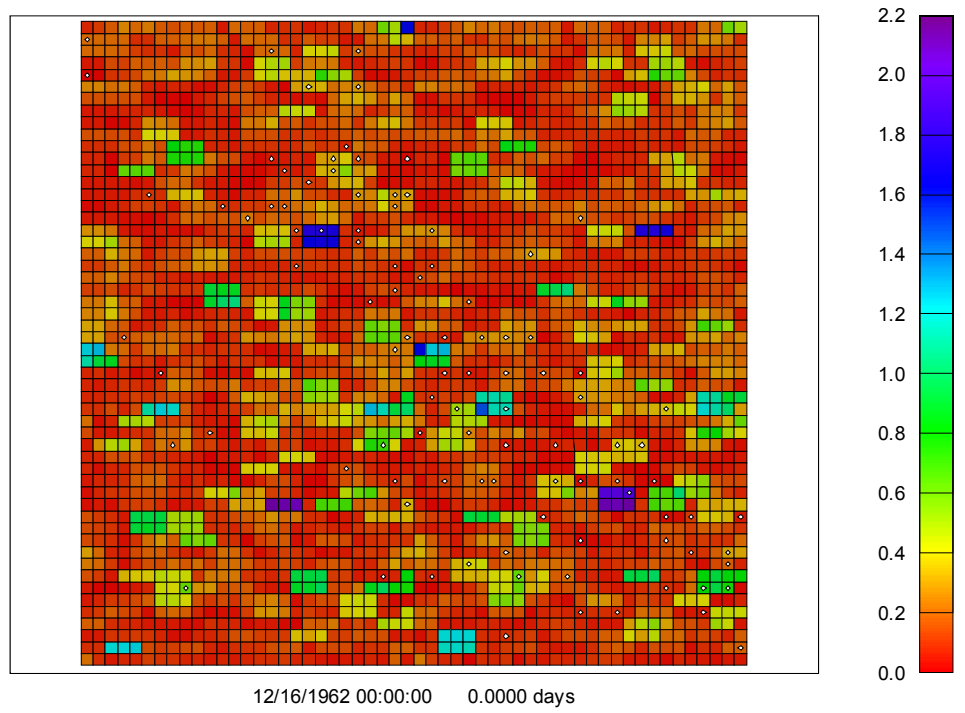


Fig. 3.4 - Actual permeability distribution for Case 4

3.2 Comparison with moving window method

3.2.1 Inversion results

History matching. I got good history matching results for all the four synthetic cases. Here I only show one of them, Case 2 which represents the quality of history match results of the other three cases. **Figs. 3.5-3.6** show fieldwide history match results for Case 2, while **Figs. 3.7-3.10** show two of the best and two of the worst individual well history matches for the same case. Apparently both field cumulative production and production rate were matched well. The matches for Well 61(Fig. 3.9) and Well 94(Fig. 3.10) are not as good as most of the other wells. I believe, it is because Well 61 is located in the upper left corner of the reservoir near two boundaries of the reservoir model. Well 94 was drilled late, so I have few observation points used in the regression. However, even though the matches for Well 61 and Well 94 are not as satisfying as most of the other wells, overall the match can still be considered to be very good.

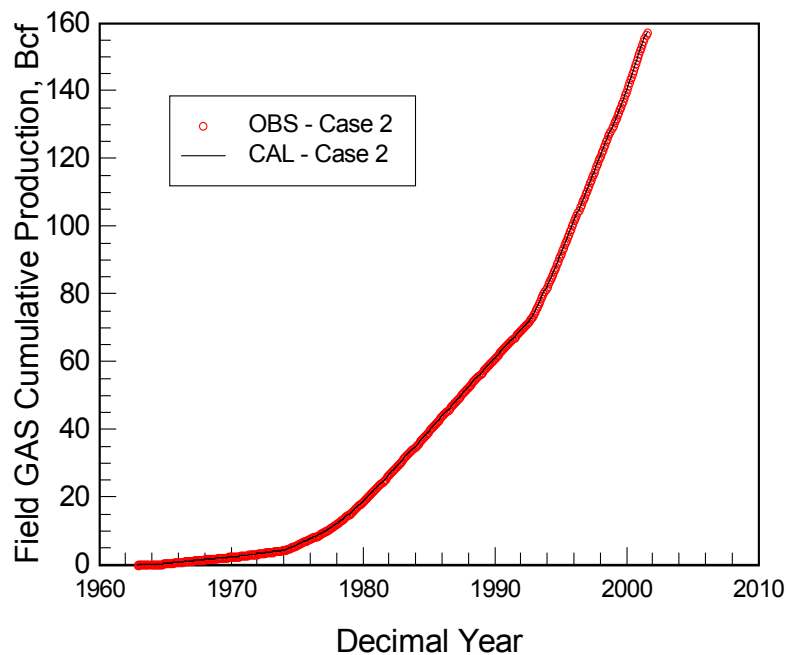


Fig. 3.5 - Field cumulative production history match for Case 2

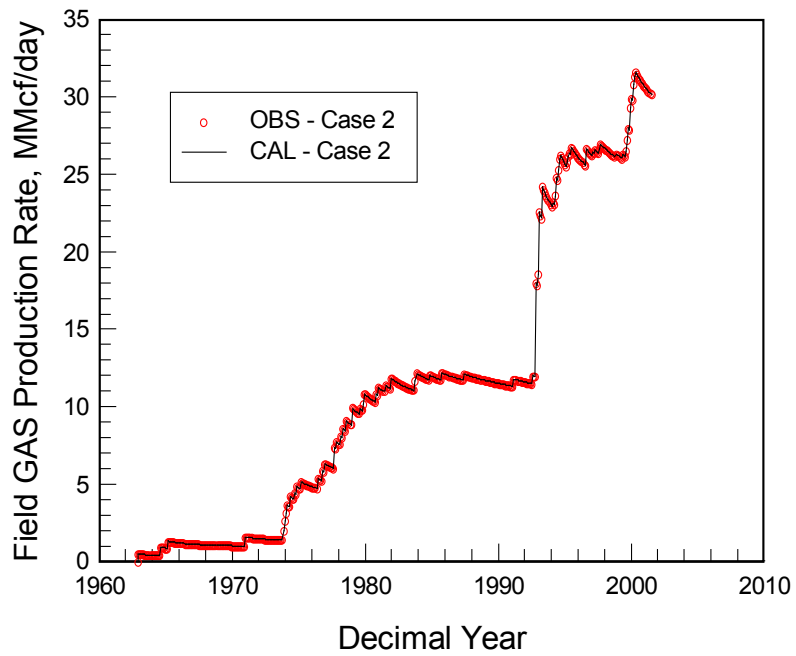


Fig. 3.6 - Field production rate history match for Case 2

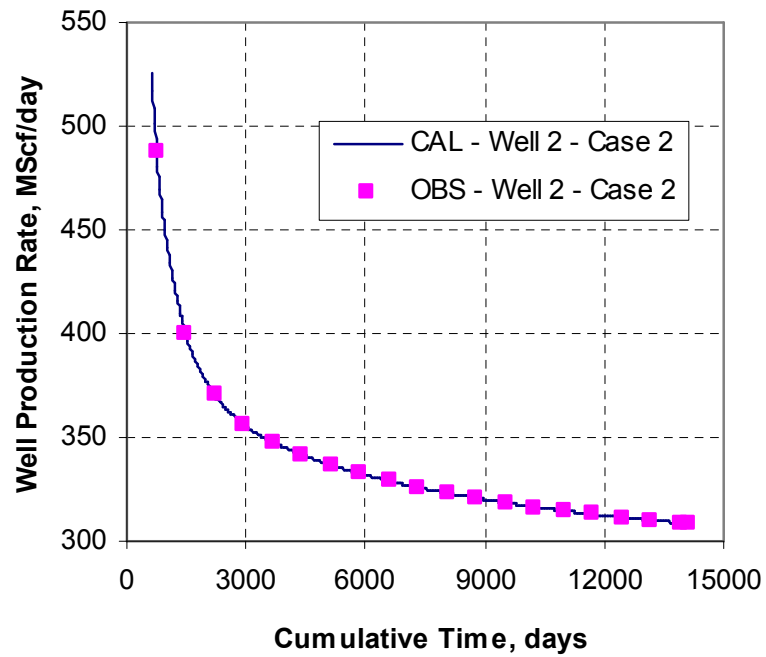


Fig. 3.7 - History match of Well 2 for Case 2

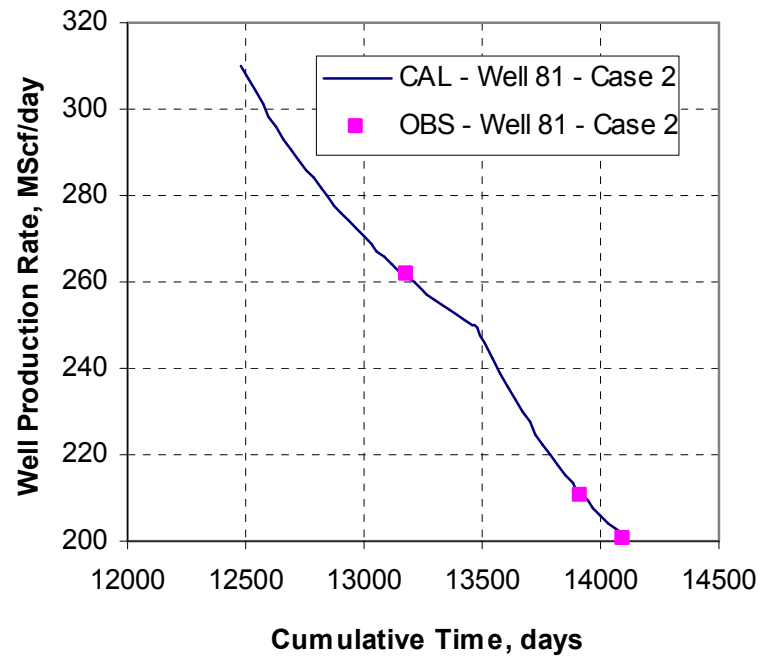


Fig. 3.8 - History match of Well 81 for Case 2

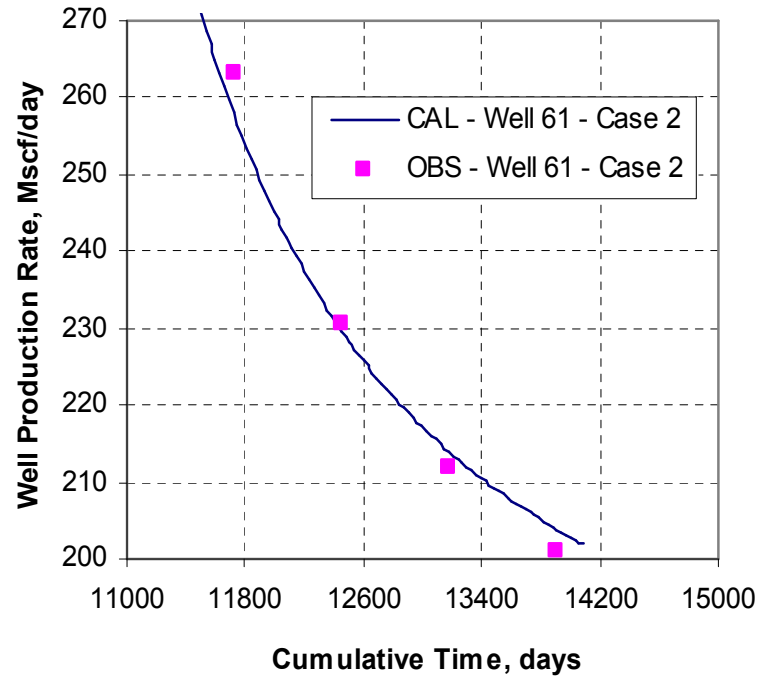


Fig. 3.9 - History match of Well 61 for Case 2

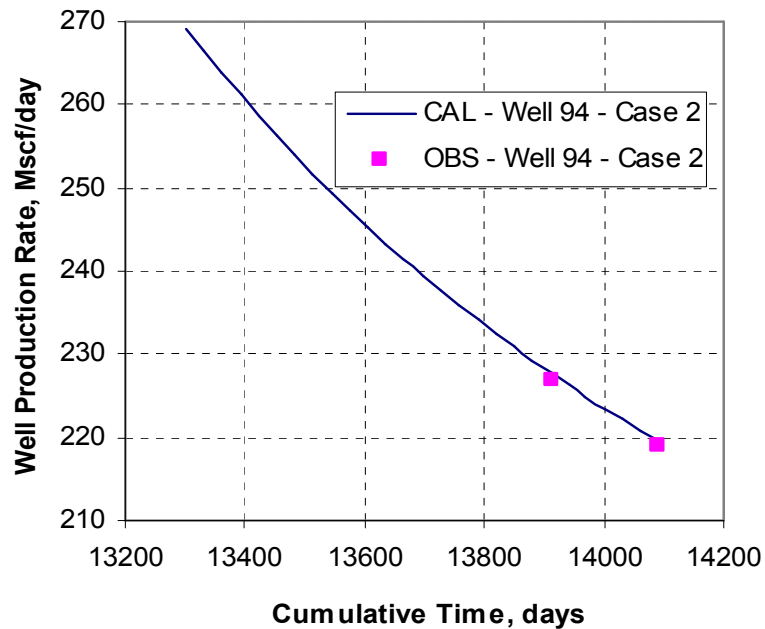


Fig. 3.10 - History match of Well 94 for Case 2

Objective function. In the four synthetic cases, convergence was achieved in 10 iterations or less with most of the decline occurring in the first 3-4 iterations (**Fig. 3.11**). As I mentioned in Chapter II (page 16), the iteration is terminated when the convergence is achieved. In these four synthetic cases, I terminated each iteration process when the objective function of each of them has not been decreased significantly in several successive iterations. Objective function decline ratio (**Table 3.3**) is the ratio of the objective function between the first and the last iteration. I use it to quantify how much the objective function decreases when the convergence occurs. Table 3.3 shows that the objective function decline ratio decreases from 148.11 to 11.71 with the increase of heterogeneity. Thus, the objective function from the cases of less heterogeneous reservoirs decreases with larger magnitude. Table 3.3 also lists smoothing and damping factors used in the four cases. Since I had no prior information, I used a smaller value for the damping

factor and started with a uniform permeability value. This is a good test for the robustness of the algorithm.

Table 3.3 – Regression results for the four synthetic cases

Case	Damping factor	Smoothing factor	No. of iterations	Objective function decline ratio	Permeability misfit, md	Normalized permeability misfit
Case 1	10	10000	10	148.11	0.0437	0.2185
Case 2	100	10000	5	34.78	0.0571	0.2855
Case 3	1000	10000	7	32.76	0.1349	0.6745
Case 4	10	50000	5	11.71	0.2247	1.1235

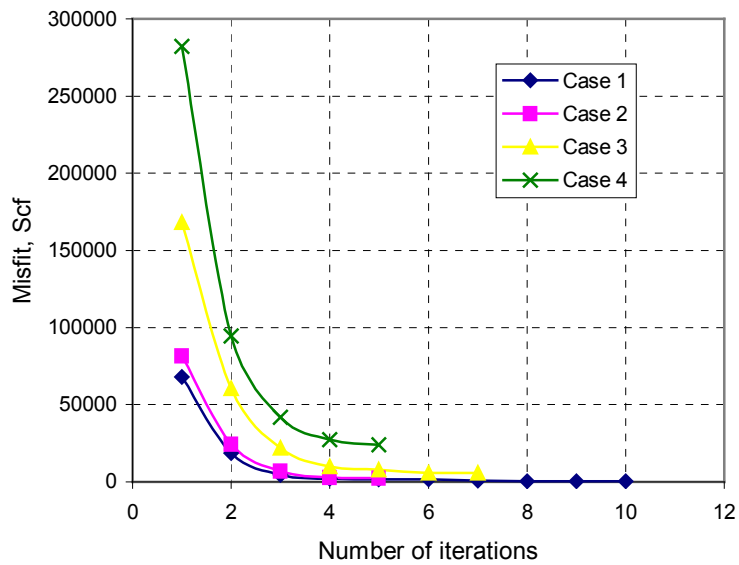


Fig. 3.11 - Objective functions for the four synthetic cases

Estimated permeability field. Figs. 3.12 - 3.15 show the actual and estimated permeability distributions for Cases 1-4, respectively. Note that a significant portion of the reservoir area is

not developed with wells. Since well responses are sensitive only to permeabilities in their vicinities, permeability distribution in the areas with wells agrees closely with the actual values. In the areas undeveloped with wells, however, there is not much difference between the estimated permeability and initial input values. Table 3.3 lists permeability misfit for the four cases. Permeability misfit, the deviation of the estimated permeability field from the actual values, is defined as:

$$\text{permeability misfit} = \sqrt{\frac{\sum_{i=1}^M (k_{est,i} - k_{act,i})^2}{M}} \quad \dots\dots\dots (3.1)$$

where, $k_{est,i}$ and $k_{act,i}$ denote the estimated and actual permeability values for grid block i , and M is the total number of grid blocks. To make it easy to compare, I also listed normalized permeability misfit, which is the permeability misfit divided by average permeability, 0.2 md, in each case. Table 3.3 shows that with increase in heterogeneity (increasing case number) normalized permeability misfit increases. This means the accuracy of estimated permeability field decreases with increase of reservoir heterogeneity.

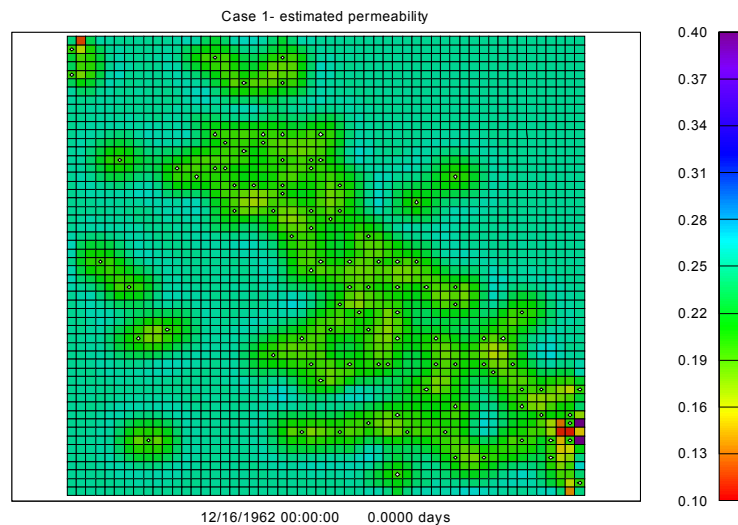


Fig. 3.12 - Estimated permeability distribution for Case 1

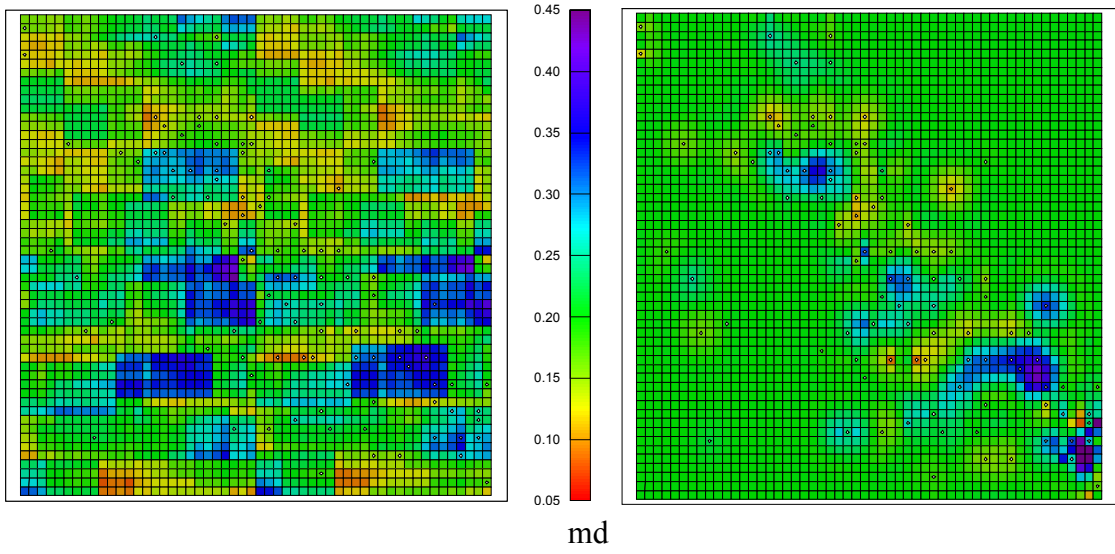


Fig. 3.13 - Actual and estimated permeability distribution for Case 2

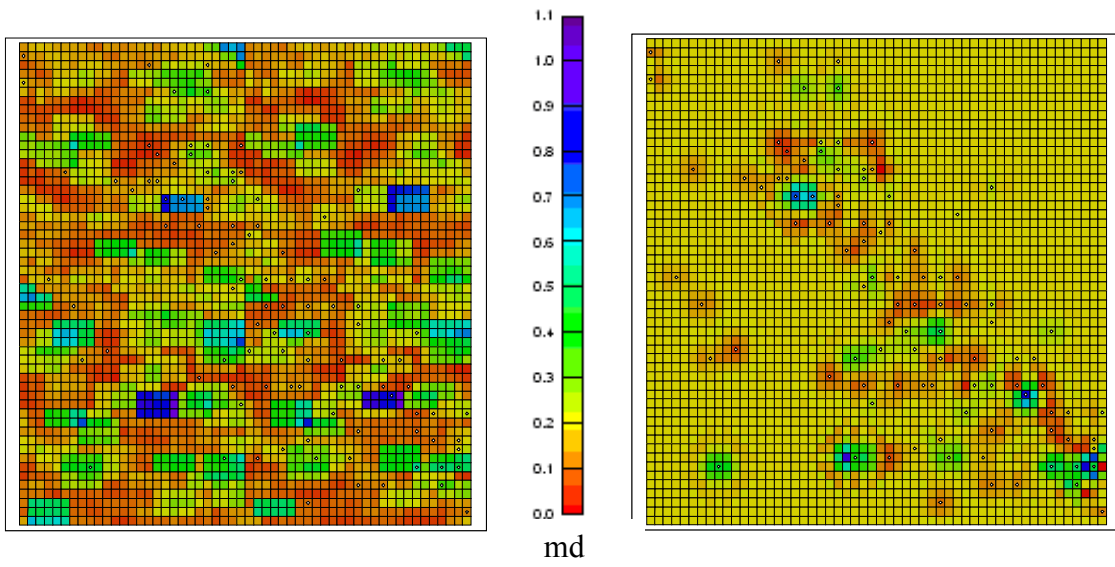
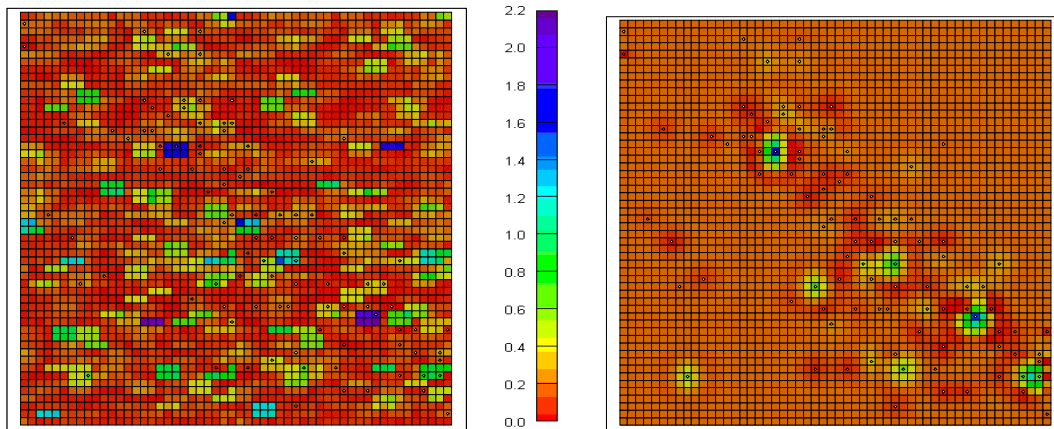


Fig. 3.14 - Actual and estimated permeability distribution for Case3



md

Fig. 3.15 - Actual and estimated permeability distribution for Case 4

The effect of smoothness factor on regression accuracy. Smoothness factor plays an important part in the regression. I use Case 2 to investigate how smoothness factor affect permeability misfit and objective function.

I did regression on Case 2 by giving 4 different smoothness factors, 0, 100, 1000 and 10000 respectively. **Fig. 3.12** shows both permeability misfit and objective function decrease with the increase of smoothness factor. This means the accuracy of regression increases with the increase of smoothness factors.

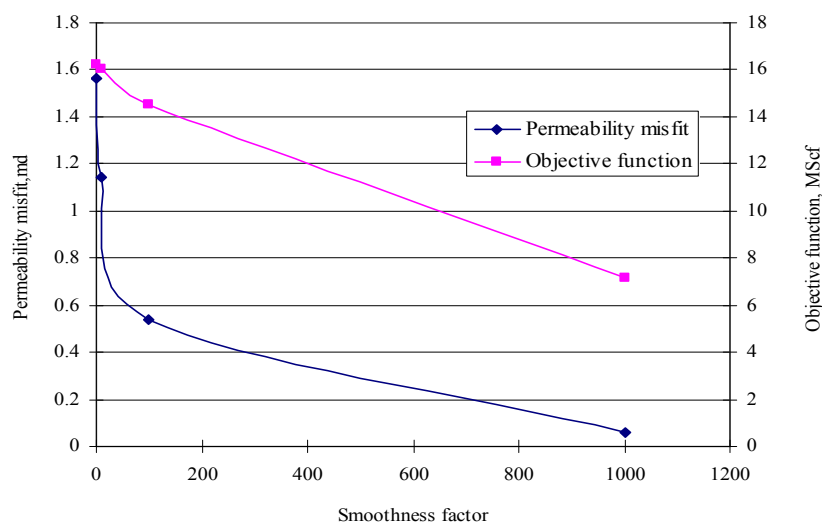
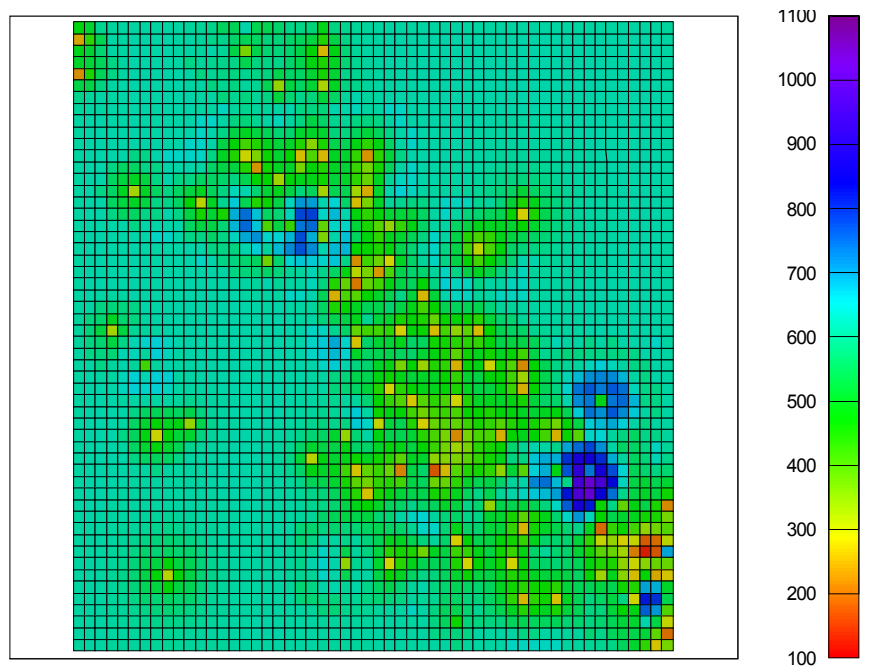


Fig.3.16 - The effect of smoothness factor on permeability misfit and objective function

3.2.2 Calculation of infill potential

Using the estimated permeability distributions and forward model, I calculated infill potential for each case. **Fig. 3.17** shows calculated infill potential for Case 2. It is the incremental fieldwide production gained by an infill in each grid block. The unit for infill potential is thousand cubic meters. The infill potentials shown include the effects of reservoir quality (permeability), depletion (pressure), and proximity to existing wells. The color in this map represents the magnitude of infill potentials. In the areas with blue color shown in Fig. 3.16, there are higher infill potentials due to the high permeability distribution indicated in Fig. 3.13 and the less depletion shown in Fig. 3.18. So these areas are the better candidates for infill drilling. While, in those areas with yellow or red color, the reservoir has been depleted very much and also has a low permeability distribution. Thus, infill drilling may not be very optimistic in these areas.



MM3

Fig. 3.17 - Infill potential map for Case 2

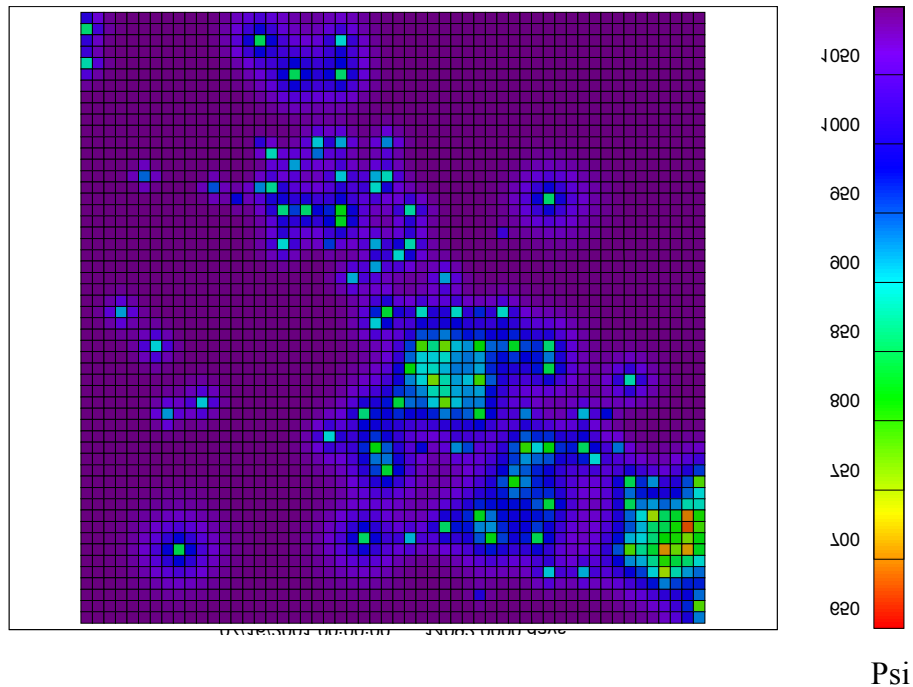


Fig. 3.18 – Pressure map for Case 2

3.2.3 Comparison with moving window method

In this section, we compare infill potential calculated using the inverse method to results calculated using the moving window method described in Guan *et al.*¹⁰ When I calculated infill potentials in all 4 synthetic cases using the simulation-based method, I made the predictions for 1 year. In the moving window method, performance of existing wells is characterized using the best year, BY, production indicator. BY is defined as the best 12 conservative months of production divided by 12, and has been demonstrated to be a reasonable proxy for estimated ultimate recovery (EUR).⁷ I term the additional fieldwide production to be gained by an infill well offsetting each existing well BY_{inf} .

The moving window technique estimates infill well performance on a well basis; *i.e.*, it calculates the additional production to be gained by a new infill well offsetting each existing

well. The simulation method estimates infill well performance on a cell basis. Thus, it was necessary to convert the simulation-based results from a cell basis to a well basis in order to compare the simulation results to those from the moving window technique. I first determined, for each well, the region consisting of all simulation cells closer to that well than to any other well, *i.e.*, the gridded Voronoi region (**Fig. 3.19**). For unbounded wells, I limited the radius of the region to a value consistent with the maximum search radius used in the moving window analysis, 3000 acres. I next calculated infill potential for a new well offsetting each existing well by averaging the individual cell values within the region for each existing well. I calculated infill potential from simulated results using both the calculated and actual permeability fields. The true infill potential determined using the actual permeability field provided the basis for determining the relative accuracies of the moving window and simulation-based inverse methods, and we named it as simulation method in the following comparison. The simulation software used for calculating the infill potential is SABRE and Simulation Manager from Schlumberger.

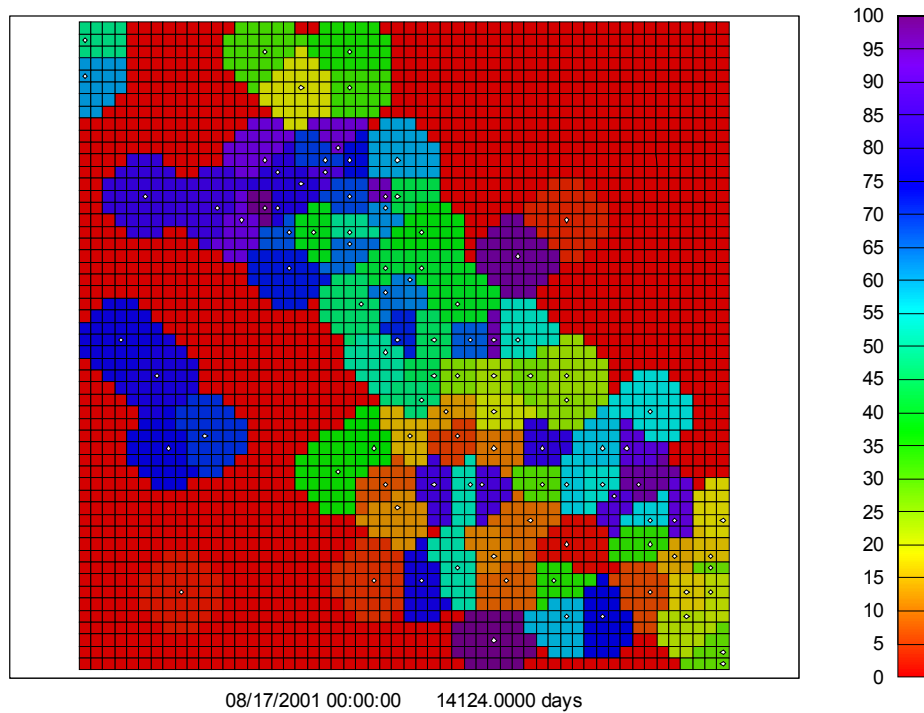


Fig. 3.19 - Simulation well regions

In the above, I used Case 2 as example case in the discussion of history matching results. Here, I present first the results of inverse and moving window method for Case 2. **Figs. 3.20 and 3.21** compare the inverse and moving window method by comparing the results of each to the true results determined using the actual permeability distribution. In each plot in Fig. 3.20 and 3.21, the true infill potential is on the y-axis, while the infill potential from either the inverse or moving window method is on the x-axis. The five lines in each plot show the extent of deviation of estimated BY_{inf} for the particular method from the true values. These figures are used to demonstrate the accuracy of inverse and moving window method clearly. If the estimated BY_{inf} are accurate, the estimated values in these figures should fall on the unit-slope line. The more scattered the estimated points in these figures, the less accurate is the estimated BY_{inf} from this particular method. In Figs. 3.20 and 3.21, I notice that most points are between the lines of +/-

30% for the inverse method, but a lot of values from the moving window method are beyond these two lines, and some are even outside the -50% line. In addition, more data points of estimated BY_{inf} from the inverse method fall on the unit-slope line compared with the moving window method.

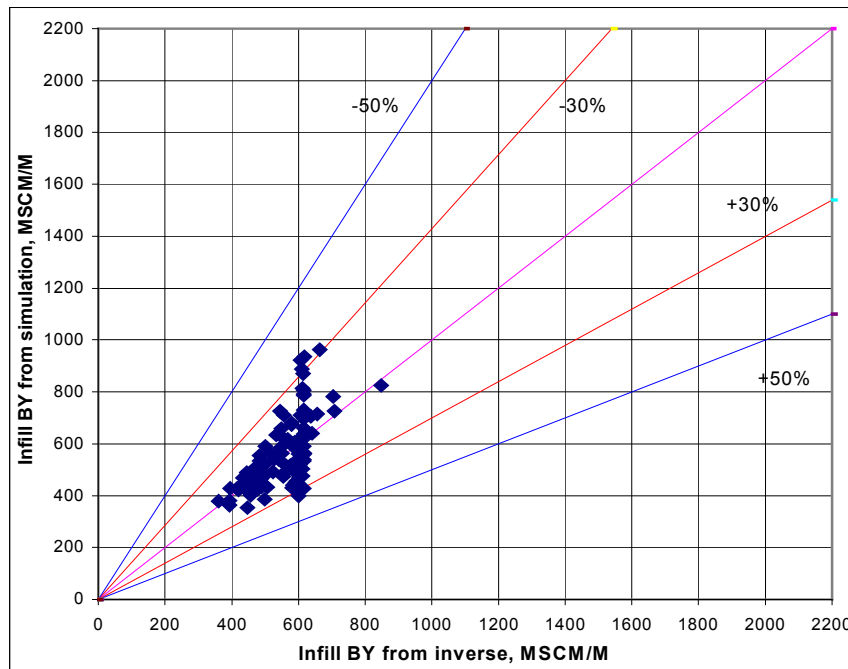


Fig. 3.20 - Infill BY from simulation and inverse method for Case 2

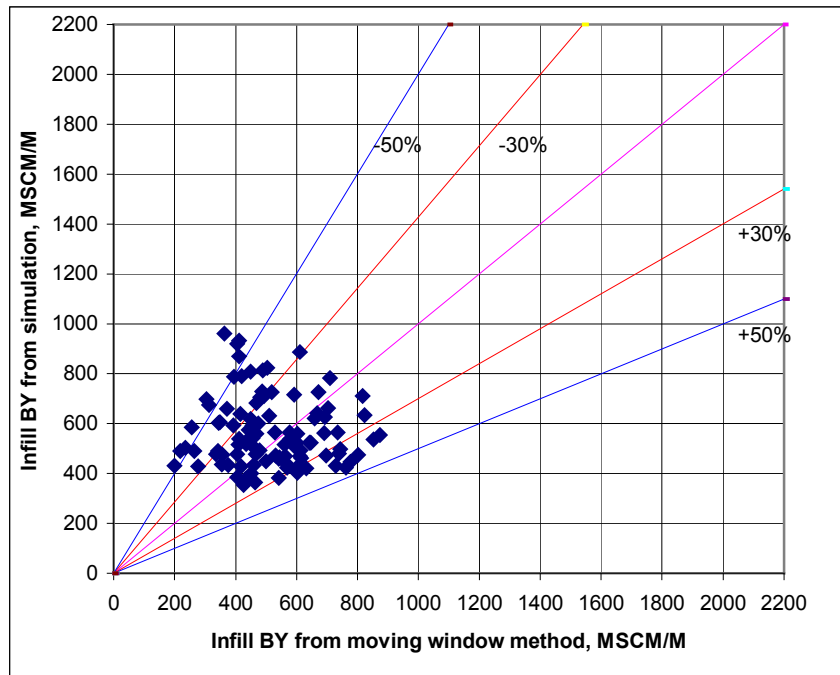


Fig. 3.21 - Infill BY from simulation and moving window method for Case 2

The comparison is also summarized in Table 3.4, which uses relative error and average percent error (APE) to quantify the overall and individual well accuracy of the inverse and moving window methods. Relative error is the error in fieldwide average BY_{inf} between each method and the true value (labeled as “Simulation” in Table 3.4). It is defined as:

$$relative\ error = \frac{average\ estimated\ BY_{inf} - average\ true\ BY_{inf}}{average\ true\ BY_{inf}} \times 100 \quad \dots\dots\dots (3.2)$$

For Case 2, both the inverse and moving window method underestimate average BY_{inf} . However, the relative error for the inverse method (-2.1%) is much less than that for the moving window method (-8.3%). Average percent error (APE) quantifies the error in the individual-well values, and is another way of evaluating the accuracy of the calculation methods. APE (average percent error) is the average of all the individual well percent errors. It is defined as:

$$\text{percent error of well } i = \left| \frac{(\text{estimated } BY_{\text{inf}} - \text{true } BY_{\text{inf}})_i}{(\text{true } BY_{\text{inf}})_i} \times 100 \right| \quad \dots\dots\dots (3.3)$$

$$APE = \frac{\sum_{i=1}^{N_w} (\text{percent error})_i}{N_w} \quad \dots\dots\dots (3.4)$$

where i is well number and N_w is the number of wells.

APE is the average deviation from the unit-slope line in Figs. 3.20 and 3.21, and increases as the scatter about the unit-slope line increases. The APE for the inversion method is 12.6%, compared to 31.7% for the moving window method. The inverse method is clearly more accurate than the moving window method for Case 2.

Table 3.4 also compares the standard deviations of inverse, moving window and true BY_{inf} . The variability in BY_{inf} from the moving window method is too high; however, the variability in BY_{inf} from the inverse method is significantly less than actual. This results primarily from the uniform starting permeability value used in the regression and the norm constraint, which dampens change from the starting values when there is not enough response for the data misfit term to dominate.

Thus, for Case 2, based on the comparison of the individual and average predicted infill well performance from the inverse and moving window methods, the inverse method is considered more accurate than the moving window method.

Table 3.4 Comparison of the inverse and moving window method

Case	Average BY_{inf} , MSCM/M			Relative error of Average BY_{inf} , %		Average percent error, %		Standard deviation of BY_{inf} , MSCM/M		
	Simulation	Moving window	Inverse	Moving window	Inverse	Moving window	Inverse	Simulation	Moving window	Inverse
Case 1	542.67	513.08	530.87	-5.45	-2.17	16.51	6.97	70.38	40.5	89.92
Case 2	564.28	517.09	551.66	-8.33	-2.15	31.70	12.61	137.64	149.52	79.68
Case 3	517.24	458.51	531.17	-11.35	2.69	38.57	24.20	195.01	188.49	90.00
Case 4	520.78	532.54	530.90	2.3	1.9	56.13	33.80	259.19	350.92	102.45

Case 1 is the homogeneous case. **Figs. 3.22** and **3.23** show that the estimated infill potentials from the inverse method are much closer to the true BY_{inf} than the moving window method, since most BY_{inf} values from the inverse method are along the unit-slope line, while, for the moving window method, the estimated BY_{inf} is more deviated between the +/-30% lines. Table 3.4 shows the relative error for the inverse method (-2.17%) is less than that for the moving window method (-5.45%). The APE for the inverse method is 6.97%, less than 16.51% for the moving window method. Thus in this homogenous case, the inverse method predicts infill performance better than the moving window method.

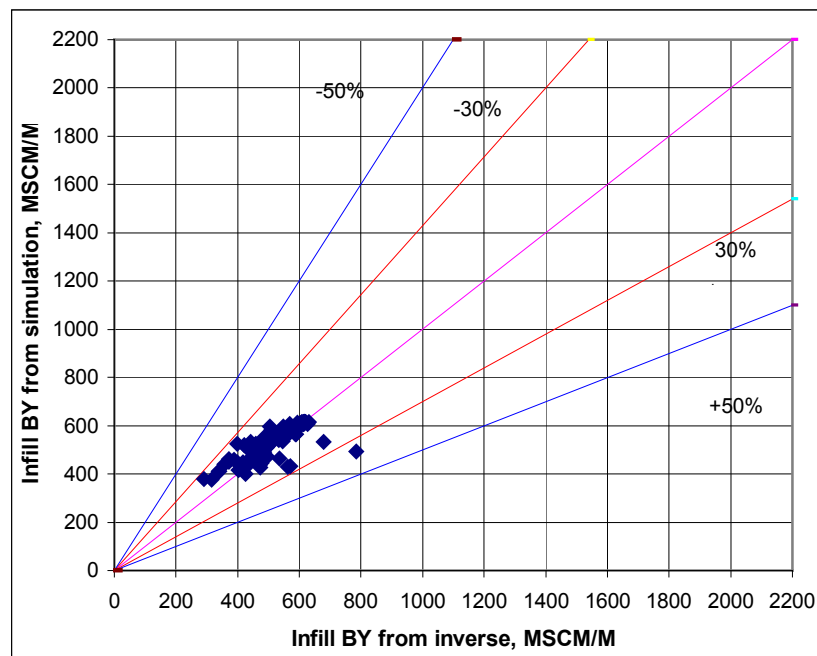


Fig. 3.22 - Infill BY from simulation and inverse method for Case 1

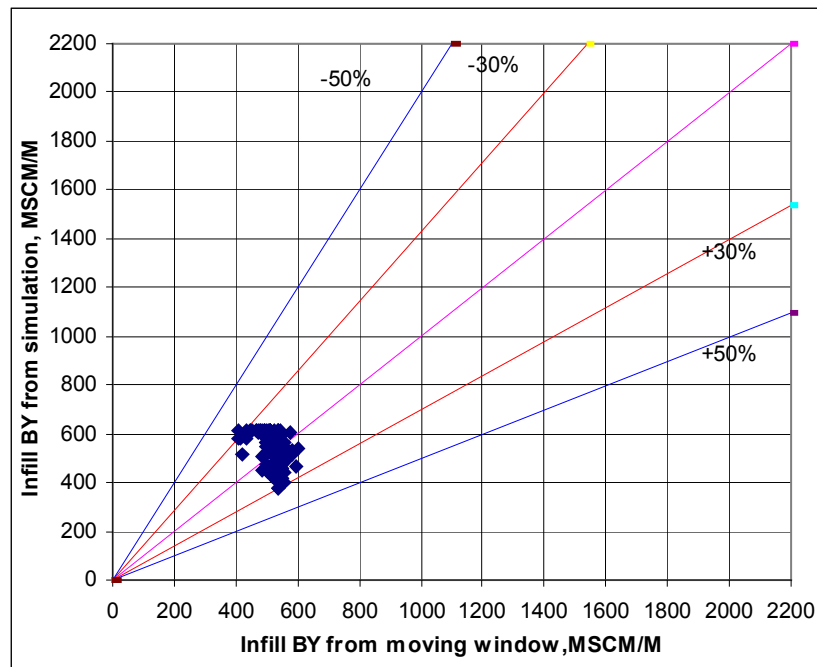


Fig. 3.23 - Infill BY from simulation and moving window method for Case 1

Case 3 and Case 4 are more heterogeneous cases compared with Case 2. **Figs. 3.24 - 3.27** show that compared with the moving window method, there are a lot fewer data points outside the $\pm 50\%$ lines for the inverse method. The relative error in Table 3.4 also indicates that the average BY_{inf} from the inverse method is much closer to the “true” average predicted BY_{inf} than the moving window method for both Case 3 and Case 4. Therefore, the inverse method outperforms the moving window method in all four synthetic cases. However, the prediction accuracy of infill performance decreases with the increase of reservoir heterogeneity as well. It is shown in Table 3.4 that the APE goes up from Case 1 to Case 4 for both the inverse and moving window method. However, the APE from the inverse method only increases from 6.97% to 33.80%, but for the moving window method, it increases from 16.51% to 56.13%.

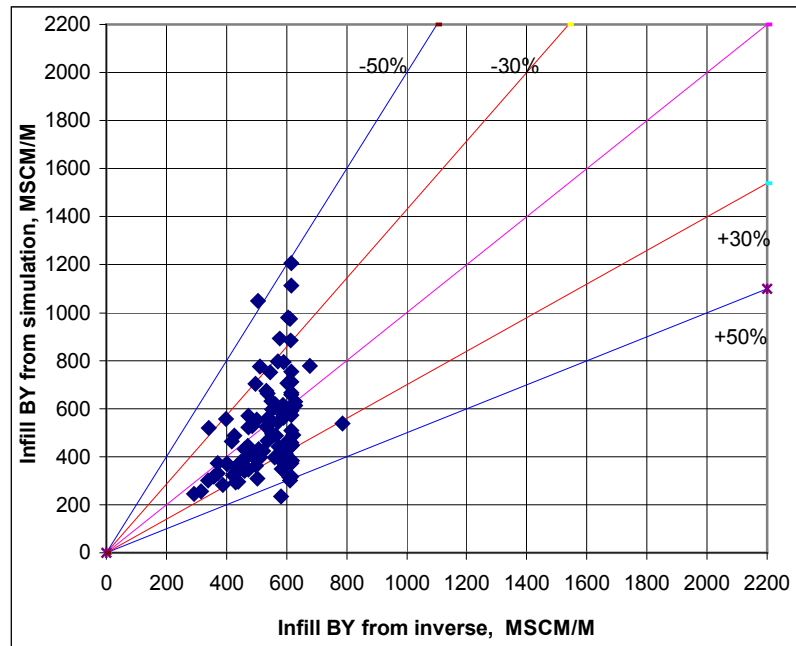


Fig. 3.24 - Infill BY from simulation and inverse method for Case 3

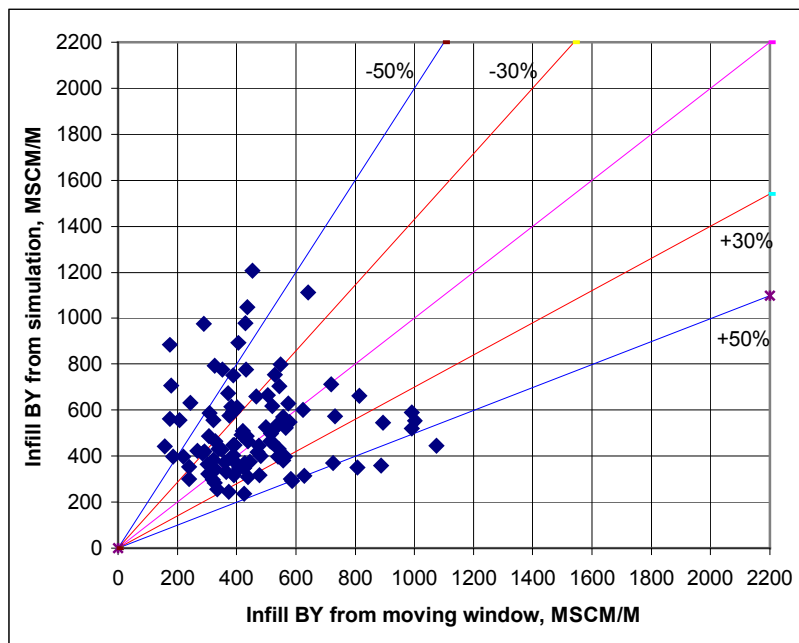


Fig. 3.25 - Infill BY from simulation and moving window method for Case 3

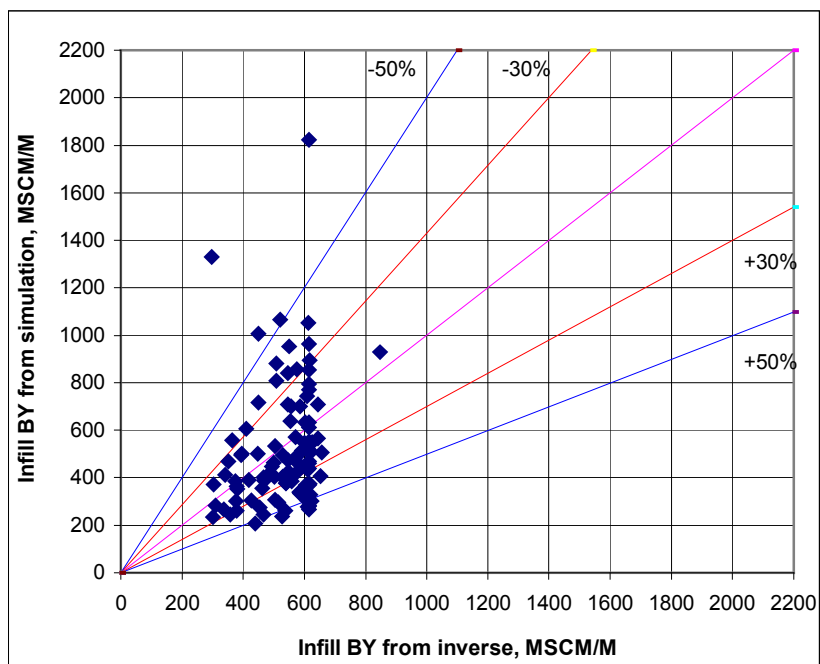


Fig. 3.26 - Infill BY from simulation and inverse method for Case 4

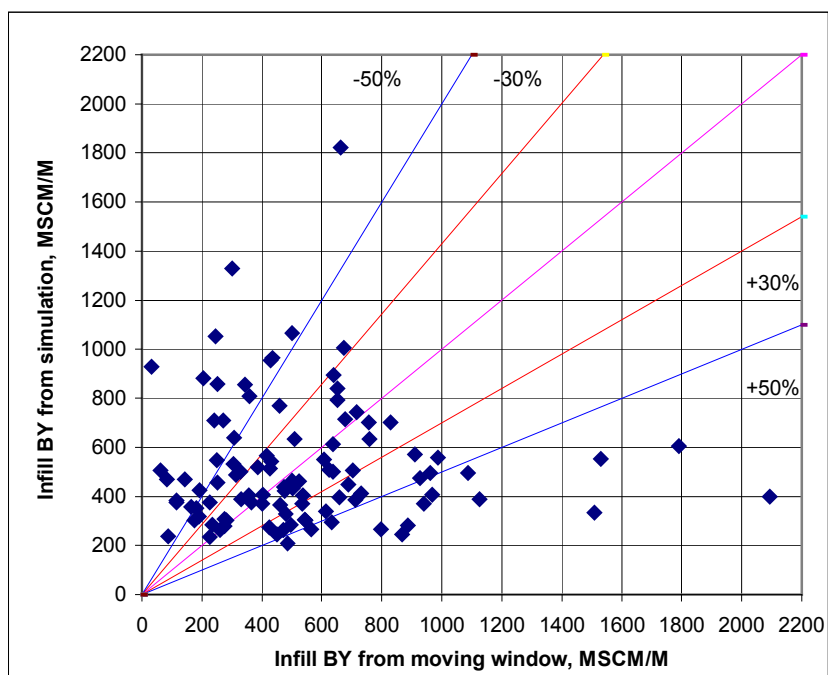


Fig. 3.27 - Infill BY from simulation and moving window method for Case 4

Based on the above comparisons, I conclude that the inverse method is more accurate than the moving window method for both average BY_{inf} and individual well BY_{inf} for all the 4 synthetic cases. However, as with the moving window method, accuracy of the inverse method decreases with increasing heterogeneity, particularly for individual well predictions. The method appears to predict infill potential of a group of wells accurately. The inverse method requires about the same data preparation and computation times as the moving window method. Thus, the simulation inversion approach appears to be superior to the moving window method for rapid assessment of infill potential. It can be very useful in targeting areas for infill development or in scoping studies that precede more detailed evaluations. Another advantage of the inverse method is that, being simulation based, it is easier to transition from scoping analyses to more detailed analyses by simply refining the reservoir description to include additional data and interpretations, which is an important improvement over the moving window method.

3.3 Comparison of inverse method with SimOpt for Case 2

3.3.1 Introduction

SimOpt²⁵ is a computer program included with Eclipse which can aid a history matching of observed reservoir data with Eclipse 100/300 simulation models. In this chapter I compare the accuracy, efficiency and speed of the inverse method with Eclipse/Simopt based on one of the synthetic cases used above, Case 2.

3.3.2 Technical description of SimOpt

SimOpt uses mathematical optimization techniques to vary specified reservoir parameters, such as permeability and pore volume, to minimize the difference between observed and simulated

production data. It can also take into account prior geological information, when available, in the regression.

The objective function, f , that is minimized in SimOpt is a modified form of the commonly used simple sum-of-the-squares.

$$f = \gamma \cdot f_{prior} + \frac{\alpha}{2} r^T r \quad \dots\dots\dots (3.5)$$

Where

α, γ - the overall weights for production and prior terms respectively.

f_{prior} - the objective function prior term, which accounts for prior knowledge of the statistical distribution of parameter modifier values.

r - the weighted production difference between an observed and a simulated response, which is defined as

$$r_i = w_d w_i \frac{(o_i - c_i)}{\sigma_d} \quad \dots\dots\dots (3.6)$$

where

d - one set of observed data of a given type at a given well

i - an individual data point for the d 'th item of observed data

o_i, c_i - the observed and calculated values, respectively

σ_d - the measurement error for the d 'th data set

w_d - an overall weighting for the d 'th production data set

w_i - a weighting for the i 'th production data point

The algorithm that SimOpt uses to minimize the objective function is Levenberg-Marquardt, which is a combination of the Newton method and a steepest descent scheme.

Denoting the vector of current parameter normalized modifier values as v^k , then the algorithm estimates the change, dv^k , required to minimize the objective function as

$$dv^k = (H + \mu I)^{-1} \nabla f(v^k) \quad \dots\dots\dots (3.7)$$

where the Hessian matrix, H , is the matrix of second derivatives of f and I is the identity matrix. The parameter μ is free and is varied so that, away from the solution where the quadratic Newton model may have less validity, it takes large values and biases the step towards the steepest descent direction. While near the solution, it takes small values to make the best possible use of the fast quadratic convergence rate of the Newton step.

In solving Eq. 3.7, SimOpt requires the first and second derivatives of the objective function (Eq. 3.5) with respect to the normalized parameter modifiers. The first derivatives are the components of the gradient vector of the objective function,

$$[\nabla f(v)]_j = \gamma \cdot \nabla f_{prior} + \alpha r^T (\nabla r) \quad \dots\dots\dots (3.8)$$

The second derivatives are the components of the Hessian matrix of the objective function

$$[H]_{jk} = \nabla^2 f = \gamma \cdot \nabla^2 f_{prior} + \alpha \{ (\nabla r)^T (\nabla r) + r^T \nabla^2 r \} \quad \dots\dots\dots (3.9)$$

It is common to ignore the term involving second derivatives of the simulated value in Eq. 3.9; this is the Gauss-Newton approximation. A justification for this is that it is frequently small in comparison to the first term. Also, it is premultiplied by a residual term, which is small near the solution, although the approximation is used even when it is far from the solution. Thus, the second term in Eq. 3.9 can be solved with first derivatives of the simulated quantity with respect to the parameters. These derivatives are obtained from the run of Eclipse 100 at the same time as the simulated quantities themselves, and in just one run.

SimOpt expresses the overall measure of the history match as a Root Mean Square (RMS) index formed from the regression objective function:

$$RMS = \sqrt{\frac{2f}{m_{obs}}} \quad \dots\dots\dots (3.10)$$

where m_{obs} is the total number of observations over which the index is formed, and f is the objective function. This RMS index provides a normalized value of the deviation between simulated and observed data.

3.3.3 Comparison of inverse method and SimOpt by synthetic case

One synthetic case, Case 2, is used to compare the accuracy and efficiency of the inverse method and SimOpt. In the inverse method, I match on reservoir properties (permeability in this case) on a cell basis. Instead of matching on individual cell values of reservoir properties (permeability in this case), SimOpt matches on constant values of permeability within the Voronoi regions around each well. Thus, the number of regression parameters is reduced to the number of wells in SimOpt. However, SimOpt is limited in the number of regression parameters. Thus, it is not suited for the reservoirs with large number of wells, such as 1000-well case.

Figs. 3.28 and 3.29 show the decreasing RMS by the inverse method and SimOpt. For both these two methods, objective function goes down smoothly. But RMS from inverse method has more decrease in fewer iterations.

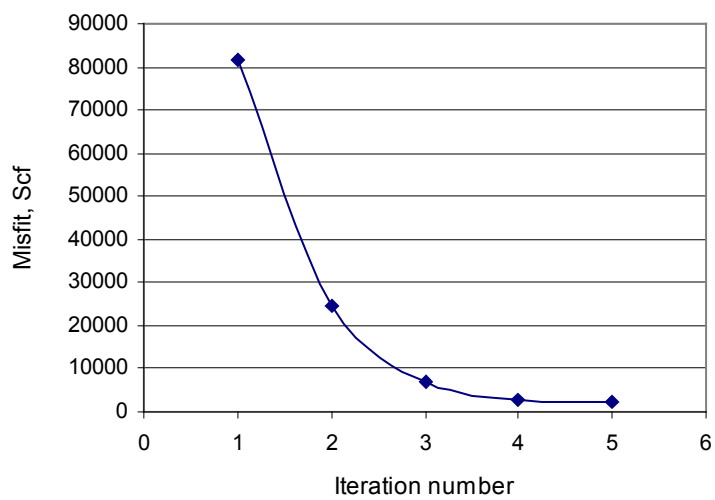


Fig. 3.28 - Objective function by inverse method

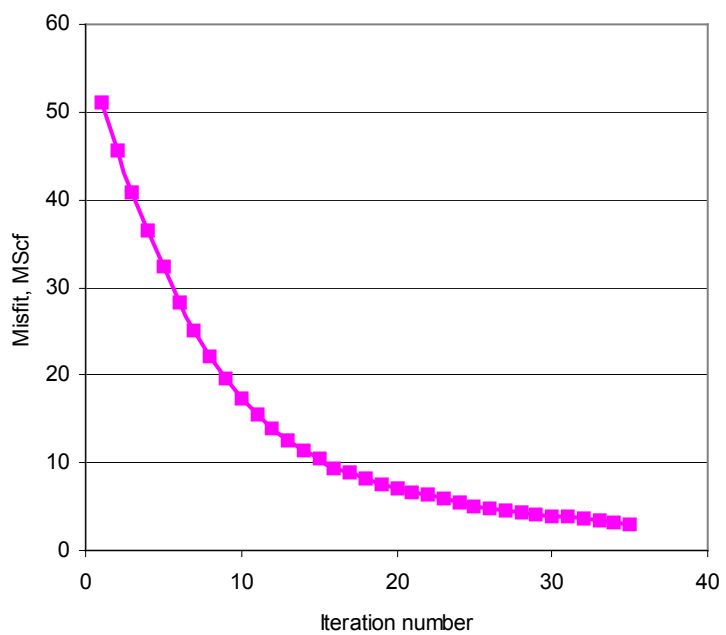


Fig. 3.29 - Objective function by SimOpt

Fig 3.30 shows history match of fieldwide production rate from SimOpt, which is as good as the match from the inverse method (Fig. 3.6). Figs. 3.30 and 3.31 show some of the best and worst well matches by SimOpt, which were selected based on the RMS index.

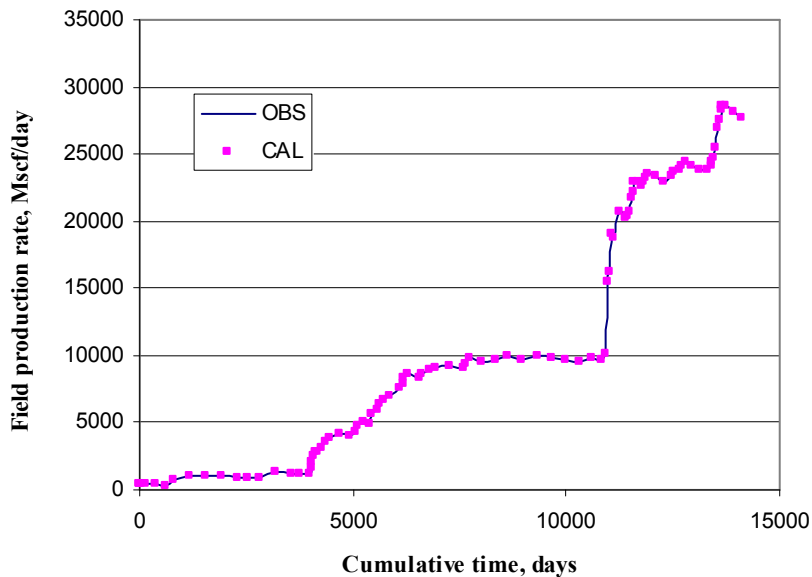


Fig. 3.30 - History match of field production rate by SimOpt

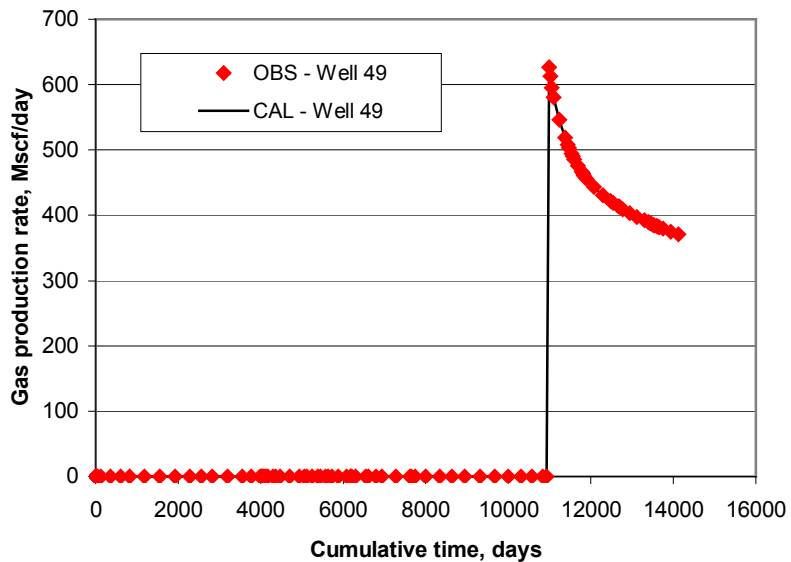


Fig. 3.31 - Good individual history match from SimOpt for Case 2 – Well 49

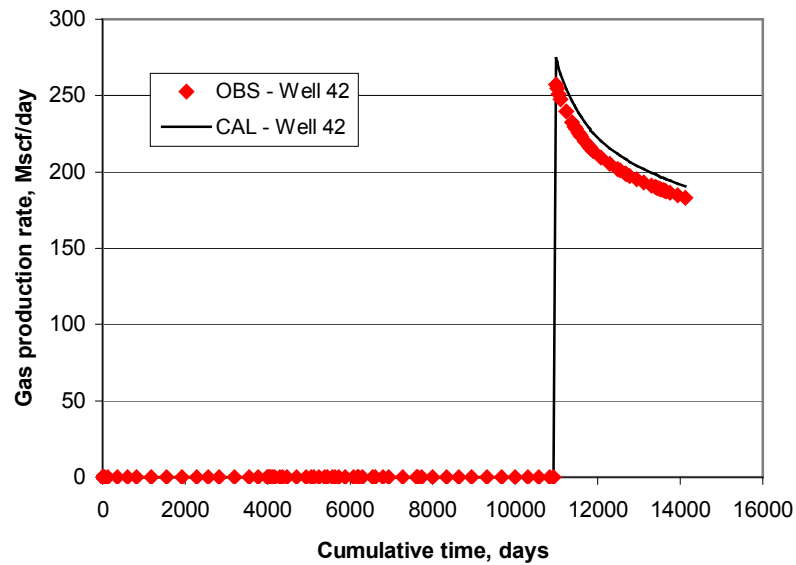


Fig. 3.32 - Bad individual history match from SimOpt for Case 2 – Well 42

Since production responses are sensitive only to permeabilities in their vicinities, both of these methods regenerate permeability distribution only in areas with producing wells. The estimated permeability distributions in **Figs. 3.14** and **3.33** do not replicate exactly the actual permeability distribution. However, the regressed permeability field resembles the heterogeneity of the known permeability field in the areas where production data and well locations are available.

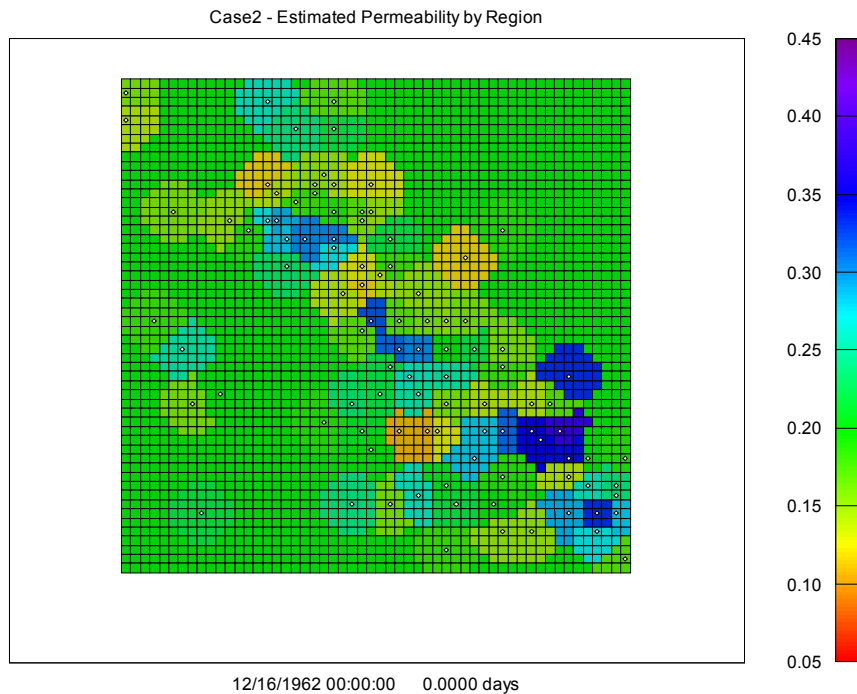


Fig.3.33 - Estimated permeability distribution for Case 2 by SimOpt

Table 3.5 compares the accuracy of the inverse method, the moving window method and SimOpt. BY_{inf} from simulation method is the true BY_{inf} using from actual permeability distribution. For Case 2, all the three methods underestimate average estimated BY_{inf} . However, the relative error from the inverse method (-2.15%) is still less than that from SimOpt (-4.10%) and the moving window method (-8.13%). **Table 3.6** summarizes the comparison of average percent error for individual wells from all three methods. The APE for the inversion method is 12.6%, compared to 12.97% for SimOpt and 31.7% from the moving window method. Therefore, SimOpt has approximately the same accuracy as the inverse method and thus, more accuracy than the moving window method. **Table 3.7** compares the computation efficiency of the inverse method and SimOpt. It takes about 3 minutes to finish one regression for the inverse method as opposed to 8 minutes for SimOpt. To have approximately the same objective function

value, the inverse method needs only 5 iterations, fewer than 35 iterations needed with SimOpt. Thus, the inverse method I proposed works more efficiently than SimOpt with approximate accuracy.

Table 3.5 - Comparison of average BY_{inf} for three methods

Case 2 BY_{inf}	Calculated from simulation method	Calculated from moving window method	Calculated from inverse method	Calculated from SimOpt
Average BY_{inf} , MSCM/M	564	517	551.65	540.86
Standard deviation, md	137.64	149.52	79.68	93.65
Relative error, %	-	-8.33	-2.15	-4.10

Table 3.6 - Comparison of average percent error of individual wells for three methods

Case 2	Calculated from moving window method	Calculated from inverse method	Calculated from SimOpt
APE, %	31.70	12.61	12.97

Table 3.7 - Comparison of computation efficiency of the inverse method and SimOpt in synthetic case

Method	Inverse method	SimOpt
CPU time for 1 iteration	3 mins 27 secs	8 mins
Iteration number needed	5	35
Total time required	18 mins	280 mins

CHAPTER IV

RESERVOIR PARAMETERS SENSITIVITY STUDY

As I discussed in Chapter II, I do not conduct a detailed reservoir characterization study in the presented inverse method, since my goal is rapid, approximate estimation of infill potential. In an initial application, I simply use whatever data are available. I initialize my reservoir model with uniform average values if the reservoir property maps are not available. For example, I assume a uniform value of the individual well skin factors for all wells if skin factor estimates are not available. I use constant pore volume in the reservoir model as well, if the porosity and thickness maps are not available. But these estimated uniform pore volume and skin factors may be far off from the actual values, and may affect the prediction accuracy of infill potential significantly. In this chapter, I made a sensitivity study to investigate and quantify the influence of the estimated uniform pore volume and skin factors on the prediction accuracy for infill drilling.

To do this, I generated a synthetic case (called base case in the following) with variable permeability, porosity and thickness distributions. The skin factor for each well is generated randomly, and ranges from -3 to 7. In the sensitivity study, I matched on permeability only as well. I quantified the influence of pore volume and skin factors on the prediction accuracy from several cases with different pore volume or skin factors in the reservoir model. The following sections provide give detailed description of the sensitivity study.

4.1 Introduction of synthetic case generated for sensitivity study

A synthetic case was generated as the actual field for the sensitivity study (labeled as the base case). The base case is similar to Case 2, one of synthetic cases I used in Chapter III for

comparing the accuracy of the inverse and moving window methods. The base case was defined on a 54*54*1 simulation grid of a 9-township area. There are 130 wells in the reservoir, which were drilled at different dates over approximately 40 years. **Fig. 4.1** shows the date of first production for the 130 wells, which represents several rounds of infill drilling. The distributions of current well spacing and first production date are realistic as they were derived from actual well data from a shallow gas basin in North America. The actual porosity, thickness and permeability distributions are shown in **Figs. 4.2, 4.3** and 3.2. The average thickness and porosity in this base case is 110 ft and 8.5%. I use variable skin factors in the base case. The property of skin factors for the base case is shown in section 4.3. Other parameters used in the simulation are listed in **Table 4.1**.

The regression is based on the synthetic production history from 1962 to 2000. After this I made a prediction for 3 years (2001-2003). In the prediction time, 30 new wells have been drilled, as indicated in **Fig. 4.4**.

I generated the synthetic production history using the actual permeability distribution, then inverted the synthetic production data to determine the permeability field for the sensitivity study. I matched on average production rate of every other year, yielding a total of about 700 observation points.

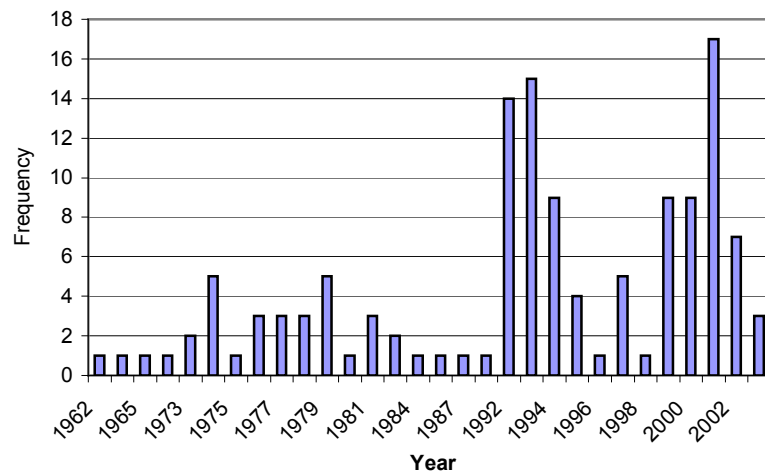


Fig 4.1 - The distribution of date of first production for the base case

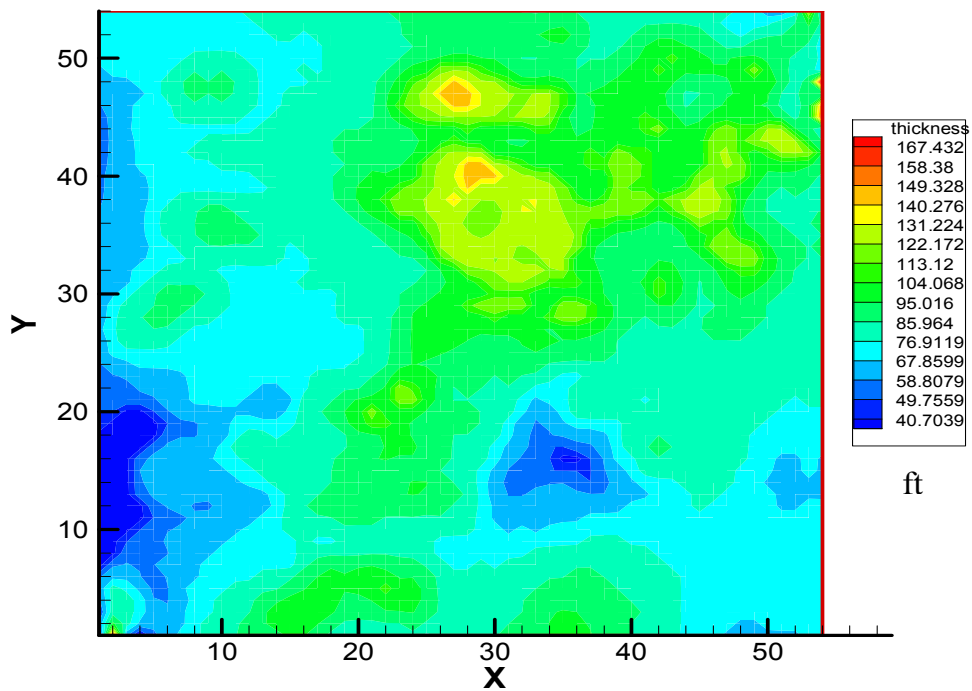


Fig 4.2 - The distribution of actual thickness for the base case

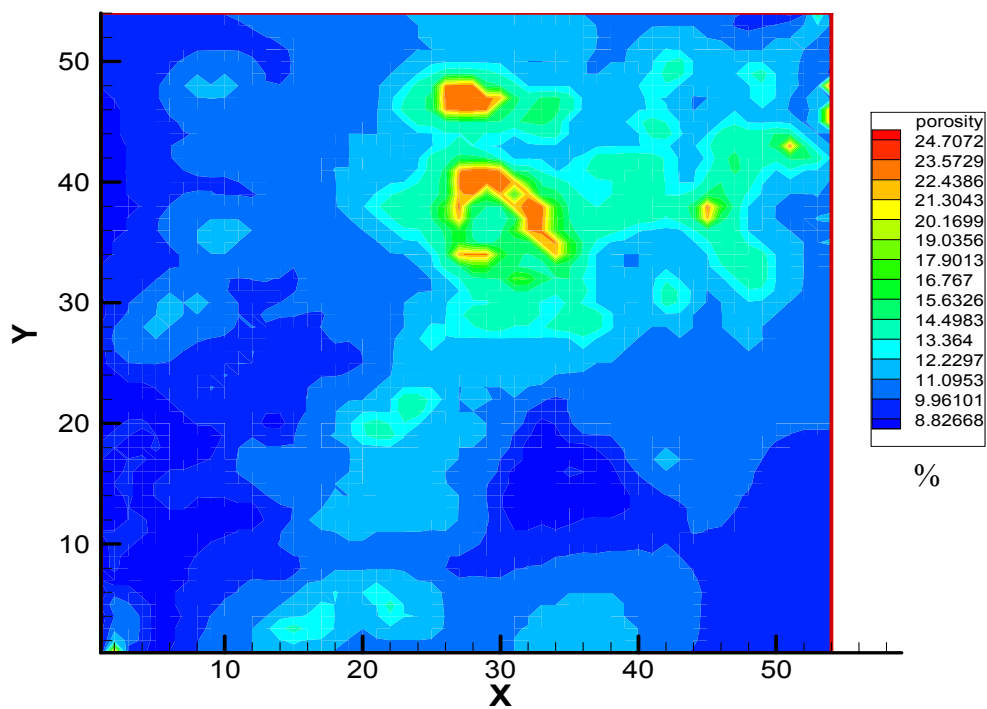


Fig 4.3 - The distribution of actual porosity for the base case

Table 4.1 – The parameters used in the base case

Number of wells	130
Initial reservoir pressure (psia)	1100
Flowing bottom hole pressure (psia)	250
Well bore radius (ft)	0.3

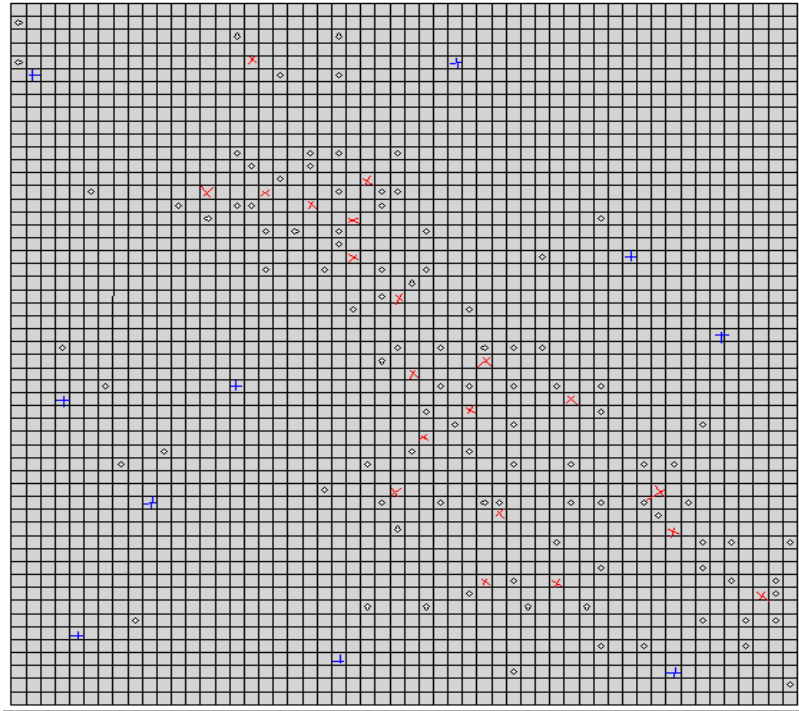


Fig. 4.4 - Well locations in the base case

(° - existing well, × - infill well, + - step-out well)

4.2 The effect of pore volume on predicted infill performance

To quantify the influence of pore volume on predicted infill performance, I built reservoir simulation models with four different pore volume distribution. **Table 4.2** shows the names and descriptions of cases involved in this study. The first case, Pv1_actual, uses the actual pore volume distribution based on actual thickness (Fig. 4.2) and porosity (Fig. 4.3) maps, which represent variable thickness and porosity distributions. The second case is Pv2_average, which initializes the reservoir model with average uniform thickness (110 ft) and porosity values (8.5%) that yield a total pore volume very close to the actual value. The third case is called Pv3_high, which uses uniform thickness (150 ft) and porosity (15%) values. The pore volume input in Pv3_high is about 1.5 times higher than the average pore volume. The fourth case,

Pv4_low, has very low uniform thickness (60 ft) and porosity values (5%) in the reservoir model. The pore volume in Pv4_low is about 1.7 times lower than the average value.

In all 4 cases, all the other parameters are known and fixed except permeability which is the only parameter to be matched. I started the regression with a uniform permeability field of $k = 0.2$ md in all 4 cases.

Table 4.2 – Description of the four synthetic cases in sensitivity study of pore volume

Cases	Net thickness ,ft	Porosity, %
Pv1_actual	actual	actual
Pv2_close	110	8.0
Pv3_high	150	15.0
Pv4_low	60	5.0

4.2.1 History matching results

Fig. 4.5 shows the decreasing objective function in the four cases. In all the 4 cases, objective functions decrease greatly in the first 3 iterations, and go into a slow decline after that. Compared with Pv3_high and Pv4_low, Pv1_actual and Pv2_average have a lower misfit with the same number of iterations. This is because I use either the actual pore volume or average uniform pore volume in each grid of reservoir model, instead of a uniform value far from the average value as in Pv3_high and Pv4_low. Pv3_high shows a lower misfit than pv4_low. But this is not the case all the time. In some other studies I did, the misfit with high pore volume input sometimes has a higher value than that with low pore volume input. It is evident that the objective function can decrease to a lower value if the reservoir model has a reasonable pore volume distribution input.

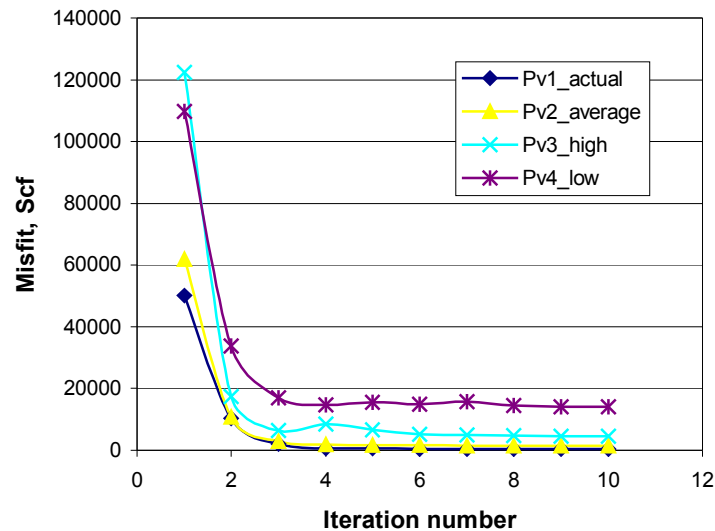


Fig. 4.5 - Objective function for the four synthetic cases

Figs. 4.6-4.9 show estimated permeability distribution for all the four synthetic cases. As I mentioned in Chapter III, the inverse method only reproduces the local permeability. For the reservoir areas which are not developed with wells, the estimated permeability keeps the initial input values. Compared with the actual permeability distribution (Fig. 3.2), the estimated permeability distribution based on actual pore volume resembles the true heterogeneity in the areas with wells and production data very well (Fig. 4.6). The estimated permeability distribution from *pv2_average* regenerates the heterogeneity of actual permeability field in the areas with wells (**Fig. 4.7**). But the estimated permeability values from *Pv2_average* are a little higher compared with actual values. For *Pv3_high* and *Pv4_low*, the estimated permeability distributions based on high and low pore volume input are far off the actual distribution. Both of them could not regenerate the heterogeneity of the actual permeability distribution. The estimated permeability values are a lot lower in the high pore volume case, and higher in the low

pore volume case. This means the estimated permeability compensates the inaccuracies in pore volume. As shown by the high objective function values in Fig. 4.5 for these two cases, the extent of the compensation is limited. Thus, poor pore volume estimation appears to have a significant effect on the estimated permeability distribution.

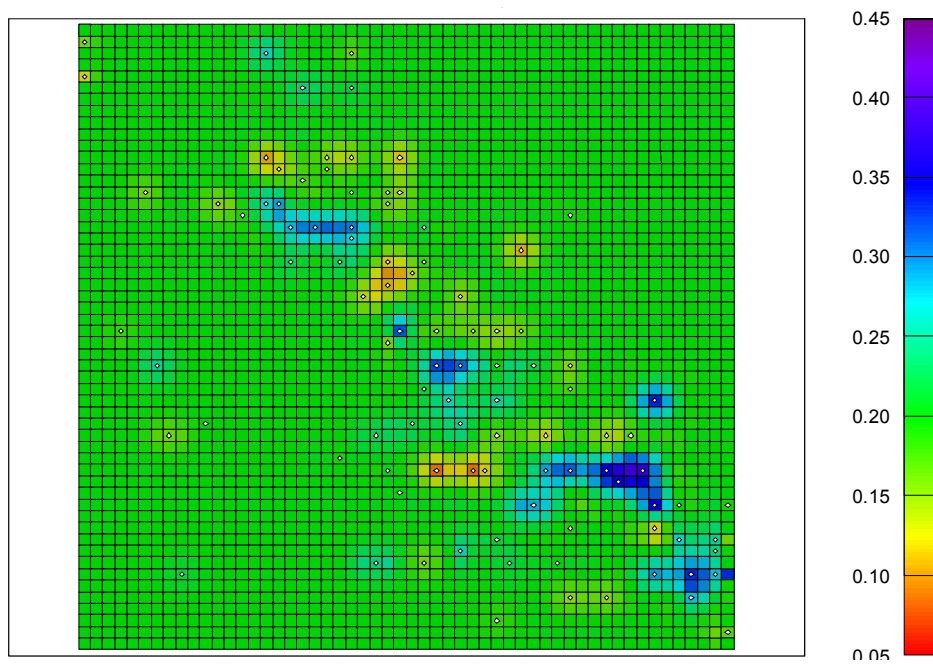


Fig. 4.6 - Estimated permeability for Pv1_actual

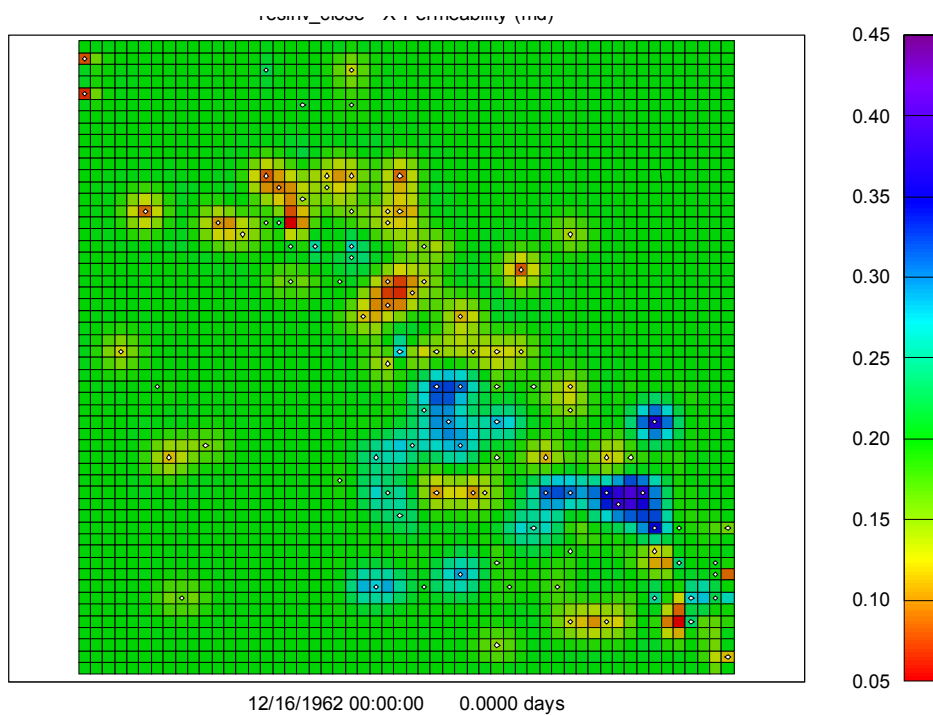


Fig. 4.7 - Estimated permeability for Pv2_average

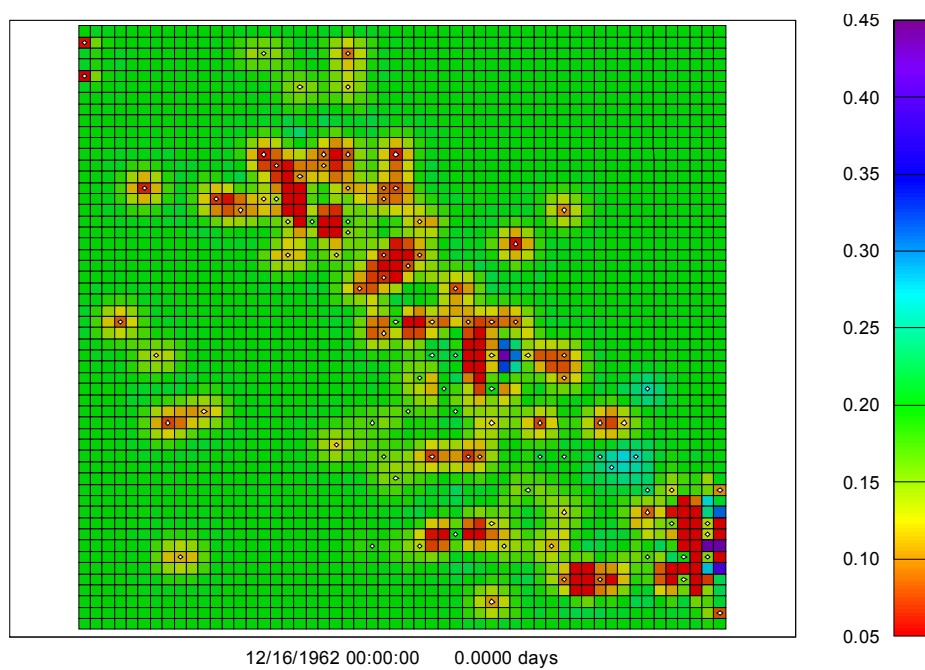


Fig. 4.8 - Estimated permeability for Pv3_high

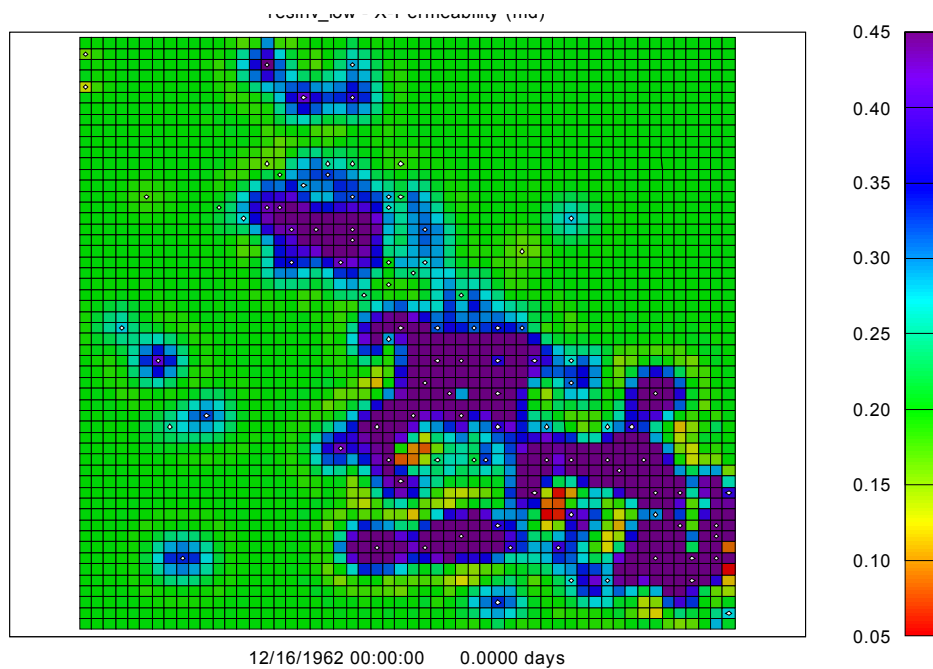


Fig. 4.9 - Estimated permeability for Pv4_low

4.2.2 Infill performance prediction

Based on the estimated permeability distribution of each case (Figs. 4.6-4.9), I calculated infill well performance. When I calculated infill potentials in all 4 synthetic cases, I made the prediction for 3 years. In this sensitivity study, I use Inf_Per to represent the infill performance of the 30 new wells. I calculated relative error and average percent error of individual-well Inf_Per in each case to quantify the prediction accuracy.

Table 4.3 demonstrates the relative error for the four synthetic cases. Relative error of Inf_Per is the error in the 130-well Inf_Per between each case and the true value. For infill wells, notice that, relative errors from Pv1_actual (9.5%) and Pv2_average (11.6%) are a lot lower than that from Pv4_low (30.94%). But relative error from Pv3_high (6.84%) is very low as compared to those from other 3 cases. I think this is just coincidence because I got very high relative error in most of other cases I studied.

Table 4.4 shows average percent error for the four synthetic cases. Average percent error quantifies the error on an individual well basis. For infill wells, Table 4.4 shows that average percent error from Pv1_actual (14.62%) and Pv2_average (21.21%) are a lot lower than that from both Pv3_high (47.16%) and Pv4_low (33.48%).

From the above discussion, I conclude that if I construct my reservoir model with a uniform thickness and porosity values that are about 1.5 higher than their average values as in Pv4_low, the infill prediction errors can be off by 30% to 40% on both a fieldwide and individual-well basis. Thus, pore volume has a significant effect on the prediction accuracy of infill wells. However, if I use average values of thickness and porosity in my reservoir model, like Pv2_average, there is not too much deviation of prediction accuracy from that with actual thickness and porosity maps. This is reassuring, since it will often be necessary to initialize reservoir models with estimated average values if reservoir property maps are not available.

Table 4.3 - Relative error with different pore volume

cases	Existing wells	Infill wells	Step-out wells
Pv1_actual, %	-0.019	9.50	14.59
Pv2_average, %	0.37	11.16	72.83
Pv3_high, %	1.84	6.84	142.83
Pv4_low, %	-6.69	30.94	-9.67

Table 4.4 - Average percent error with different pore volume

cases	Existing wells	Infill wells	Step-out wells
Pv1_actual, %	0.22	14.62	30.97
Pv2_average, %	0.84	21.21	70.26
Pv3_high, %	2.32	47.16	138.53
Pv4_low, %	6.39	33.48	26.52

4.3 The effect of skin factors on predicted infill performance

The skin factor is a dimensionless quantity used to quantify the additional pressure drop from a zone of altered permeability in the formation immediately adjacent to the wellbore. Because of drilling and/or completion operations, this near-wellbore zone can be damaged, resulting in a permeability that is lower than the unaltered, in-situ formation permeability. Under these conditions, the skin factor is a positive quantity. Larger positive values of skin factors indicate greater reductions in near-wellbore permeability. Conversely, if the formation around the wellbore is stimulated, such as by acidizing or fracturing, the skin factor is negative.¹¹

The skin factor for a well can be estimated in various ways. The best way is from a pressure transient test tests in the same formation and in wells with similar completions, or it can be approximated from the well's completion and/or stimulation type. If measured data are not available, it may be possible to develop from known data a correlation against stimulation type and use this where you do not have skin factor data. As I mentioned before, individual well skin factors are usually not available. In my study, I assume zero or another uniform value for skin factors of all wells.

I used two synthetic cases, one with actual skin factors and the other with zero skin factors for all the wells, to quantify how the skin factors affect the prediction accuracy. The

observed data I generated for regression is based on variable skin factors. Properties of the generated skin factor distribution for 130 wells are shown in **Table 4.5**. The synthetic case with actual skin factors is exactly same as case Pv1_actual I used above, and I called it as Sk1_actual here. The other case with zero skin factors is called Sk2_zero. The only difference between these two cases is the input value of skin factors, one with actual variable skin factors and the other using uniform zero for skin factor of each well. As in the previous sensitivity study, I inverted synthetic production data to determine the permeability field. In both cases, all the other parameters were known and fixed except permeability, which was the only parameter matched.

Table 4.5 - The property of skin factors

Mean	1.8588
Standard Error	0.2376
Median	1.8180
Standard Deviation	2.7095
Sample Variance	7.3414
Kurtosis	-1.1427
Skewness	-0.0067
Range	9.8953
Minimum	-2.9313
Maximum	6.9640
Sum	241.6492
Count	130.0000

Fig. 4.10 shows that the objective functions decrease smoothly in both cases. Note that, importantly, the misfit is lower in Sk1_actual. The objective function with actual skin factors decreases to a lower value with the same number of iterations.

The estimated permeability distribution for Sk1_actual is shown in Fig. 4.6. **Fig 4.11** shows the estimated permeability distribution for Sk2_zero. Compared with the actual permeability distribution (Fig. 3.2), the estimated permeability in both cases regenerates the heterogeneity of the reservoir well. But in Sk2_zero, the permeability values in some areas are lower than the actual values.

Tables 4.6 and **4.7** show the relative error and average percent error of Inf_Per for both cases. For infill wells, the relative error in Sk2_zero, -3.40%, is lower than that in Sk1_actual, -9.50%. But the average percent error in Sk2_zero is 37.23%, which is about twice the error in Sk1_actual, 14.62%. Thus, skin factors have a big effect on prediction accuracy.

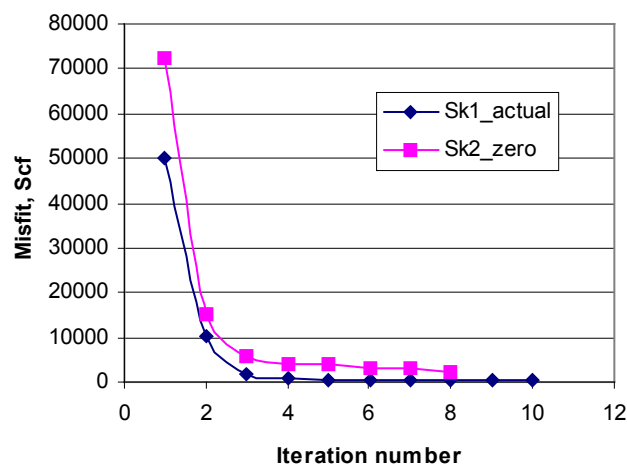


Fig. 4.10 - Objective function with different skin factors

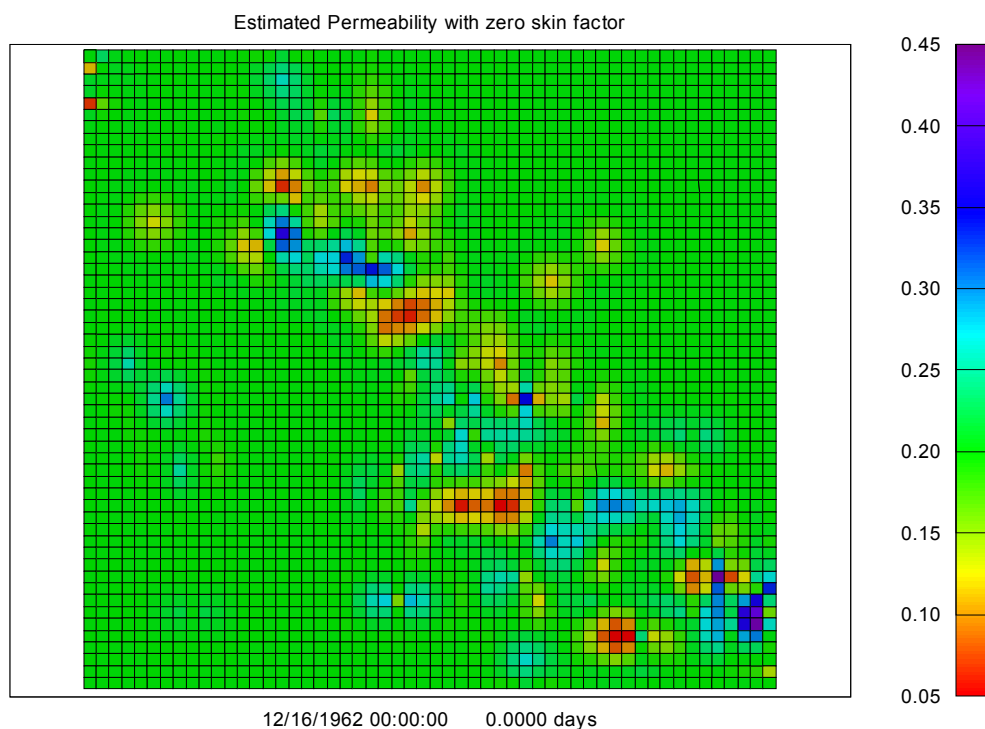


Fig. 4.11 - Estimated permeability distribution for Sk2_zero

Table 4.6 - Percent error distribution for Sk1_actual

	Existing wells	Infill wells	Step-out wells
Relative error, %	-0.019	-9.50	14.59
APE(average percent error),%	0.22	14.62	30.97

Table 4.7 - Percent error distribution for Sk2_zero

	Existing wells	Infill wells	Step-out wells
Relative error, %	-0.31	-3.40	41.99
APE(average percent error),%	1.14	37.23	61.92

CHAPTER V

FIELD CASE APPLICATION OF INVERSE METHOD

In Chapter III, I compared the inverse method with the moving window technology for four synthetic cases. In this Chapter, I applied the simulation inversion method to actual production data from the 9-township area from which the synthetic cases were derived. To evaluate the accuracy of the inverse method, I performed a blind validation study in which I excluded part of data set to compare my prediction results with observed infill performance.

5.1 Field case description

The reservoir in study is located in the Viking Formation of the Western Canada Sedimentary Basin, which is equivalent in age to the Muddy Sandstone of Wyoming and the Newcastle Sandstone of Montana and North Dakota. There are more than 75 fields in the Viking Formation. Estimated original recoverable resources for the formation are 9.8 Tcf of gas and 558 million bbl of oil. Through 1991, cumulative Viking production was 3.65 Tcf of gas and 420 million bbl of oil.²⁶

Several studies²⁷⁻³⁰ have established the geologic framework and controls on hydrocarbon producibility of the Viking Formation. Viking production is primarily from stratigraphic traps in shoreline deposits and incised-valley, channel-fill sandstones. Porosity variations and directional permeability of Viking Formation reservoirs are pronounced and are controlled by sedimentary facies, which in turn, are related to the depositional history. Viking progradational shoreface bar reservoirs are comprised of fine- to medium-grained sandstones 5-10 meters thick that were deposited during a regressive phase. Transgressive bar and sheet sandstone reservoirs range from coarse-grained sandstone to conglomeratic sandstone that are 1

to 4 meters thick. Both progradational shoreface and transgressive bar facies are tens of kilometers long, several kilometers wide, and trend northwestward. Estuary and incised valley fill reservoir sandstones occur as north-trending isolated channel sandbodies that are usually less than 10 meters thick and are comprised of fine-grained to conglomeratic sandstone.

The reservoir in study is a shallow gas reservoir with approximately 40 years of production history. There are approximately 201 wells with production through December 31, 2004. The distribution of date of first production (**Fig. 5.1**) shows that several rounds of infill drilling have already been implemented in parts of the reservoir. I produced the wells at an estimated flowing bottomhole pressure of 250 psia in the simulations, and honored shut-in periods with durations of one month or longer.

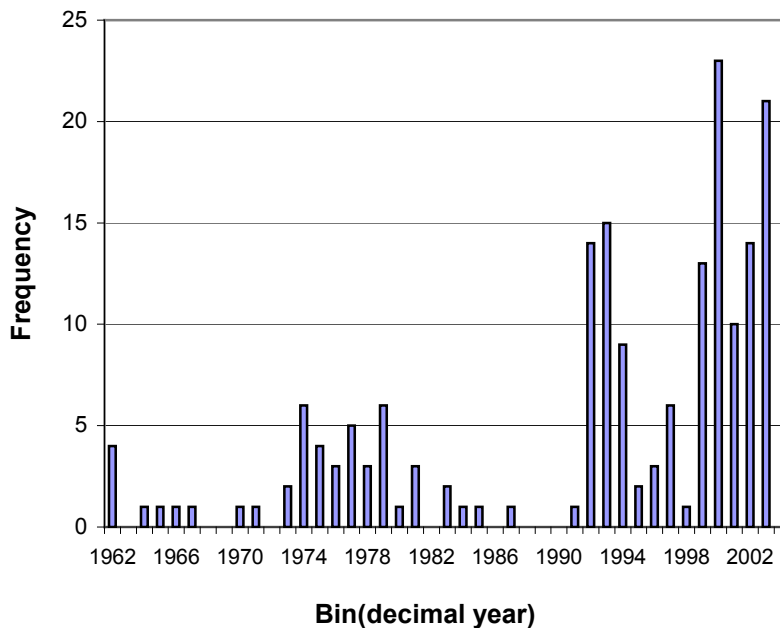


Fig. 5.1 - Histogram of date of first production for the field case

5.2 Procedures for dealing with the new field database

The field data I use to build my reservoir models are based on a database from company. This database includes two tables. One of the tables called “Texas_Accumap_Dump_9_Townships” includes well and formation information, such as UWI, well name, latitude & longitude, spud date, and formation name and so on. The other table is “Texas_A&M_9_townships_viking_production”, which provides monthly production data. In table “Texas_Accumap_Dump_9_Townships”, then some were wells, that are not from Viking and its equivalent formation, are included. These wells need to be excluded from validation study of this field case. There are also some multi-completion wells in this table, which were treated as different wells in the table “Texas_A&M_9_townships_viking_production”. It was necessary to find these wells and put their production together as one well.

From these two tables, I generated well location data and observation data needed for running my simulation model. These two tables include the well and production information of 261 wells with 40 years production history, so it is important to process these data efficiently. Following are the specific procedures I used in this field study.

3 **Step 1:** Check formation ID in the table “Texas_Accumap_Dump_9_Townships”.

- (1) There are 261 total wells in this table. The column named as “Prd Zone” summarizes all the formation IDs for each well. I need to know what this formation ID represents, so I can confirm if this well is from Viking and its equivalent formation based on the stratigraphic chart for this area. Another table called “Formation Ids Sorted by FORM_ID” gives the formation name corresponding to each formation ID. Table 5.1 lists the formation name and ID of 8 formations found in “Prd Zone”.

Table 5.1 - Formation ID corresponding to formation name

Formation ID	Formation Name
BCDS	BASAL COLORADO SS.
BSLD	BOW ISLAND
MNVL	MANNVILLE
VKNG	VIKING ZONE
CLRD	COLORADO
MLKR	MILK RIVER
MDCN	MEDICINE RIVER
SSPK	SECOND WHITE SPECKS

(2) “Stratigraphic Correlation Chart” presents the stratigraphic information about BRITISH COLUMBIA, ALBERTA, SASKATCHEWAN and so on. This charts shows that the first four formations, i.e., BASAL COLORADO SS., BOW ISLAND, MANNVILLE AND VILING, are in Viking and its equivalent formation. Wells from the remaining four formations were found to not be Viking equivalent and were not included in this Viking study.

(3) Remove all the wells in the database that were not found to be Viking equivalent wells.

There are 49 of these wells, so the total number of wells in this field case study was 212.

- **Step 2:** Define well locations and grids.

(1) In table “Texas_Accumap_Dump_9_Townships”, I found that the UWI showed in this table has different format as that shown in table “Texas_A&M_9_townships_Viking_production”. So I need to modify the name of UWI in these two tables to correlate them for finding multi-completion wells and

summarizing the well and observation data for each well. To do this, I generate “UWI(revised)” based on “UWI” given based on the format with “UWI” in table “Texas_A&M_9_Townships_Viking_Production”. Second, I sorted all the wells by “On Prod” which give the date of first production, to give the order of producing date. Based on this production date, I gave a new well ID such as “A1”, “A2”, to each well which is easy to tell early or late wells.

- (2) Generate structure map and well location map based on the longitude and latitude given in table “Texas_Accumap_Dump_9_Townships”. I used GeoGraphix in this study.
- (3) Input structure map and well location map into a software (CMG in my study) to choose grid to make sure all the wells included. The way I calculated grids is:

It is a 9 township areas, so the length of the study area is 95040 ft since one township is 6 miles long. I define one grid size as 1760 ft, like what I used in the four synthetic cases in Chapter III. So the number of grids is 54.

- **Step 3:** Generate observation data for doing regression

Calculate the average gas production rate in each year for each well, i.e., yearly production divided by the actual producing days. But since I did regression for 152 wells with 40 years of production history, too many data points were involved in the regression if I used observation data from each year, which makes the regression very slow. Thus, I selected the observation data of each well from every other year.

5.3 Construct reservoir model

I used the same 54x54x1 simulation grid as in the synthetic cases. I started with a uniform permeability of 0.1 md, and inverted the actual production data using the methodology described in Chapter II to determine the permeability field. I matched on average production rate of every

other year, generating a total of 1180 data points for regression. Other reservoir and well parameters used in the reservoir model are listed in **Table 5.2**, which are estimated average values from actual field data. I conducted a blind validation study in which I performed regression on production data from 1962 to December 31, 2000, then compared the predicted to observed performance from January 1, 2001 through January 31, 2004. The regression consisted of 2916 parameters (permeability in this case).

Table 5.2 - Other parameters used in the field case

Number of wells	212
Porosity (%)	15
Initial reservoir pressure (psia)	1100
Flowing bottom hole pressure (psia)	250
Well skin factor	-3
Well bore radius (ft)	0.3
Net thickness (ft)	15

5.4 Field test results

Field test results include objective function, estimated permeability distribution, history matching production data and validation.

5.4.1 Objective function and estimated permeability distribution

Fig. 5.2 shows that the objective function declines rapidly in the first few iterations then settles into a slower, constant decline. The iteration of regression is terminated when convergence is achieved, i.e, the objective function in this case does not decrease significantly for several

successive iterations. **Fig. 5.3** shows the estimated permeability distribution after 10 iterations. I did not use norm constraints in the regression, because we had no prior information on the permeability distribution. Smoothness constraints provide the spatial continuity that is exhibited in Fig. 5.3. The selection of smoothness factor is somewhat subjective.^{15,22,23} I tried it with different values based on my experience. The final selection is based on a compromise between having a small misfit and having a geologically reasonable permeability distribution. Note that the permeability distribution is affected only in the vicinity of wells, where the influence of production is felt.

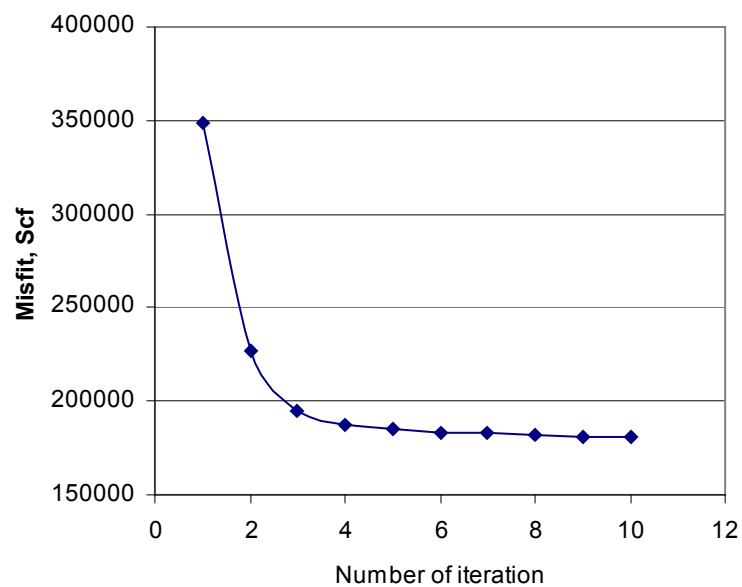


Fig. 5.2 - Objective function for the field case

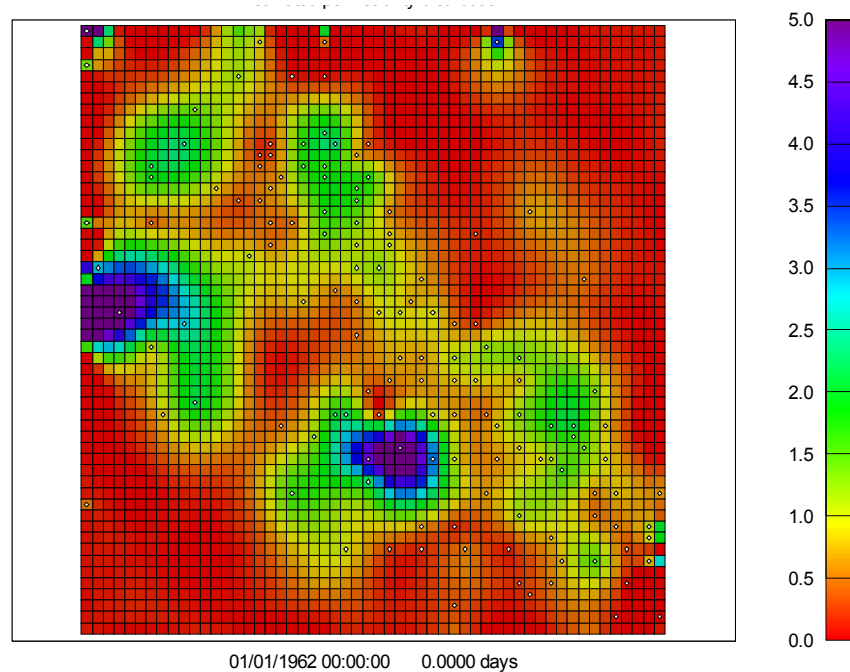


Fig. 5.3 - Estimated permeability for the field case at the end of the 152-well history

5.4.2 History matching

From 1962 to December 31, 2000, there are 152 wells that produce during this period. **Figs. 5.4-5.5** show field-wide history match results. I believe the results are acceptable over most of the history, given that I have used only well locations, production data, and estimated average values for other reservoir properties. The calculated results began to diverge from the observed values near the end of history. I think this divergence results from the large number of new wells drilled in the last two years of history (Fig. 5.1). For these new wells, I usually only have one or two observed data points in the regression, which limits the accuracy of the calculated permeability around these wells. **Figs. 5.6-5.9** show four examples of individual well history matches. Good matches are obtained for Wells 12, 48 and 53 (Figs. 5.6-5.8). A poorer match is obtained for Well 2 (Fig. 5.9), which began producing in the 1960's. Well 2 is close to the boundary in the reservoir model, which does not necessarily correspond to the reservoir boundary, since I am

modeling only a part of the reservoir. This may affect the accuracy of the history match for this well.

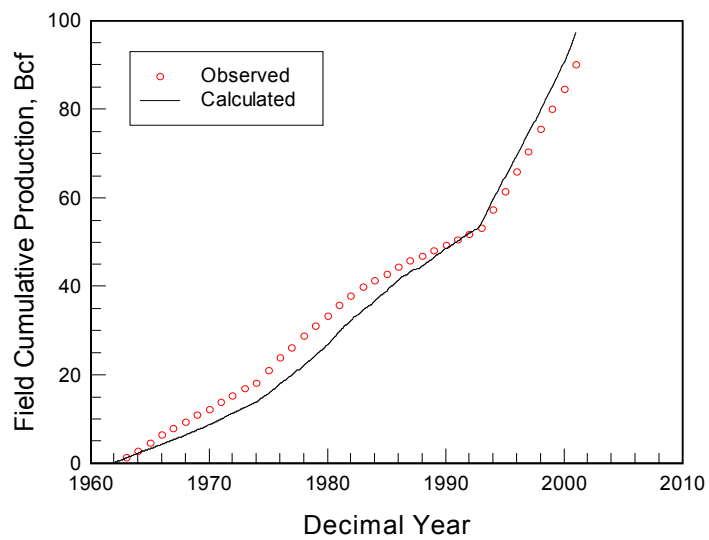


Fig. 5.4 - History match of field cumulative production

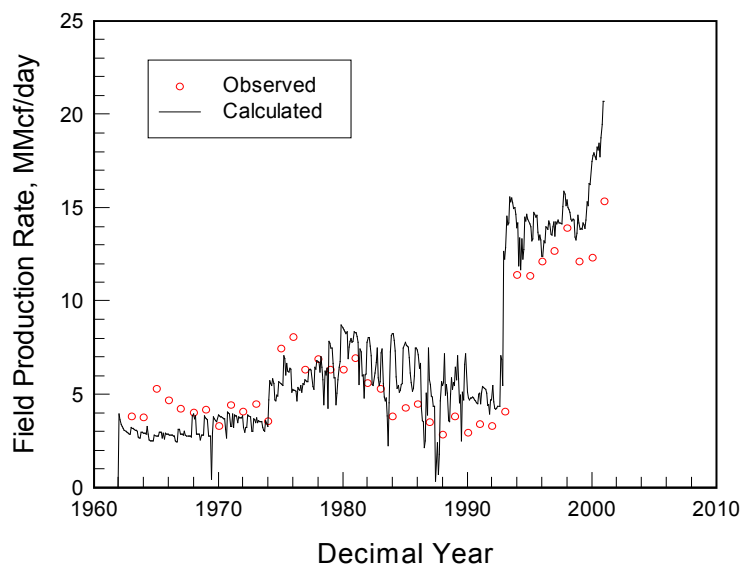


Fig. 5.5 - History match of field production rate

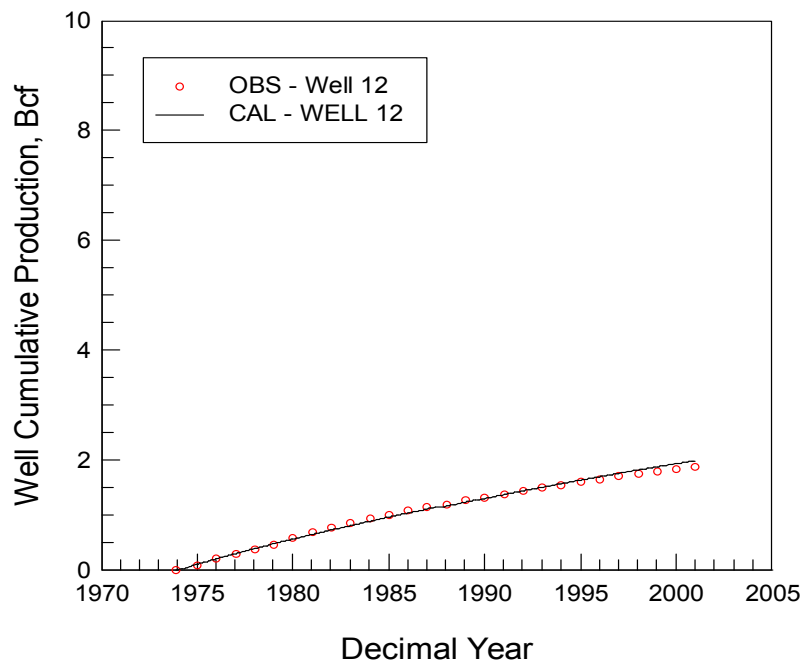


Fig. 5.6 - History match of Well 12

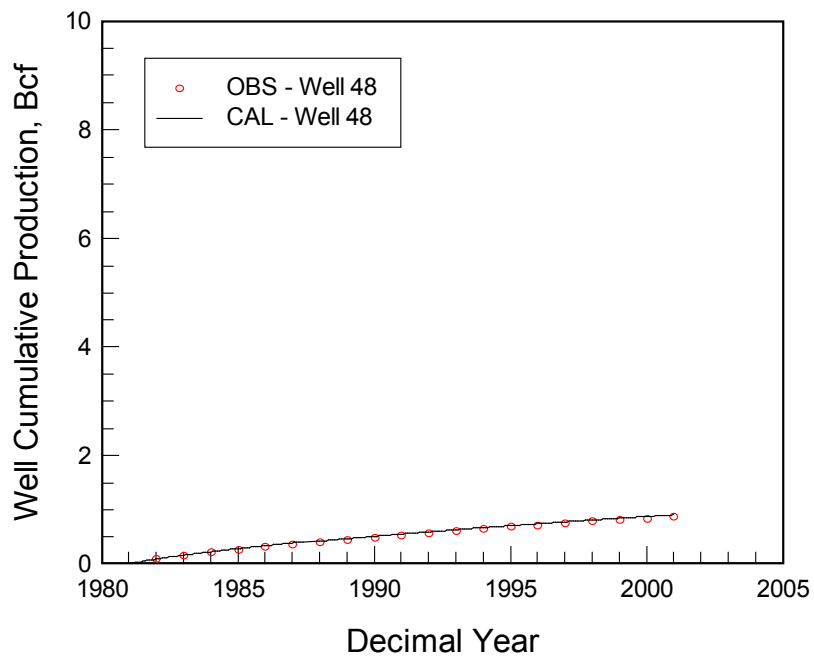


Fig. 5.7 - History match of Well 48

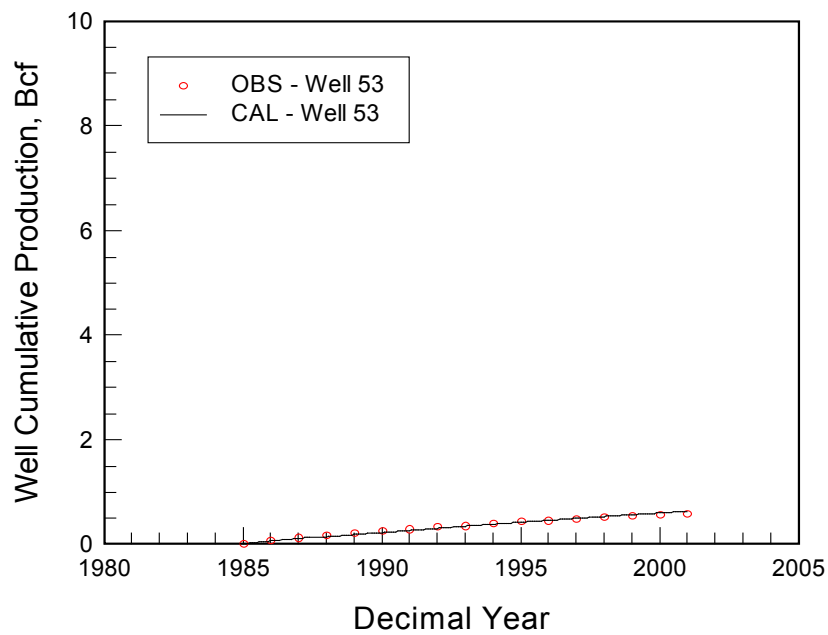


Fig. 5.8 – History match of Well 53

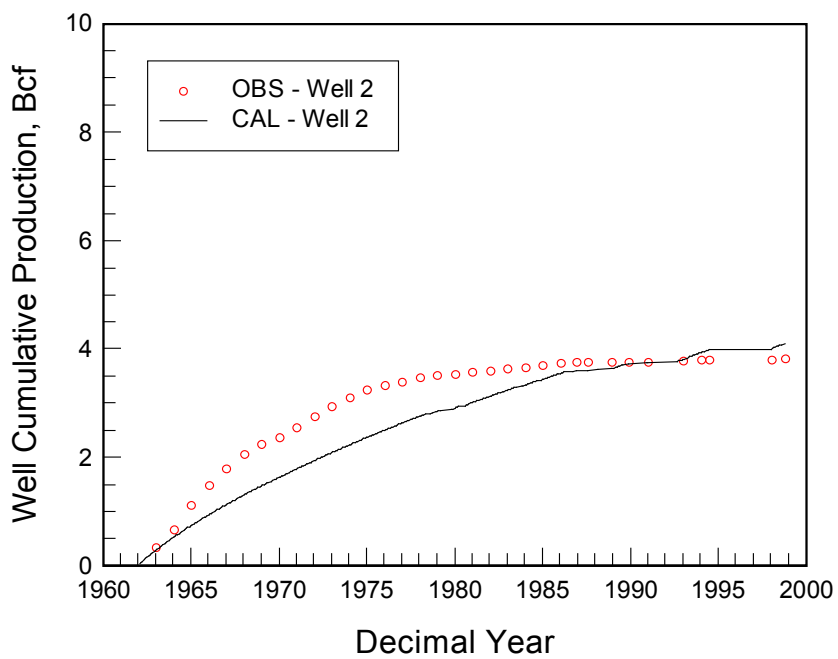


Fig. 5.9 – History match of Well 2

5.4.3 Validation

Using the estimated permeability distribution I obtained by history matching production data through 12/31/2000, I forecasted reservoir performance through 1/31/2004. There were 49 new wells that began production during this 3-year period, which are indicated by symbols “+” or “x” in Fig. 5.10. Figs. 5.11-5.13 show fieldwide predicted performance for three different groups of wells. Fig. 5.11 is the prediction for existing wells, i.e., those wells first produced before 1/1/2001. Among 152 existing wells, some of them stopped producing before 1/1/2001, so there is only 105 existing wells included in the prediction. Fig. 5.12 is the prediction for infill wells, those wells first produced after 2001 and close to existing wells. Fig. 5.13 is the predicted performance for step-out wells, those wells first produced after 2001, but far from existing wells. Infill wells are indicated by the symbol “+” in Fig. 5.10, while step-out wells are indicated by the symbol “x”.

I expected performance to be predicted more accurately for infill wells than step-out wells since infill wells benefit from the more accurate permeability distribution resulting from the production influence of nearby existing wells. However, Figs. 5.12, 5.13 and Table 5.3 show that, on a group average basis, there is not much difference in fieldwide predictions for these two groups of wells, and step-out wells get predicted even a little better. Table 5.3 shows that, on an individual well basis, the prediction error of infill wells is 62.67% compared with 311.68% in step-out wells. Thus, the field case demonstrates that infill wells can be better predicted than step-out wells as expected. I expected to obtain the most accurate prediction for existing wells because of their involvement in history matching. However, Fig. 5.11 shows that this is not the case. Prediction error for the existing wells, even on an individual well basis, is larger than the error for the infill wells. I attribute this poor prediction for existing wells to the larger error in the last couple of years of the history match, due to the addition of many new wells late in history. In

the next section, I investigated use of different weighting factors to put more weight on late wells to improve this prediction.

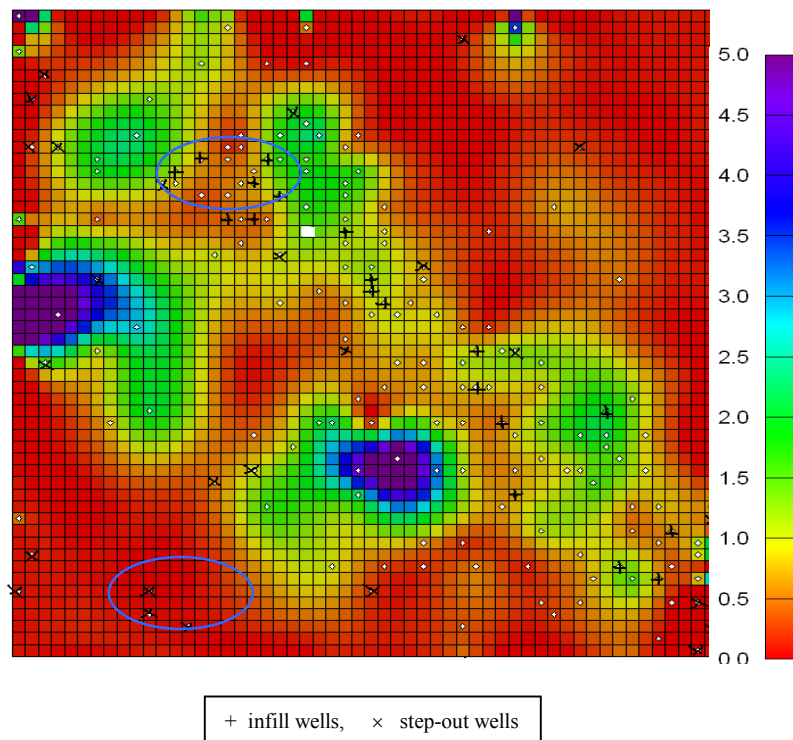


Fig. 5.10 Estimated permeability distribution for the field case

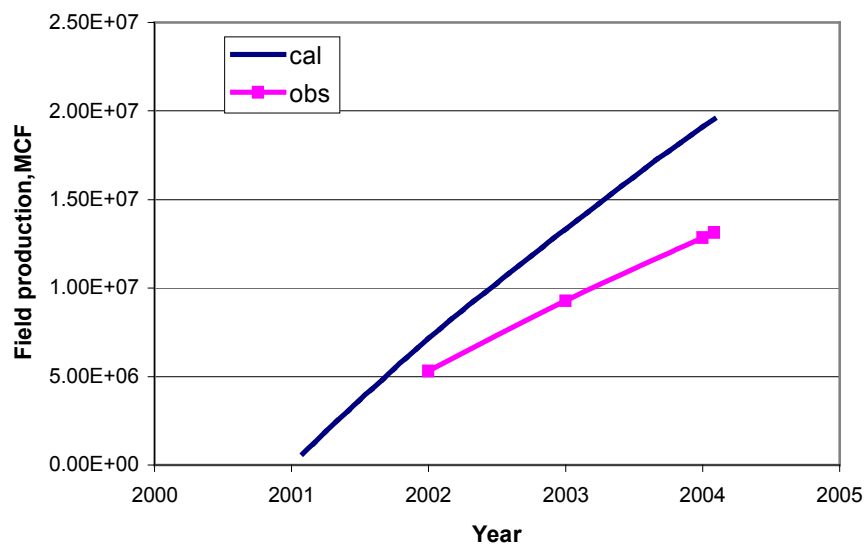


Fig. 5.11 - Predicted field cumulative production for the 105 existing wells that produced during the prediction period

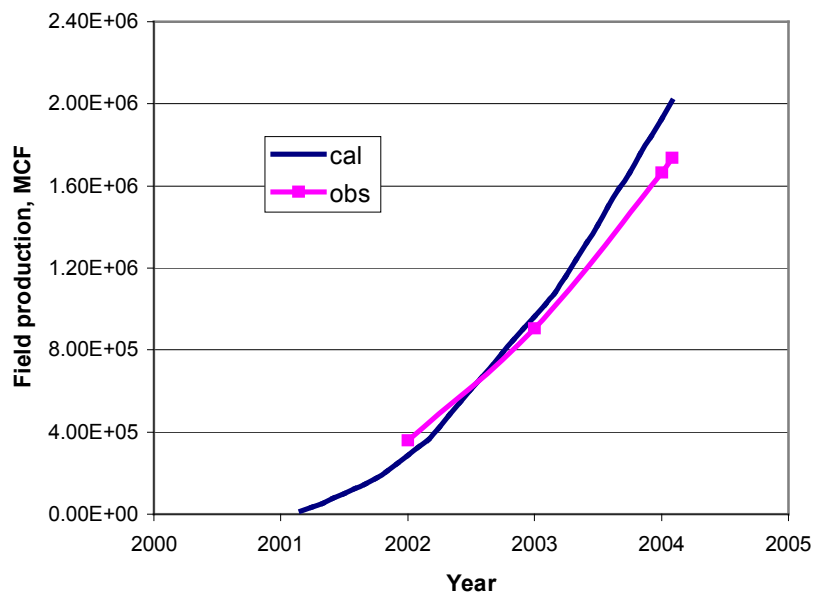


Fig. 5.12 - Predicted field cumulative production for 19 infill wells

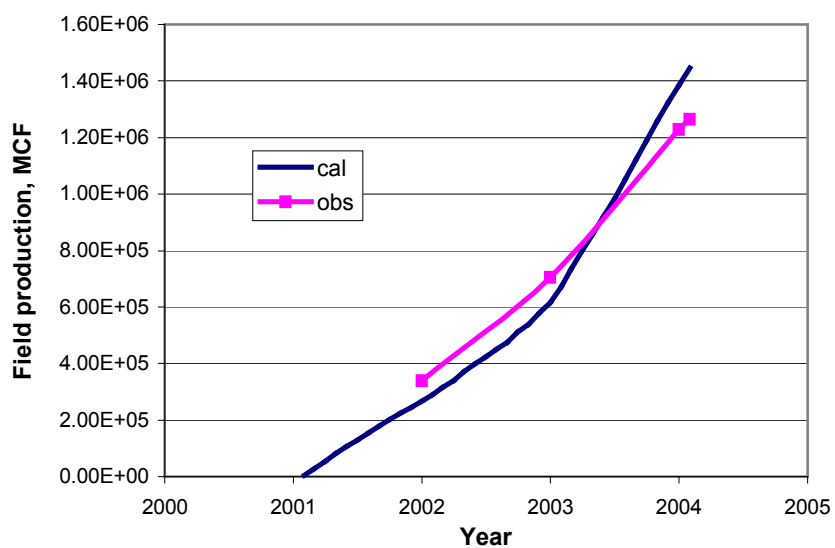


Fig. 5.13 - Predicted field cumulative production for 26 step-out wells

Table 5.3 - Summary of percent error for group wells

	Existing wells	Infill wells	Step-outs wells
Relative error, %	48.56	15.96	14.96
APE(average percent error),%	240.48	62.67	311.68
Median of percent error, %	61.72	31.78	81.94

Figs. 5.14-5.17 show example predictions for four individual wells. Well 163 (Fig. 5.14) and Well 173 (Fig. 5.15), two infill wells located in the northern ellipse in Fig. 5.10, have good predictions of cumulative production. Large errors in predicted cumulative production are obtained for Well 170 (Fig. 5.16) and Well 177 (Fig. 5.17), two step-out wells located in the southern ellipse in Fig. 5.10.

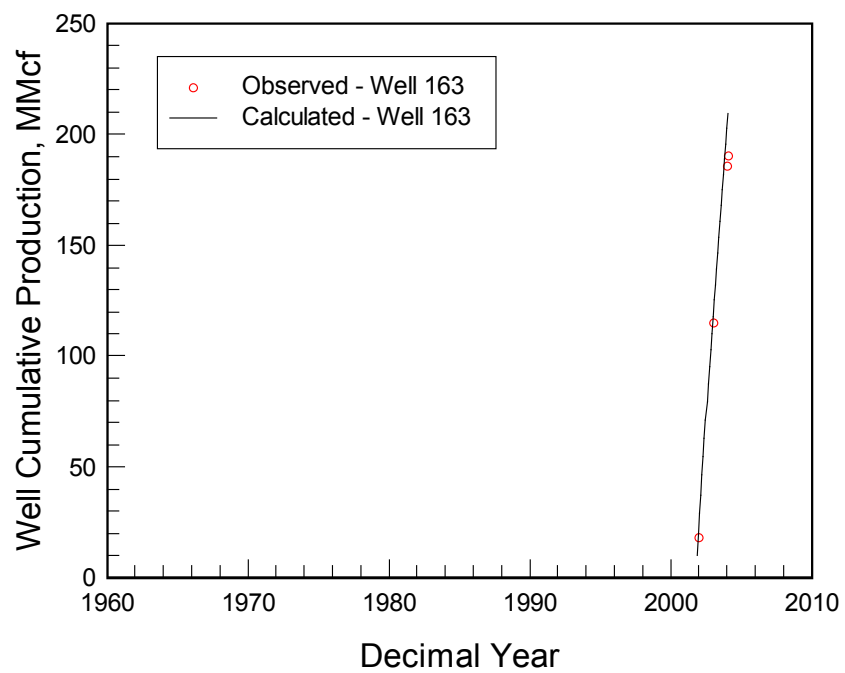


Fig. 5.14 - Prediction for infill Well 163

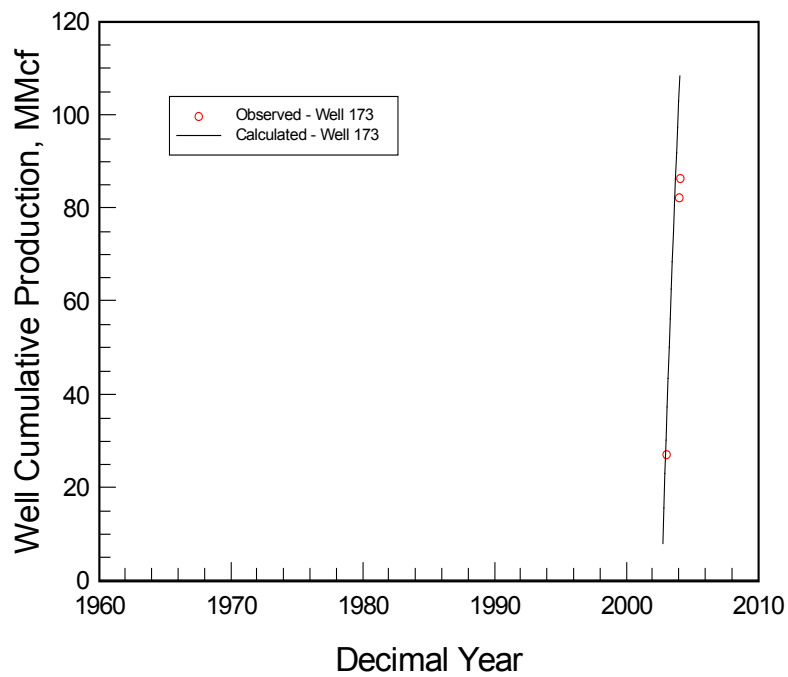


Fig. 5.15 - Prediction for infill Well 173

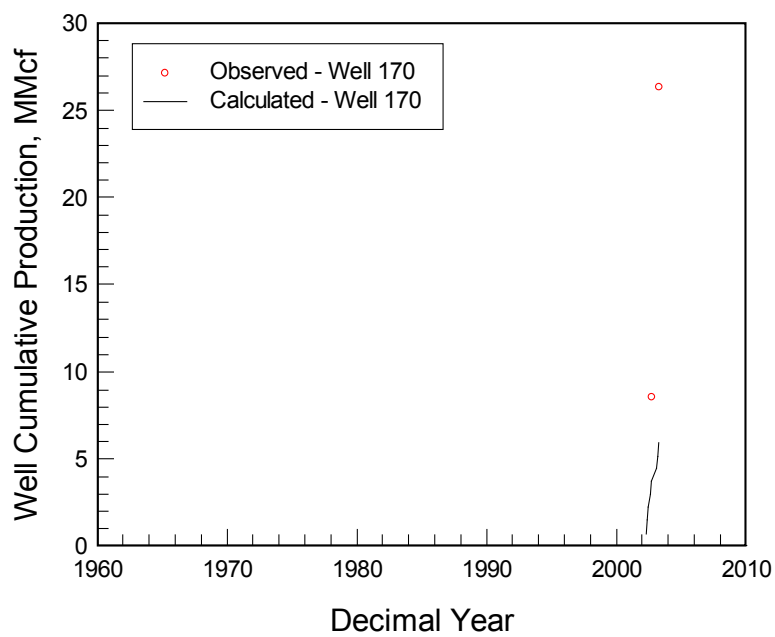


Fig. 5.16 - Prediction for step-out Well 170

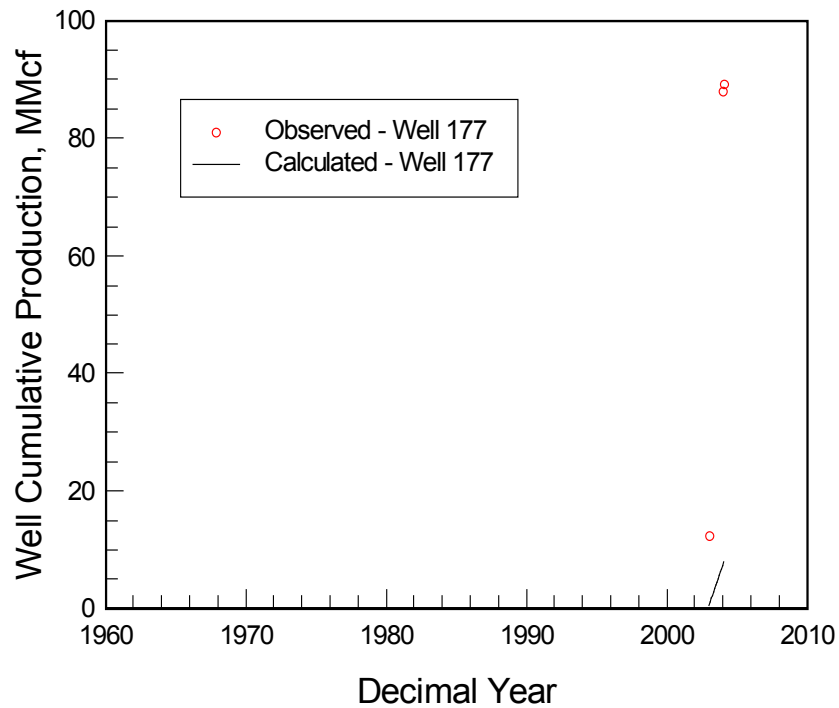


Fig. 5.17 - Prediction for step-out Well 177

These results show that in areas with existing wells with sufficient production data to quantify reservoir quality, it may be possible to accurately predict the production potential of infill wells. Since the method is based primarily on well locations and production data for a rapid screening evaluation, predictions for individual well locations can be substantially in error for step-out wells or locations without sufficient production data. Predictions for step-out wells can be improved only by including other types of data, e.g., seismic data. Of course, this will require transitioning to more rigorous reservoir characterization, at greater costs. However, this transition is greatly facilitated because the screening method is simulation based.

5.5 Sensitivity to weighting factors

In the analysis above, I give the same weight to all the observation data points. I tried to improve the prediction results by assigning different weightings to particular production data points. In the following sections, I discuss four different ways for assigning weighting factors.

5.5.1 Objective function with weighting factors

I am trying to minimize

$$\|\omega(d - g[m])\|_2^2 = \sum_{i=1}^N (\omega_i (d_i - g_i[m]))^2 \quad \dots\dots\dots (5.1)$$

At the l -th iteration step, I take a first order Taylor series expansion of $g[m]$ around m_l ,

$$g[m] = g[m_l] + G\delta m \quad \dots\dots\dots (5.2)$$

where m_l is the vector of M parameters at the l -th iteration step, G is the sensitivity coefficients matrix, and δm is the vector of parameter changes at the l -th iteration step. Thus, I obtain the data misfit vector ε at the l -th iteration step,

$$\varepsilon = d - g[m_l] = G\delta m \quad \dots\dots\dots (5.3)$$

Substituting Eq. 5.3 into Eq. 5.1, I obtain

$$\begin{aligned} \sum_{i=1}^N (\omega_i (d_i - g_i[m]))^2 &= \sum_{i=1}^N (\omega_i (\varepsilon_i - \sum_{j=1}^M G_{i,j} \delta m_j))^2 \\ &= \sum_{i=1}^N (\sqrt{\omega_i} \varepsilon_i - \sum_{j=1}^M \sqrt{\omega_i} G_{i,j} \delta m_j)^2 \end{aligned} \quad \dots\dots\dots (5.4)$$

5.5.2 Different types of weighting factors investigated

To evaluate how the weight factors affect the prediction results, I generated four different types of weighting factors, which put emphasis on late wells.

Type 1 : I use the same weighting factors for all the wells.

Type 2 : For each well, weighting factors are inversely proportional to the number of observation data points for the well. So the more data points we have a well, the less weight we give to each data point for the well.

$$\omega_{i,j} = \frac{1}{(N_{obs})_i} \dots\dots\dots (5.5)$$

where $\omega_{i,j}$ is the weighting factor of well i for j -th observation point, and $(N_{obs})_i$ is the total number of observation data points of well i .

Type 3 : Data points in late wells and data points at late times in the same well have more significant weightings. For example, if I have four data points for well i , the sum of these four data points are $1+2+3+4=10$. Then the weight factors will be $\frac{1}{10}, \frac{2}{10}, \frac{3}{10}, \frac{4}{10}$. Thus,

$$\omega_{i,j} = \frac{j}{\sum_1^{(N_{obs})_i} (j)} \dots\dots\dots (5.6)$$

Type 4 : Late wells have greater weightings than earlier wells.

$$\omega_{i,j} = \frac{1}{time_{i,j}} \dots\dots\dots (5.7)$$

where $\omega_{i,j}$ is the weighting factor corresponding to the j -th observation data point for well i , and $time_{i,j}$ is the cumulative production days corresponding to the j -th observation data point for well i .

I repeated the field case using these different types of weighting factors and some combinations of the different types.

5.5.3 Summary of results with different weighting factors

I investigated 6 different schemes for weighting factors as shown in **Table 5.4**. In this field case, I used BY_{inf} to represent the well cumulative production in 3 years for each well. For the 3 different types of group wells (existing, infill and step-out wells), I calculated percent error of BY_{inf} both on a groupwide and on an individual well basis. **Figs. 5.18** and **5.19** summarize relative error of BY_{inf} for 6 different weighting schemes. It is apparent that for existing and infill wells, combinations 3 and 6 work better both on a groupwide and on an individual well basis. **Tables 5.5 – 5.10** list the prediction results for all 6 schemes. **Figs. 5.20-5.22** demonstrate how the predicted field cumulative production and field rate matches changed after using weighting scheme 6. Compared to the prediction of field cumulative production for infill wells shown in Fig. 5.12, there is significant improvement in prediction using weighting scheme 6 (Fig. 5.21). Fig. 5.20 shows that the prediction of field cumulative production for existing wells is not much different from that without using weighting factors. Thus, it is helpful for infill well prediction to put more emphasis on late wells and/or at late times for the same well. But this does not cause much change for existing wells. I believe the reason for poor prediction in existing wells is probably the minimum shut-in time I assigned in my model. As I mentioned above, I honored shut-in periods of one month or longer. But some existing wells did not produce for the entire month in months in which there is non-zero monthly production. This could be responsible for the calculated cumulative production being higher than the observed value, even far off in some cases.

Table 5.4 - Different combination of weighting factors

Schemes	Weighting types
1	Type 1
2	Type 2
3	Type 3
4	Type 4
5	Type 2 and Type 3
6	Type 3 and Type 4

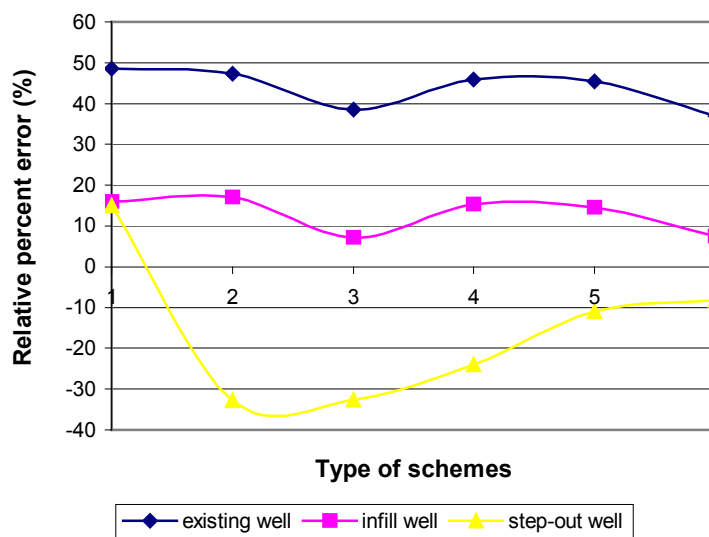


Fig. 5.18 - Distribution of relative percent error for 3 group wells

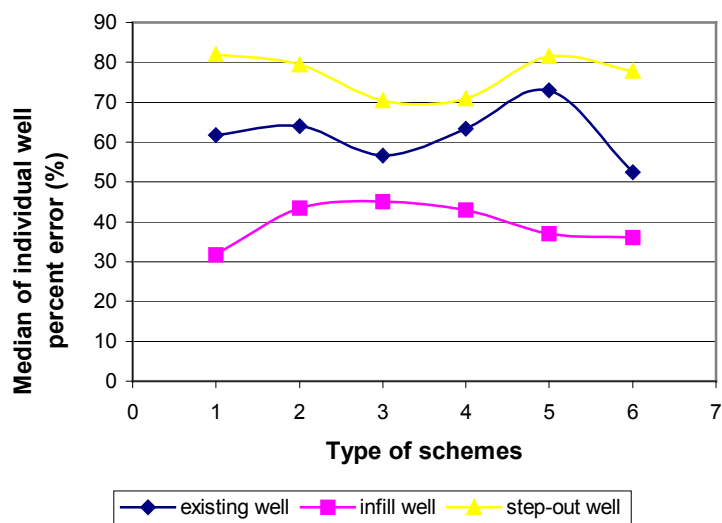


Fig. 5.19 - Distribution of median of percent error for 3 group wells

Table 5.5 - Percent error distribution using weighting factors as 1(Type 1)

	Existing wells	Infill wells	Step-out wells
Relative error, %	48.56	15.96	14.96
APE(average percent error),%	240.48	62.67	311.68
Median of percent error, %	61.72	31.78	81.94

Table 5.6 - Percent Error distribution with Type 2 weighting factors

	Existing wells	Infill wells	Step-out wells
Relative error, %	47.23	17.12	-32.81
APE(average percent error),%	227.55	67.58	179.72
Median of percent error, %	63.98	43.49	79.40

Table 5.7 - Percent error distribution with Type 3 weighting factors (normalized)

	Existing wells	Infill wells	Step-out wells
Relative error, %	38.60	7.25	-32.62
APE(average percent error),%	138.37	63.16	149.39
Median of percent error, %	56.58	45.06	70.45

Table 5.8 - Percent error distribution with Type 4 weighting factors

	Existing wells	Infill wells	Step-out wells
Relative error, %	45.91	15.35	-24.06
APE(average percent error),%	161.74	68.91	192.71
Median of percent error, %	63.42	43.07	70.87

Table 5.9 - Percent error distribution with schemes of Type 2 and Type 3 weighting

	Existing wells	Infill wells	Step-out wells
Relative error, %	45.35	14.61	-10.94
APE(average percent error),%	163.22	65.03	294.74
Median of percent error, %	73.03	37.00	81.51

Table 5.10 - Percent error distribution with schemes of Type 2 and Type 4 weighting

	Existing wells	Infill wells	Step-out wells
Relative error, %	37.02	7.57	-8.17
APE(average percent error),%	118.06	58.08	269.67
Median of percent error, %	52.53	36.09	77.86

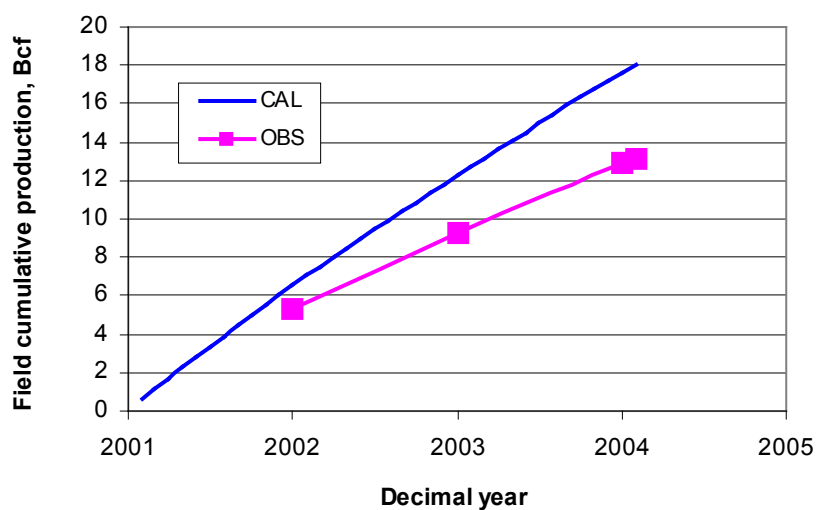


Fig. 5.20 - Predicted field cumulative production for 105 existing wells with weighting scheme 6

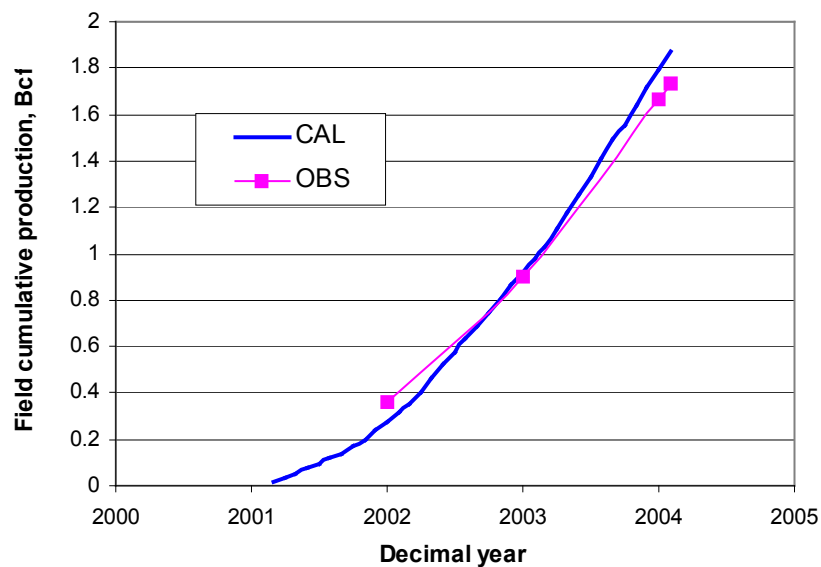


Fig. 5.21 - Predicted field cumulative production for 19 infill wells with weighting scheme 6

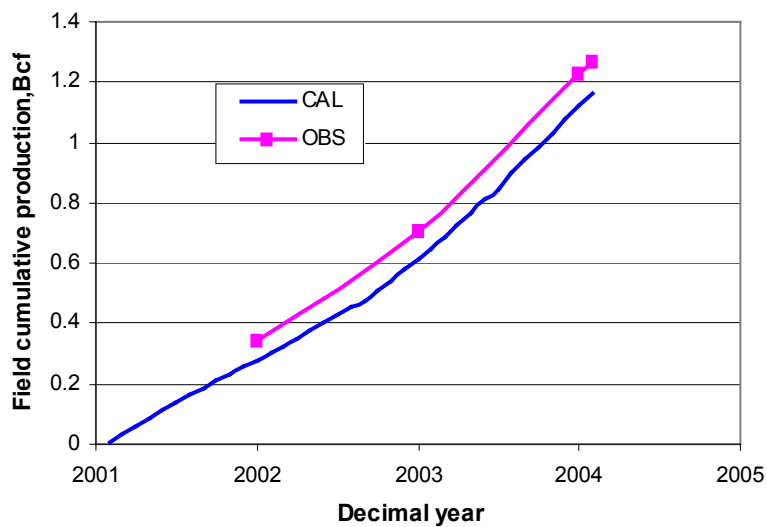


Fig. 5.22 - Predicted field cumulative production for 26 step-out wells with weighting scheme 6

5.6 Comparison of inverse method and SimOpt by field case

I also applied SimOpt in this field case to compare the accuracy and efficiency of these two methods. In addition, since SimOpt can estimate two parameters (permeability and pore volume) at the same time rather than one (permeability) estimated with the inverse method, I tried to quantify how much the prediction results can be improved by matching both pore volume and permeability. Note that, when I match only the permeability field either by the inverse method or SimOpt, I start regression with a uniform value for pore volume.

5.6.1 History matching results

Figs 5.23 and 5.24 show the decreasing objective functions from SimOpt by matching on permeability field only and by matching on both permeability and pore volume. The objective function in Fig. 5.24 is continuing to decrease at the point of termination. There are two reasons why I terminated it at this iteration. First, the misfit does not change very much after iteration 16. Second, I want to compare the misfits in Fig. 5.23 and 5.24 when they are terminated with the same number of iterations. The misfit by matching on two parameters is less than that by only matching the permeability field, but there is not much practical difference. Compared to the misfit from inverse method in this field case (Fig. 5.2), the misfit from SimOpt by either matching on permeability only (Fig. 5.23) or pore volume and permeability (Fig. 5.24) has less decrease with the same number of iterations.

Figs. 5.25 and 5.26 show the estimated permeability distributions for matching only permeability and both permeability and pore volume by SimOpt, which are very similar. As I mentioned before, SimOpt is matching by regions, as is apparent in these two figures. The two maps also indicate that permeability can only be estimated in the areas with or near wells. **Fig.**

5.27 is the estimated pore volume distribution from SimOpt, which was estimated by regions as well.

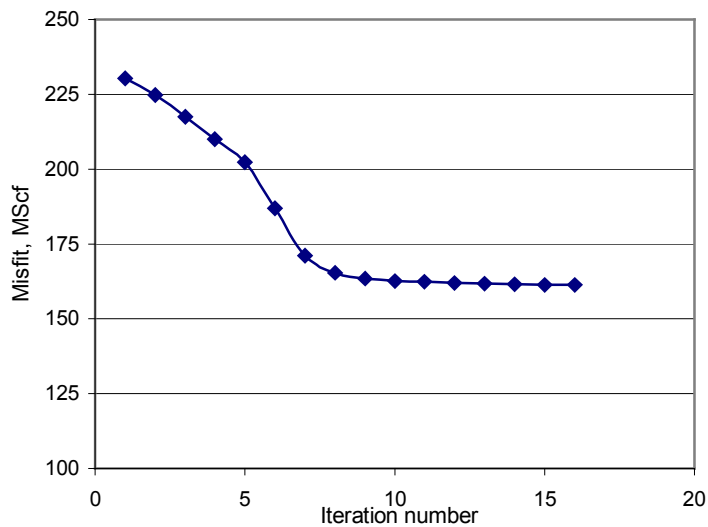


Fig. 5.23 - Objective function by SimOpt matching only on permeability

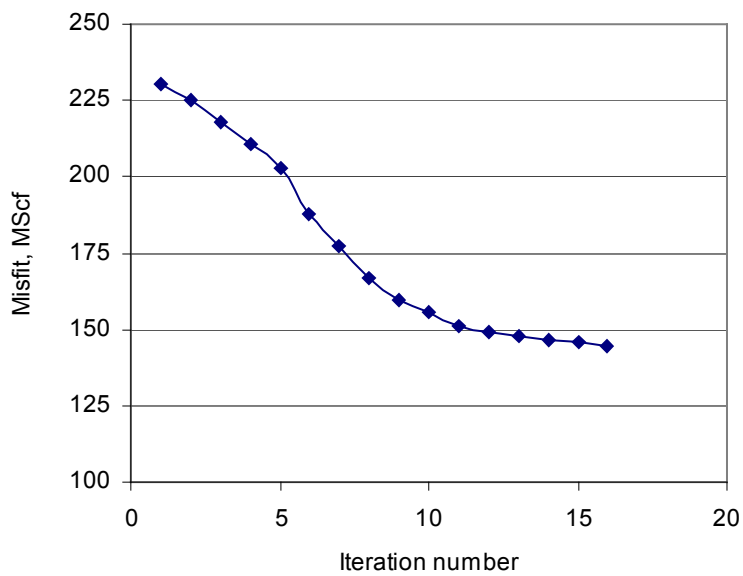


Fig. 5.24 - Objective function by SimOpt matching on both permeability and pore volume

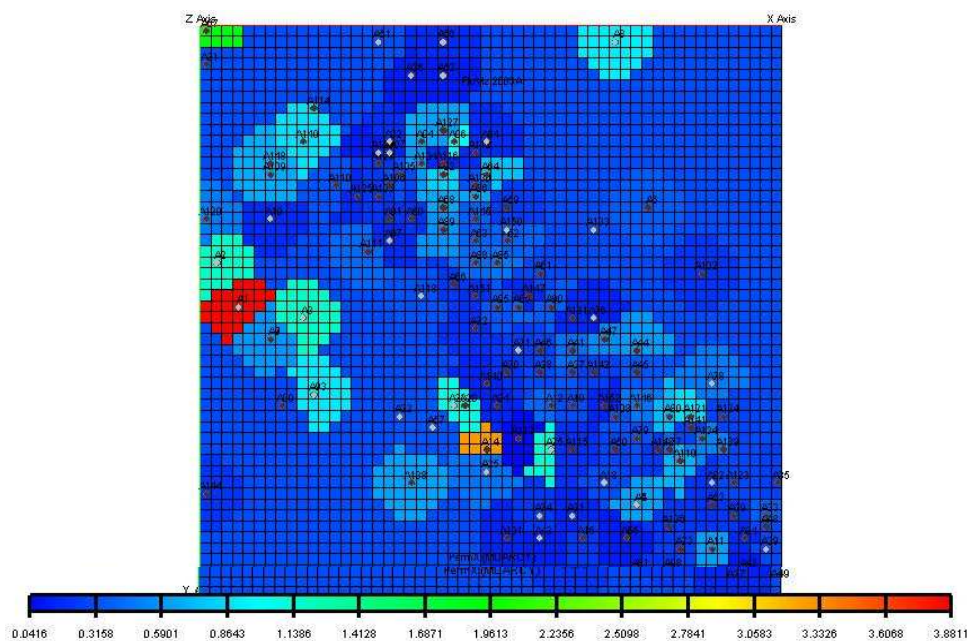


Fig. 5.25 - Estimated permeability distribution by SimOpt matching on permeability only

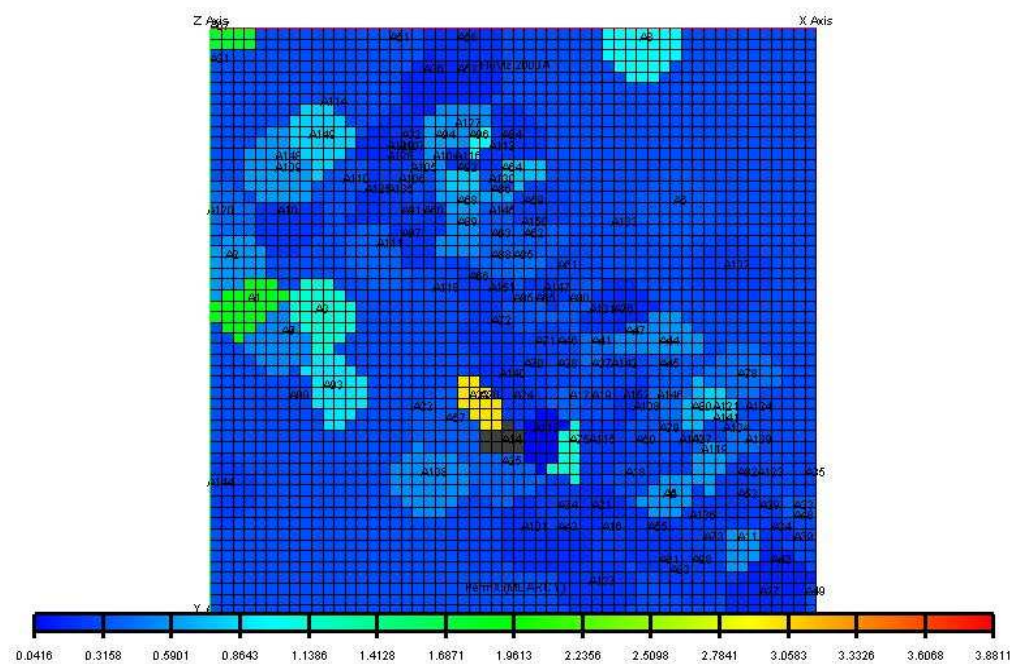


Fig. 5.26 - Estimated permeability distribution by SimOpt matching on permeability and porosity

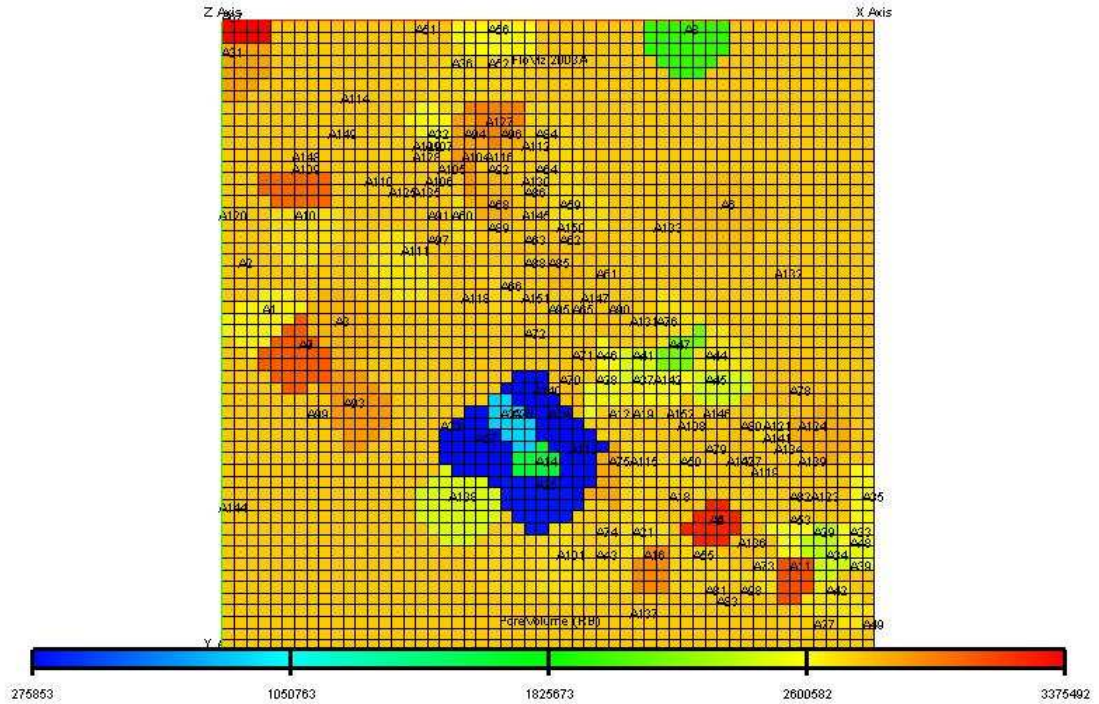


Fig.5.27 Estimated pore volume distribution by SimOpt matching on permeability and porosity

5.6.2 Infill drilling predictions

Tables 5.11-5.13 show the prediction error for the inverse method and SimOpt. Inverse method gives better predictions than SimOpt in all 3 groupings of wells. Thus, the inverse method predicts infill potential more accurately than SimOpt. There is not much improvement in prediction accuracy by matching on both pore volume and permeability instead of matching on permeability only by SimOpt. This may be due to matching by regions with SimOpt.

Table 5.11 - Percent error by inverse method

	Existing well	Infill well	Step-out wells
Relative error, %	48.56	32.01	-76.35
APE(average percent error),%	240.48	130.17	77.70
Median of percent error, %	61.72	48.32	77.59

Table 5.12 - Percent error by SimOpt matching only on permeability

	Existing wells	Infill wells	Step-out wells
Relative error, %	60.23	69.22	38.56
APE(average percent error),%	438.85	170.50	245.65
Median of percent error, %	77.96	62.16	128.63

Table 5.13 - Percent error by SimOpt matching both on permeability and pore volume

	Existing wells	Infill wells	Step-out wells
Relative error, %	56.16	70.33	40.44
APE(average percent error),%	437.87	186.20	232.56
Median of percent error, %	76.12	60.06	128.38

Table 5.14 shows it takes about 8 minutes to finish one regression for the inverse method as opposed to 45 minutes for SimOpt. To have similar objective function value, the inverse method only needs 10 iterations, fewer than 16 needed from SimOpt. Total CPU time

need for the inverse method is only 1 hour 20 minutes, much faster than the 12 hours required for SimOpt. Thus, inverse method is considerably more efficient than SimOpt.

Table 5.14 - Comparison of computation efficiency in field case

	CPU time for 1 iteration	Total iterations	Total CPU time
Inverse Method	8 mins	10	1 hour 20 mins
SimOpt	45 mins	16	12 hours

Based on the above study, it is demonstrated that the inverse method is more accurate than SimOpt in prediction accuracy. In addition, inverse method is a lot faster than SimOpt. The difference in speed is due in part to the different minimization methods they used. The inverse method uses LSQR in minimization, which is an extremely efficient method compared with the Levenberg-Marquardt used in SimOpt.

CHAPTER VI

SUMMARY AND CONCLUSIONS

A simulation-based inversion approach has been presented to predict infill drilling potential as an alternative to conventional reservoir studies and moving window statistical methods. This proposed method combines reservoir simulation with automatic history matching. It does not include detailed reservoir characterization, and uses available data only. It relies primarily on well location and production data, inverting production data with constant flowing bottomhole pressure well constraints. The focus is on large-scale, coarse-resolution rather than small-scale, high-resolution modeling.

The calculation of sensitivity coefficients is the critical part to improve the efficiency of the whole process. In the past decades, many methods for calculating sensitivity coefficients have been proposed. I used the MGPST method due to its high efficiency. Inverse modeling is used to minimize the difference between observed and calculated values, and adjust reservoir parameters based on the difference. In order to remedy the ill-posedness of the inverse problem, I augmented the objective function by adding two terms, norm constraints which ensures that the final model is not too deviated from the initial geologic model, and smoothness constraints, which help to keep spatial continuity. I used LSQR, a mathematic optimization method and also an iterative sparse matrix solver, to solve this augmented linear system. The calculation of infill predictions is based on the above reservoir model and estimated permeability distributions. My infill performance is quantified on a cell basis.

To validate the proposed method, I applied the inverse method to four synthetic test cases with varying degrees of heterogeneity. Followings are the conclusions of the synthetic case study.

- The inverse method can predict infill drilling performance more accurately compared with the moving window statistical method.
- Predictions with the inversion approach were more accurate for both individual wells and the average infill potential for a group of wells.
- Pore volume has a significant effect on prediction accuracy. In the reservoir model with a uniform pore volume about 1.5 higher than average values, the fieldwide prediction error was off by 30%, and the individual-well basis prediction error was approximately 40% high.
- Skin factors have a large effect on prediction accuracy.

I also applied inverse method to a field case, in the Viking Formation of the Western Canada Sedimentary Basin. To validate my predictions, I excluded part of the data set and compared the predicted with observed performance for 3 years. The conclusions are as followed:

- The predictions for existing wells are not as good as what I expected. I attributed this to the minimum shut-in time I assigned in my model. My analysis is based on monthly production data, so I produce wells in the simulation at constant flowing bottomhole pressure for the entire month in months in which there is non-zero monthly production. This results in an overprediction of production when wells do not produce for the entire month.
- The inverse method was able to accurately predict performance for infill wells in areas with sufficient production from existing wells to effectively quantify reservoir quality. Predictions for step-out wells were also good on a fieldwide basis, but much less accurate on an individual well basis.
- Predictions for step-out wells or infill wells in areas with insufficient production can be improved only by including other types of data. Since the proposed method is simulation based, it can easily incorporate other types of data and enables a smooth transition to more

detailed studies, which is an improvement over moving window statistical methods.

Finally, I compared my inverse method with SimOpt in both synthetic cases and field cases. SimOpt is a computer program included with Eclipse that uses mathematical optimization techniques to vary specified reservoir parameters, such as permeability and pore volume, to minimize the difference between observed and simulated production data. The minimization method SimOpt uses is Levenberg-Marquardt method, which is different with the inverse method uses, LSQR method. Both synthetic cases and field cases demonstrate the inverse method is more accurate and efficient compared with SimOpt. Predictions did not get much improved by matching two parameters (permeability and pore volume) rather than one (only permeability) using SimOpt in my study. I think using regions to match may be part of reasons for the poor results. The presented inversion approach matches on reservoir properties on a cell basis. However, instead of matching on individual cell values of reservoir properties, SimOpt matches on constant values of permeability within the gridded Voronoi regions around each well because of the limited number of parameters SimOpt can use in the regression.

Based on all the studies using the inverse method, I conclude that the inverse method is able to identify potential areas or groups of wells for infill development quickly and inexpensively. Prediction accuracy can be increased commensurate with reservoir characterization effort, time and costs. Thus, the method can be a useful and reliable screening tool in large gas infill drilling projects.

Future work should focus on continuing improvement of the accuracy and efficiency of this simulation based inversion method. The specific recommendations are as follows:

- Match using two reservoir parameters, i.e. permeability and porosity, as opposed to just permeability. I should also investigate trying to match using porosity and permeability

on a cell basis rather than matching on constant values of permeability or porosity within the regions.

- Modify the code to match on a region as well as cell basis. Compare the accuracy and efficiency of these two different ways of matching reservoir properties.
- Provide for incorporation of pressure data in the inversion. Incorporating shut-in pressure data will require additional sensitivity calculations, while flowing pressure data may be incorporated through the well constraint mechanism.
- Test the method on larger problems – 1000's to 10,000's of wells.
- Quantify the uncertainty of the infill and recompletion performance predictions.

NOMENCLATURE

- A = the matrix of flow element
- a_N, a_W = north and west flow coefficient, scf · cp/psi² · D
- a_E, a_S = east and south flow coefficient, scf · cp/psi² · D
- a_C = main diagonal of coefficient Matrix A, scf · cp/psi² · D
- APD = average percent difference, %
- b = the knowns including wellblock pressure of last time step and bottomhole pressure, psi
- BY = best 12 conservative months of production divided by 12, MSCM/M
- BY_{inf} = infill drilling production, MSCM/M
- c_i = the calculated production value
- d = the vector of N observation data
- d = right-side column vector of Eq. 2.2
- f = objective function in SimOpt
- f_{prior} = the objective function prior term
- g = forward model
- G = the matrix of sensitivity coefficients
- H = the Hessian matrix
- \mathbf{I} = unity matrix
- J_l = well constant of well l
- J' = well index

- k_j = permeability in wellblock j , md
 $k_{est,i}$ = estimated permeability value for gridblock i
 $k_{act,i}$ = actual permeability value for gridblock i
 kh = permeability in wellblock j , md.ft
 L_h = second-order spatial-difference operator
 M = the number of parameters
 m = the vector of M Parameters
 m_{obs} = the total number of observations
 MSCM/M = thousand standard cubic meter per month
 N = the number of observed data
 N_w = number of wells
 o_i = the observed production value
 p = the vector of well block pressure, psi
 p_p = real-gas pseudopressure, m/Lt^3 , psi^2/cp
 p_{pwf} = real-gas pseudopressure at bottomhole, m/Lt^3 , psi^2/cp
 $p_{pi,j}^n$ = real-gas pseudopressure in (i,j) grid at n time step, m/Lt^3 , psi^2/cp
 $p_{pi,j-1}^{n+1}$ = real-gas pseudopressure in $(i,j-1)$ grid at $n+1$ time step, m/Lt^3 , psi^2/cp
 $p_{pi-1,j}^{n+1}$ = real-gas pseudopressure in $(i-1,j)$ grid at $n+1$ time step, m/Lt^3 , psi^2/cp
 $p_{pi+1,j}^{n+1}$ = real-gas pseudopressure in $(i+1,j)$ grid at $n+1$ time step, m/Lt^3 , psi^2/cp
 $p_{pi+1,j}^{n+1}$ = real-gas pseudopressure in $(i+1,j)$ grid at $n+1$ time step, m/Lt^3 , psi^2/cp
 q = production rate, L^3/t , scf/D

- r = the weighted production data difference
 r_o = equivalent radius of well gridblock, L, ft
 r_w = wellbore radius, L, ft
 RMS = the root mean square
 s = skin factor, dimensionless
 $STDEV$ = standard deviation
 T = temperature, T, °R
 T_{sc} = temperature at standard condition, °R
 Δt = timestep, t, days
 V_p = pore volume of gridblock, L³, ft³
 x_l = a row in matrix A (Eq. 2.10) with corresponding to well l
 z = z factors
 α = coefficient in Eq. 2.4
 γ = weighting factor
 μ = viscosity, m/Lt, cp
 v^k = the vector of current parameter normalized modifier
 ε = data misfit vector, L³/t, scf/D
 δm = perturbation of permeability field, md
 ϕh = pore volume, ft
 w_d = an overall weighting for the d 'th production data set
 w_i = a weighting for the i 'th production data point

REFERENCES

1. McCallister, T.: "Impact of Unconventional Gas Technology in the Annual Energy Outlook 2000," [HTTP://eia.doe.gov](http://eia.doe.gov), (2000).
2. Hudson, J.W., Jochen, J.E. and Spivey, J.P.: "Practical Methods to High-Grade Infill Opportunities Applied to the Mesaverde, Morrow, and Cotton Valley Formations," paper SPE 68598 presented at the SPE Hydrocarbon Economics and Evaluation Symposium, Dallas, 2-3 April, 2001.
3. Coats, K.H., Dempsey, J.R. and Henderson, J.H.: "A New Technique for Determining Reservoir Description from Field Performance Data," paper SPE 2344 presented at the 43rd Annual Fall Meeting held in Houston, Sept. 29 – Oct. 2, 1968.
4. Chung, C.B. and Kravaris, C.: "Incorporation of a Priori Information in Reservoir History Matching by Regularization," paper SPE21615, (2005), unpublished.
5. Coats, K.H.: "An Approach to Locating New Wells in Heterogeneous, Gas Producing Fields," paper SPE 2264 presented at 43rd Annual SPE Fall Meeting, Houston, Sept. 29-Oct. 2, 1968.
6. McCain Jr., W.D., Voneiff, G.W., Hunt, E.R. and Semmelbeck, M.E.: "A Tight Gas Field Study: Carthage (Cotton Valley) Field," paper SPE 26141 presented at the 1993 SPE Gas Technology Symposium, Calgary, 28-30 June.
7. Voneiff, G.W. and Cipolla, C.L.: "A New Approach to Large Scale Infill Evaluations Applied to the Ozona (Canyon) Gas Sands", paper SPE 35023 presented at the 1996 Permian Basin Oil and Gas Recovery Conference in Midland, TX, 27-29 March.

8. Kyte, D.G. and Meehan, D.N.: "Horizontal Spacing, Depletion, and Infill Potential in the Austin Chalk", paper SPE 36721 presented at the 1996 SPE Annual Technical Conference and Exhibition in Denver, CO, 6-9 October.
9. Hudson, J.W., Jochen, J.E. and Jochen, V.A.: "Practical Technique to Identify Infill Potential in Low Permeability Gas Reservoirs Applied to the Milk River Formation in Canada," paper SPE 59779 presented at the 2000 SPE/CEPI Gas Symposium, Calgary, 3-5 April.
10. Guan, L., McVay, D.A., Jenson, J.L. and Voneiff, G.W.: "Evaluation of a Statistical Method for Assessing Infill Production Potential in Mature, Low-permeability Gas Reservoirs," *Journal of Energy Resources Technology* (2004) **126**, No.3, 241.
11. Lee, J. and Wattenbarger, R. A.: *Gas Reservoir Engineering*, SPE, Richardson, Texas, (2000).
12. Wu, Z.: "A Newton-Raphson Iterative Scheme for Integrating Multiphase Production Data into Reservoir Models," *SPE Journal*, (September 2001).
13. Wu, Z. and Datta-Gupta, A. "Rapid History Matching Using a Generalized Travel Time Inversion Method," paper SPE 66352 presented at the SPE Reservoir Simulation Symposium, Houston, 11-14 February 2001.
14. Sen, M.K., Datta-Gupta, A., Stoffa, P.L., Lake, L.W. and Pope, G.A.: "Stochastic Reservoir Modeling Using Simulated Annealing and Genetic Algorithm," paper SPE 24754 presented at the 87th Annual Technical Conference and Exhibition of SPE held in Washington, DC, 4-7 October, 1992.
15. Cheng, H., Kharghoria, A., He, Z. and Datta-Gupta, A.: "Fast History Matching of Finite-Difference Models Using Streamline-Derived Sensitivities," paper SPE 89447 presented at

the 2004 SPE/DOE Fourteenth Symposium on Improved Oil Recovery held in Tulsa, OK, 17-21 April.

16. Jorge Nocedal and Stephaen J. Wright, *Numerical Optimization*, Springer-Verlag, New York Berlin Heidelberg,(1999).
17. Chu, L., Reynolds, A.C. and Oliver, D.S.: “Computation of Sensitivity Coefficients for Conditioning the Permeability Field to Well-test Pressure data,” *In Situ* (1995) **19**, 179.
18. Wu, Z., Reynolds, A.C. and Oliver, D.S.: “Conditioning Geostatistical Models to Two-Phase Production Data,” *SPE Journal*, **4**(2), (June 1999) 142.
19. Yeh, W.: “Review of Parameter Identification Procedures in Groundwater Hydrology: the Inverse Problem,” *Water Resour. Res*(1986), **22**, 95-108.
20. Anterion, F., Eymard, R. and Karcher, B. “Use of Parameter Gradients for Reservoir History Matching,” paper SPE 18433 presented at the 1989 SPE Symposium on Reservoir Simulation, Houston, 6-8 February.
21. Tang, Y. N. and Chen, Y.M.: “Generalized Pulse-Spectrum Technique for 2-D and 2-Phase History Matching,” *Applied Numerical Mathematics* (1989) **5**, 529.
22. Yoon, S., Malallah, A.H., Datta-Gupta, A. and Vasco, D.W. : “A Multi-scale Approach to Production Data Integration Using Streamline Models,” paper SPE 56653 presented at the 1999 SPE Annual Technical Conference and Exhibition, Houston, 3-6 October.
23. Vega.L., Rojas, D. and Datta-Gupta, A.: “Scalability of the Deterministic and Bayesian Approaches to Production Data Integration into Field-Scale Reservoir Models,” paper SPE 79666 presented at the 2003 SPE Reservoir Simulation Symposium, Houston, 3-5 Februray.
24. Paige, C.C. and Saunders, M.A.: “LSQR: An Algorithm for Sparse Linear Equations and Sparse Least Squares,” *ACM Trans. Math. Software* (1982), **8**(1), 43-71.
25. *SimOpt*, Vers. 2002a, Geoquest Schlumberger, Houston,(2002).

26. Hay, P. W., 1994, "Oil and gas resources of the Western Canada Sedimentary Basin", in *Geologic Atlas of the Western Canada Sedimentary Basin*, G.D. Mossop and I. Shetson (comp.), Canadian Society of Petroleum Geologists and Alberta Research Council, Alberta, Chapter 32, URL http://www.ags.gov.ab.ca/publications/atlas_www/atlas.shtml, (accessed on May 3, 2004).
27. MacEachern, J. A., and S. G. Pemberton, 1994, "Ichnological Aspects of Incised-valley Fill Systems from the Viking Formation of the Western Canada Sedimentary Basin, Alberta, Canada", in *Incised-valley Systems: Origin and Sedimentary Sequences*, SEPM Special Publication No. 51, P.129-157, SEPM, Tulsa, OK, (1994)
28. Reinson, G. E., "Comparison of Transgressive and Regressive Clastic Reservoirs, Late Albian Viking Formation, Alberta Basin," *American Association of Petroleum Geologists Bulletin*,(1996) **80**, 980.
29. Reinson, G. E., 1988, "Reservoir Geology of Crystal Viking Field, Lower Cretaceous Estuarine Tidal Channel-bay Complex, South-Central Alberta," *American Association of Petroleum Geologists Bulletin*, (1988) **72**, 1270.
30. Reinson, G. E., W. J. Warters, J. Cox, and P. R. Price, "Cretaceous Viking Formation of the Western Canada Sedimentary Basin," in *Geologic Atlas of the Western Canada Sedimentary Basin*, G.D. Mossop and I. Shetson (comp.), Canadian Society of Petroleum Geologists and Alberta Research Council, Alberta, Chapter 21, URL(1994).

VITA

Name: Hui Gao

Permanent Address: 3116 TAMU - 507 Richardson Building
College Station, TX 77843-3116
USA

Education: Ph.D., Petroleum Engineering (May 2005)
Texas A&M University, College Station, Texas, USA

M.S., Petroleum Engineering (June 2000)
University of Petroleum (Bei Jing), P.R. China

B.S., Petroleum Engineering (July 1995)
University of Petroleum (East China), P.R. China

Experience: Reservoir Engineer, ShengLi Oilfield, P.R. China (1995-1997)